Secondary Bending Stresses in High-Strength Hollow Section Joints

Prishilla S. Kisoensingh

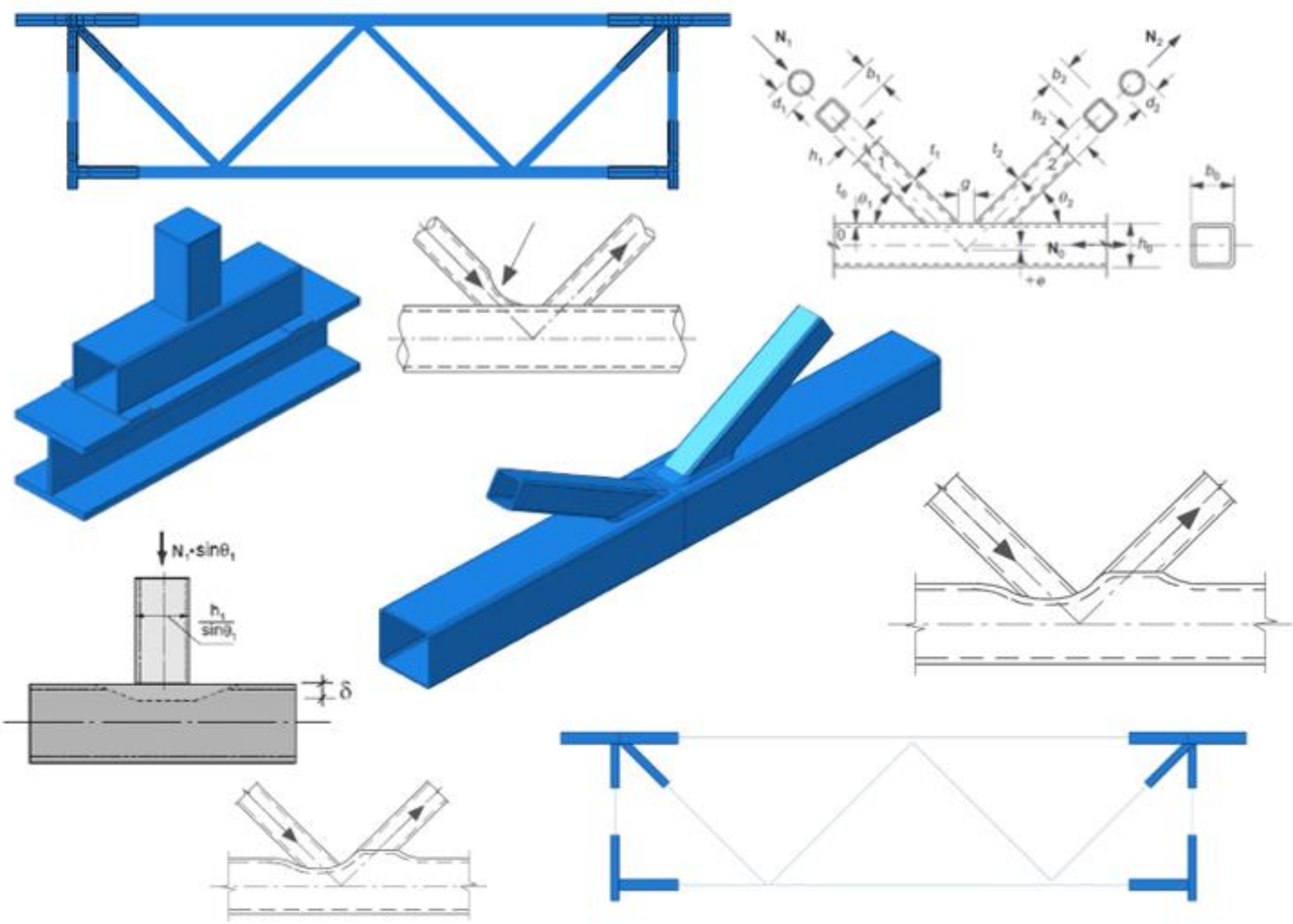

TU Delft

Secondary Bending Stresses in High-Strength Hollow Section Joints

by

Prishilla Kisoensingh

in partial fulfilment of the requirement for the degree of

Master of Science
in Civil Engineering

at the Delft University of Technology,
to be defended publicly on Friday May 10, 2019 at 14:00 pm.

Thesis committee:	*Prof. Dr. M. Veljkovic*	*TU Delft, Chairman*
	Dr. M.A.N. Hendriks	*TU Delft*
	Dr. Haohui Xin	*TU Delft*

TU Delft

PREFACE

This thesis is my final work of MSc. in structural engineering at the Delft University of Technology. The goal of the thesis is to investigate the secondary bending stresses in high-strength hollow section joints through a parametric study. The scope of the work is limited to square hollow section.

I would like to express my gratitude to the members of the graduation committee. Firstly, Prof. Dr. M. Veljkovic and Dr. Haohui Xin for their professional guidance throughout this research and provided me the opportunity to participate at ICEARC’19 (International Civil Engineering and Architecture Conference 2019) held in Trabzon, Turkey. Secondly, Dr. M.A.N. Hendriks. for sharing his insight and prof. Wardenier for providing valuable information which greatly assisted this research.

Finally, I would like to thank my family and friends in Suriname and in Netherlands for their constant support and encouragement during my study.

Prishilla S. Kisoensingh
Delft, May 2019

ABSTRACT

Background: The interest in high strength steel (HSS) shows an increasing trend mainly due to its high yield strength, low weight to strength ratio, decreasing costs of the base material and fabrication [1-3]. The proposed 2020 version of the Eurocode 3 part 1-8 [4], still under discussion at the time of writing of this thesis, covers steel with yield strength up to 700 MPa. This standard has recommended high material reduction parameter for joints with steel grades above S355 to S700. This is done to consider the low deformation observed for steel between 450 MPa and 460 MPa, to include the insufficient knowledge of the material properties of HSSs and the impact of these properties on the current standards [3]. Secondary bending stresses are omitted for the static design strength of mild strength hollow section joints. But for high-strength joints rules regarding these stresses need to be re-analyzed, since the impact of HSS on hollow section joints may be different[5].

Goal: In this study the main goal is to investigate the level of the secondary bending stresses in hollow section joints made of high-strength steel using numerical analyses. Furthermore, the magnitude of the material reduction factors recommended by the proposed 2020 version of the Eurocode 3 part 1-8 [4] are evaluated.

Validation study: An attempt is made to validate the FEM against test data. The commercial finite element program ABAQUS® is used to build the FEM. Roughly good agreement between the test and the FEA is obtained.

Parametric study: A parametric study is performed on an isolated gap K-joint. The joint geometries, boundary and loading conditions are taken from the literature. To study the impact of the material parameters on the secondary bending stresses in RHS joint, various parameters including material properties, gap size, brace width to chord width ratio and weld type are varied. These parameters influence the stiffness, strength, stress distribution and secondary bending stresses. A total of 32 gap K-joints is analyzed in this research. Also, an attempt is made to obtain the ultimate load resistance using the yield line theory.

Results: As results, valuable information about the joint behavior of high-strength hollow section joints is obtained. It is found that secondary bending stresses cannot be neglected when high-strength steels are used.

Keywords: Rectangular hollow section (RHS), High-strength steels (HSS), Ultimate load, secondary bending stress, level of secondary bending stress, material reduction factors, yield line.

Contents

LIST OF FIGURES

LIST OF TABLES

CHAPTER 1 INTRODUCTION

1.1 Background

The interest in high strength steel (HSS) with yield strength above 460 MPa shows an increasing trend, mainly due to its high yield strength, low weight to strength ratio, decreasing costs of the base material and decrease cost of fabrication. The HSS has potential for applications in specific structures, such as in truss girders of long spans used in sport arenas and bridges. However, HSS are not commonly used mainly due to the serviceability criteria and the limited experience in welding procedures. Furthermore, the uncertainty exists whether the current standards of tubular joints validated for mild-strength steels can be applied to HSS, because of the lack of experimental evidence [1-3].

Secondary bending stresses in tubular joints are introduced by the non-uniform stiffness of the joint, eccentricity and the large deformations of the truss girder. The calculation of the secondary bending stresses is complex because it does not only depend on the joint stiffness but also on the behavior of the joint. To simplify the strength calculation, truss girders are designed using pinned jointed brace and continuous chord. This method does not include all the joint parameters such as the local joint stiffness and secondary bending stresses [6]. The code EN1993-1-8:2005 [7] which is applicable to welded hollow section joints with steel grade up to S460 allows to neglect the secondary bending stresses for joints within the validity range. For steel grade between S355 and S460, a material reduction factor of 0.9 is considered to take into account the low deformation capacity [6].

The use of the HSS has been facilitated in the proposed 2020 version of the Eurocode 3 part 1-8 [4], which is still under discussion at the time of writing of this thesis. This code covers steel grade up to 700 MPa. Design equations, which are validated for mild strength steel, are applied to HSS. For steel grades between S460 and S700, a material reduction factor of 0.8 is recommended. Furthermore, the yield strength should not exceed 80%f_u. The reason for these high reduction factors can be due to the large deformation observed for steel with yield strength between 450 MPa and 460 MPa, the insufficient knowledge of the material properties of HSS and the impact of these properties on the current standards [3]. This arises a need to study the HSS relating secondary bending stresses.

Secondary bending stresses in mild-strength joints were previously studied by professor Wardenier [8]. In his report, it was observed that the maximum secondary bending stresses in hollow section joints varies from 40% to 60% of the axial load. Furthermore, the secondary bending stresses reduces after the redistribution of stresses in the the plastic stage. At ultimate load resistance, these stresses disappear and can therefore be neglected in the static design strength. Also, numerous studies conducted under CIDECT (Comité International pour le Développement et l´Etude de la Construction Tubulaire) were mostly performed on mild-strength hollow section joints. CIDECT has published design standards for hollow section joints [6] and these are the basis of many standards including the EN1993-1-8:2005 [7].

However, limited experimental data on high-strength hollow section joints regarding secondary bending stresses is available. Recent studies on secondary bending stresses in high-strength hollow section joints by Bjork [5] has proven that these stresses can be considerably large and affect the joint capacity. During the workshop HPSSRC (First Workshop Proceedings of High Performance Steel Structures Research Council) held at Delft University of Technology a research in high strength hollow section joints by KIT (Karlsruhe Institute of Technology) was presented [9]. A reduction factor of 0.8 was suggested to consider for the static design strength of hollow section joints. Furthermore, their research has indicated that secondary bending stresses for joints with steel grade above S460 should be considered in static design strength. This can be done by using the k_1- factors from the EN1993-1-9:2012 [10]. However, at the time of writing this thesis, this study was not published.

This research aims to investigate the secondary bending stresses in hollow section joints with steel grade up to S960. Furthermore, the magnitude of the material reduction factors recommended by the proposed 2020 version of the Eurocode 3 part 1-8 [4] is evaluated. These stresses in hollow section joints is investigated numerically using the commercial finite element software ABAQUS®. Previous test data are used to calibrate the finite element models.

1.2 Research Objective and Question

The main research objective of this thesis is to obtain the level of the secondary bending stresses in hollow section joints made of mild-strength and high-strength steel. Also, the high material reduction factors recommended by the proposed 2020 version of the Eurocode 3 part 1-8 [4] for steel grade between S460 and S700 is reviewed. The scope of this research is limited to square hollow section joints. The research questions for this thesis are:

I. Which parameters can be used to describe the secondary bending stresses in the hollow section joints?

II. What is the behavior of the rectangular hollow section joints made of HSS? Is there any high reduction parameter in the current design formulas for the RHS joints needed?

III. Should the secondary bending stresses for RHS joints be considered in the design? Which can be divided into multiple sub questions:
   a. How to determine the secondary bending moments in FEM? What is the level of the secondary bending moment?
   b. What are the effects of the parameters used in the parametric study on secondary bending stresses?
   c. Are additional reductions on the yield strength sufficient to cover the secondary bending stresses?

1.3 Research Methodology

First, a literature survey has been performed in order to obtain knowledge in the secondary bending stresses and the design rules for hollow section joints. Hereafter, an attempt has been made to calibrate finite element models against test data. Numerical analysis is used to perform the parametric study. Finally, the obtained results will be analyzed and conclusions regarding the joint behavior are drawn. The described methodology is shown in **Figure 1-1**.

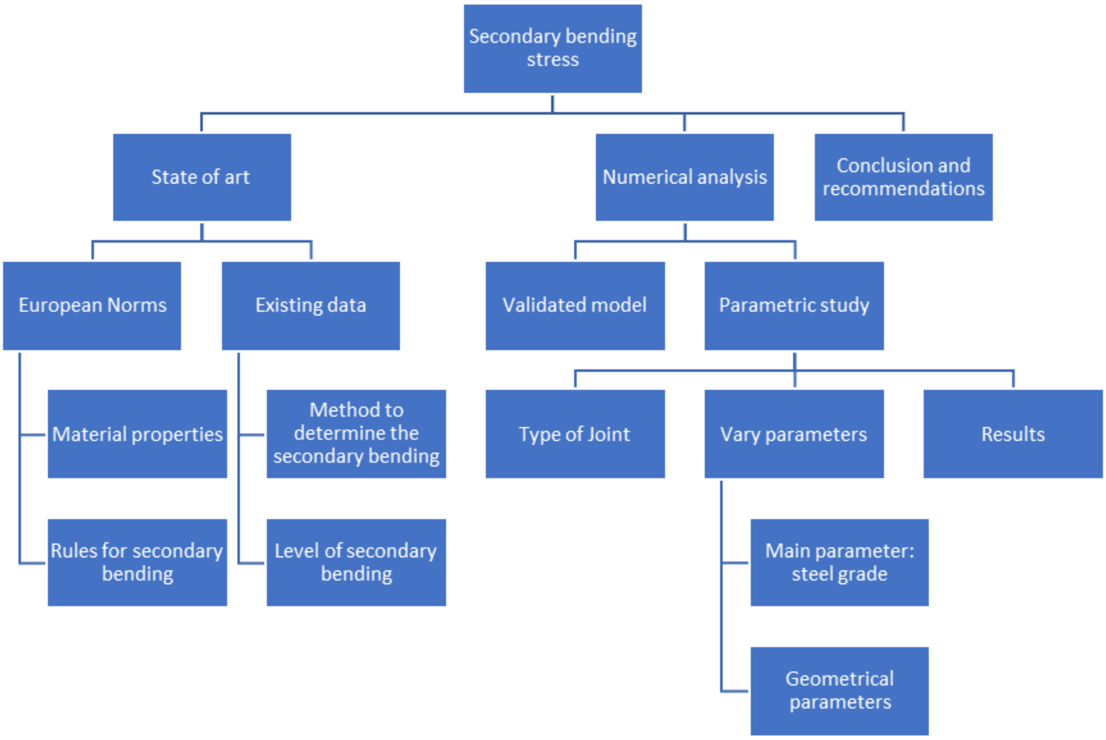

Figure 1-1: Methodology

CHAPTER 2 LITERATURE REVIEW

2.1 High-Strength Steels

2.1.1 Introduction

High-strength steel (HSS) indicates steels with yield strength greater than 460 MPa and up to 700 MPa and steels with yield strength greater than 700 MPa are defined as ulta-high-strength steel. Steels between S235 and S460 are usually referred to as mild-strength steel. Two common heat treatments to produce high-strength steels are the quenching and tempering (QT) and the thermo-mechanical controlled processing (TMCP). In the 1960s, the quenching and tempering method and in the 1970s, the thermo-mechanical rolling process was already developed. High-strength steels with yield strength up to 690 MPa were already created in the 1970s. High-strength steels were developed worldwide and used in countries such as in Japan, the United States and in Europe [11]. High yield strength of the steel is obtained by alloying and heat treatments. Adding alloying elements can improve the steel strength but reduce the weldability and ductility. Heat treatments have an effect on the microstructure and the grain size which may influence the strength, toughness and weldability [12]. Nowadays, the steel industry produces HSSs with desirable mechanical properties. The development of the steel grades is given in **Figure 2-1**. For decades, high strength steels have been extensively used in the automotive and crane industry. High-strength steels are applied in some civil structures, such as bridges, offshore platforms, tower, and lattice structures [2].

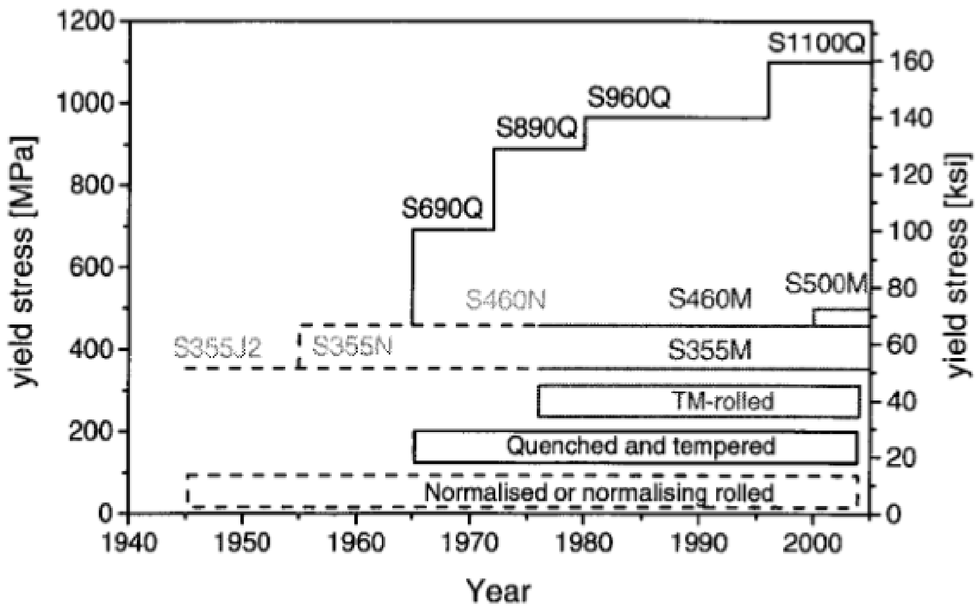

Figure 2-1: Development of high-strength steel [11]

Due to the increasing interest in high-strength steel, many studies have been carried out to investigate the mechanical properties and the structural behavior of high-strength steels. In 2007, steels up to S700 are included in the European standards [4, 10]. Additional reductions and rules are given to design with these HSSs, especially for high-strength steel tubular joints. These are needed to cover the knowledge gap and to include the different mechanical properties of HSSs. Ultra-high-strength steels greater than S700 are already in the market, but not supported by the European standards. The use of high-strength steel has many benefits. Due to their high yield strength and weight to strength ratio, lighter structures can be built which results in lower consumption of material and lower CO_2 emission.

2.1.2 Mechanical Properties

The mechanical properties of steel can be described using the stress-strain relationship. The stress-strain relationship of steel is linear elastic until the upper yielding plateau. Beyond this plateau the stress is no longer proportional to the strain (see **Figure 2-2(a)**). After the upper yield plateau the steel starts to yield. A clear lower yield plateau, strain hardening, and peak stress can be observed. The lower yield plateau, where the strain increases without a significant change in stress, is taken as the yield strength and the peak stress is considered as the ultimate stress. Normal steels have these desirable properties which is necessary for ductility.

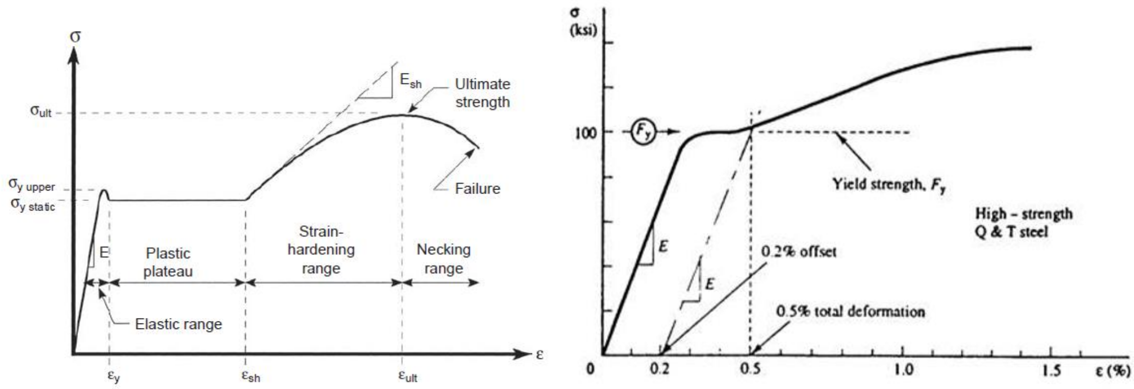

Figure 2-2: Schematic representation stress-strain curve for (a) mild-strength steel [13] and (b) HSS [2]

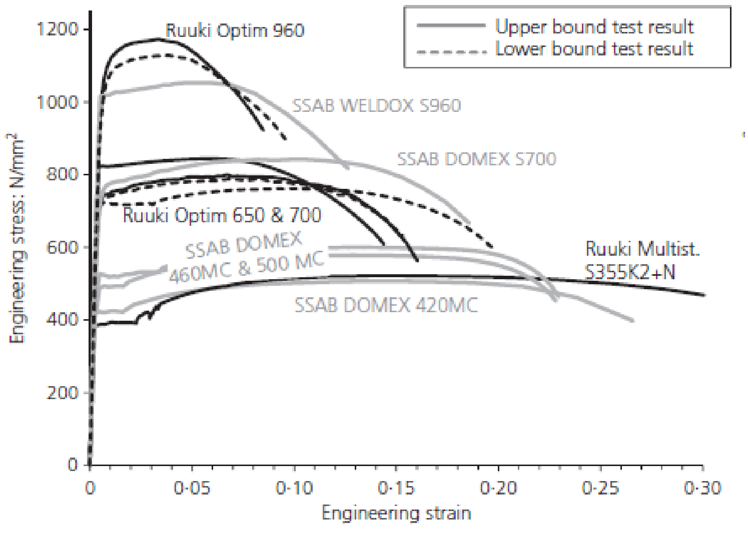

Figure 2-3: Stress-strain curve mild-strength and high-strength steel [14]

For the increasing yield strength, the ultimate strain decreases. Also, beyond the yield plateau the high-strength steel has a shorter or no yield plateau. For steel without a clear yield point, the yield strength can be defined as the 0.2% proof stress (see **Figure 2-2(b)**). Also, the difference between the yield strength and the ultimate tensile strength becomes smaller for increasing yield strength. Therefore, the proposed 2020 version of the Eurocode 3 part 1-8 has proposed to limit the yield strength 0.8 times the ultimate stress, $0.8f_u$. This is done to ensure that the material has sufficient ductility. **Figure 2-3** shows the stress-strain relationship for mild-strength steels and high-strength steels obtained by coupon test. The modulus of elasticity for all steel grades is identical, which is approximately 210 GPa [2, 13-15].

Ductility and toughness
Sufficient ductility is necessary to allow the material to deform plastically and to redistribute stresses without a brittle failure. Therefore, the standards have given limitations to the material parameters that affect the ductility. For steel up to S460, the limitations are[16]:

- $f_u / f_y \geq 1.1$
- Elongation at failure greater than 15%
- $\varepsilon_u \geq 15 f_y / E$

These ductility requirements for steel greater than S460 and up to S700 are[10]:

- $f_u / f_y \geq 1.05$
- Elongation at failure greater than 10%
- $\varepsilon_u \geq 15 f_y / E$

Compared to mild-strength steel with yield strength up to S460, high-strength steels have lower f_u / f_y ratio. High f_u / f_y ratio is considered to provide high deformation capacity before brittle failure occurs. Therefore, high-strength steels have lower ductility than mild-strength steel. Due to this high-strength steel materials have lower deformation and rotation capacity. The elongation at failure is the ratio of the elongation of the specimen at fracture over the original length. Furthermore, this parameter reduces with increasing yield strength. The strain at ultimate strength should be greater than or equal to $15 f_y / E$ [3, 10, 16]. High toughness is required to avoid the brittle failure. The toughness can be measured by Charpy-V notch test. Material with toughness of 27J or higher at the test temperature is considered as ductile. Tests done on mild and high-strength steel indicate that HSS have good toughness. This is due to the improved manufacturing processes and micro-alloying [2, 17].

2.2 Welded Connection

The connection between hollow section joints can be made using weld – designed in such a way that the joint resistance has sufficient stiffness and deformation capacity. These are necessary for the non-uniform stress distribution and the redistribution of moments. In case of gap joints, the entire perimeter of the brace member should be welded. Butt welds and or fillet welds are often used to join the hollow section joints. To create the butt welds, the edges are usually beveled. Butt welds can be either full penetrated or partial penetrated. Fillet welds are triangularly shaped welds, which can be single or double-sided. Single sided fillet welds create locally eccentricity, which introduces additional forces and stresses. Single sided fillet welds are only applied to join hollow sections. The effective throat thickness 'a' of the fillet welds is the height of the largest triangular as shown in **Figure 2-4**. The penetration fillet weld may have a throat thickness larger than the designed throat thickness. The minimum effective throat thickness of the fillet welds should be 3 mm [4, 18].

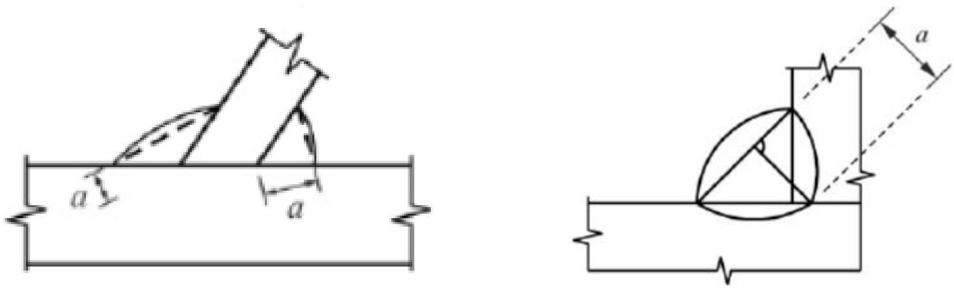

Figure 2-4: Throat thickness of a fillet and deep penetration fillet weld [18]

2.2.1 Design Resistance Fillet Welds

Various methods are recommended by the codes to design the welds [4, 18]. The fillet welds should be designed using the directional method or the simplified method. The directional method is based on the forces and moments transferred through the welds. These forces and moments are decomposed into the normal stress perpendicular to the throat ($\sigma_\perp$), the normal stress parallel to the axis of the weld ($\sigma_\parallel$), the shear stress perpendicular to the axis of the weld ($\tau_\perp$) and the shear stress parallel to the axis of the weld ($\tau_\parallel$). These stresses are shown in **Figure 2-5** [18]. To determine the resistance of the welds, both the undermentioned equations should be satisfied.

$$[\sigma_\perp + 3(\tau_\perp{}^2 + \tau_\parallel{}^2)]^{0.5} \leq \frac{f_u}{\beta_w \gamma_{m2}} \text{ and } \sigma_\perp \leq \frac{0.9 f_u}{\gamma_{m2}}$$ **Equation 2-1**

where the factor β_w is the correlation factor and it depends on the steel grade (shown in **Table 2-1**). The parameter f_u is the nominal ultimate strength of the weaker part. The parameter γ_{m2} is the partial safety factor for welded connections [4, 18].

Table 2-1: Correlation factor fillet welds [4]

Steel grade	β_w
S235	0.8
S275	0.85
S355	0.90
S460	0.85
S690	1.10

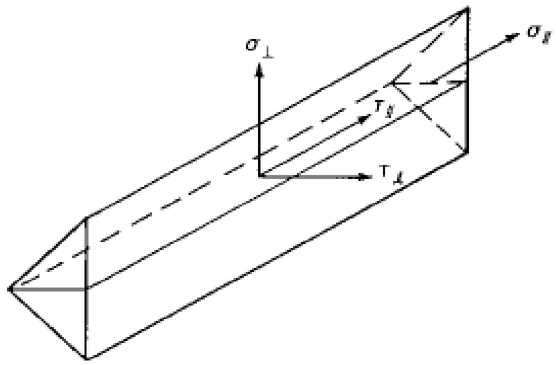

Figure 2-5: Stresses in the fillet weld [4]

This equation changes slightly for connection with steel S460 and above and different base material and filler material strength. The proposed 2020 version of the Eurocode 3 part 1-8 [4] recommends to include the strength of the filler material in design resistance. The equation becomes:

$$[\sigma_{\perp} + 3(\tau_{\perp}^{2} + \tau_{\parallel}^{2})]^{0.5} \leq \frac{0.25 f_{u,PM} + 0.75 f_{u,FM}}{\beta_{w,\mathrm{mod}} \gamma_{m2}}$$ **Equation 2-2**

where $f_{u,PM}$ and $f_{u,FM}$ are the strength of the weakest parent material and the filler material, respectively. The factor $\beta_{w,\mathrm{mod}}$ is the modified correlation factor between weld and parent material [4]. Another way to determine the weld strength is the simplified method. In this method the force transmitted by the weld should satisfy the equation:

$$F_{w,Ed} \leq F_{w,Rd}$$ **Equation 2-3**

where $F_{w,Ed}$ is the design value of the weld force per unit length and $F_{w,Rd}$ is the design weld resistance per unit length [4, 18].

Full-strength method

The full-strength method is used for welded connections with a possible brittle failure. This is the case when the rupture strength of the weld is much lower than that of the parent material. With this method, the stresses and forces needed for the directional and simplified method can be avoided. Based on **Figure 2-6** the following expressions can be obtained for a double-sided fillet weld:

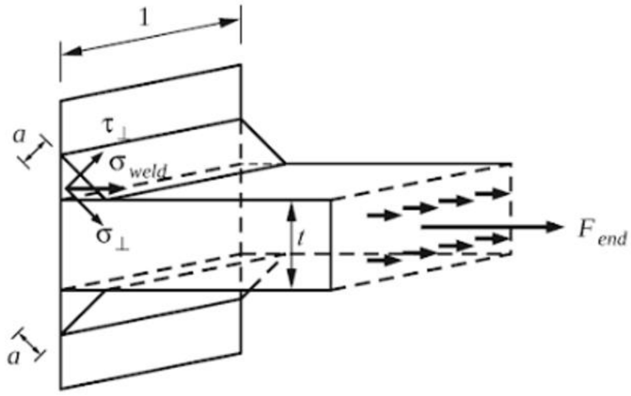

Figure 2-6: Double-sided fillet welds [18]

$$F_{end} = tlf_y$$
$$\sigma_{weld} = \frac{F_{end}}{2al} \quad \text{Equation 2-4}$$
$$\sigma_{\perp} = \tau_{\perp} = \frac{\sigma_{weld}}{\sqrt{2}} \; and \; \tau_{//} = 0$$

where *a* is the throat thickness and *l* is the unit length of the weld. The parameter γ_{m0} is the partial safety factor for steel material. Combining these expressions with the expression used for the directional method, the following expression is obtained to determine the full-strength of double-sided fillet welds [18]:

$$a \geq \frac{F_{end}\beta_w\gamma_{m2}}{f_u l\sqrt{2}} = \frac{(f_y tl)\beta_w\gamma_{m2}}{f_u l\sqrt{2}} \quad \text{Equation 2-5}$$

2.2.1.1 Single sided-fillet welds in RHS joints

Welds are usually designed “full strength” or for the external load. Full-strength welds are preferred, since sufficient deformation capacity and rotation capacity would be ensured, and the failure in the welds would be avoided. The required throat thickness of a full-strength single-sided fillet weld according to [4] can be determined using the equation:

$$a \geq \frac{F_{end}\beta_w\gamma_{m2}}{f_u l\sqrt{2}} = \frac{\sqrt{2} f_y t\beta_w\gamma_{m2}}{\gamma_{m0} f_u} \quad \text{Equation 2-6}$$

The throat thickness for each steel grade is summarized in the **Table 2-2**. The correlation factor for steel grade up to S700 is obtained from [4]. For steel grade S960 the correlation factor has been linearly extrapolated[4, 18].

Table 2-2: Required throat thickness fillet weld

Steel grade	β_w	γ_{m2}	γ_{m0}	f_y	f_u	Full-strength [4] a/t
	(-)	(-)		(N/mm^2)	(N/mm^2)	(mm)
S355	0.9	1.25	1	390	521	1.19
S460	0.85	1.25	1	460	575.5	1.20
S700	1.1	1.25	1	700	835	1.63
S960	1.24	1.25	1	960	1175	1.79

The throat thickness is dependent on the thickness of the connected plate, the strength of the weaker material and the correlation factor. In case the fillet weld is designed to resist the external axial load, the length of the fillet weld is also required to determine the throat thickness. The stiffness along the RHS brace perimeter is non-uniform and due to this a certain part is assumed to be effective in resisting the load. Therefore, an effective length of the brace perimeter is assumed to consider for the design of the weld. The effective length considered for the punching shear failure in RHS gap K-joint, shown in **Figure 2-7**, can also be considered to resist the the load[4, 6, 18]. The smallest effective length is equal to:

$$l_{eff} = 2(h_i / \sin(\theta_i) + b_{e,p})$$

with **Equation 2-7**

$$b_{e,p} = \frac{10}{b_o / t_o} b_i \leq b_i$$

In which h_i is the height of the brace, b_i is the width of the brace member, θ_i is the brace angle, b_o is the width of the chord and t_o is the thickness of the chord.

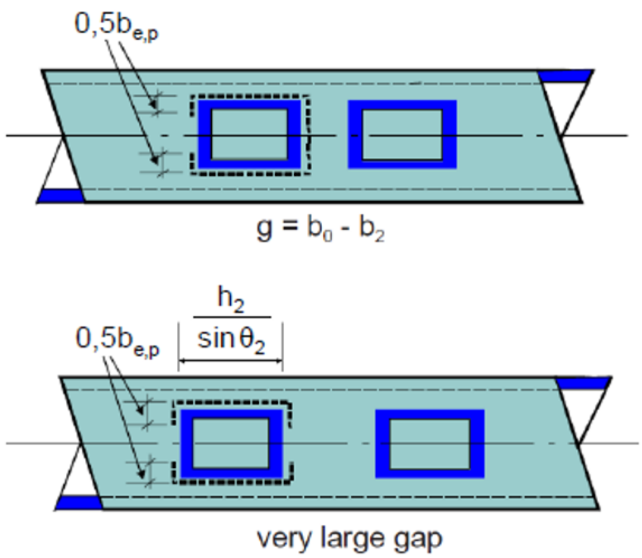

Figure 2-7: Effective length considered for punching shear failure for a gap K-joint[6]

2.3 Design Recommendations

The first investigation on circular hollow section (CHS) joints was carried out in the 1950s in Germany [19]. Investigations were mainly done on circular hollow sections joints. Due to the increasing popularity of the tubular sections, many other countries started to get involved in performing tests on CHS joints. The end preparations of the circular hollow sections, due to the circular shape were complex. New types of hollow section were therefore needed. The first rectangular hollow section (RHS) was fabricated in 1952, which were easy to connect. Many experiments on isolated joints (mainly under static axial loading) were carried out and design equations were developed. All these equations were based on a limited research and were different from each other. CIDECT and IIW (International Institute of Welding) made it possible for many researchers to share their work and to obtain general design rules for joints with hollow sections. Hereafter various studies have been carried out to gain more knowledge.

In 1981, the IIW (sub-commission XV-E) published the first edition of design rules on static strength of tubular joints. The second edition was published in 1989 and the third in 2009. The second edition is adopted by many documents and codes. CIDECT published design guidelines for hollow section joints based on the IIW publications in 1989 and 2009. The book, Hollow Section in Structural Application [6] is based on the recent publication of the IIW. The standard EN1993-1-8:2005 [20] provides design equations for hollow section joints adopted from the IIW recommendations published in 1989. The recent development of the hollow section joints is also covered in the updated design code. The design resistance according to the proposed 2020 version of the Eurocode 3 part 1-8 [4] will be discussed in this section.

2.3.1 Joint Classification

The type of joints depends on their geometry. T and Y joints, presented in **Figure 2-8** includes one brace member, which can be perpendicular (T joint) to the chord or inclined (Y joint). K joints include two inclined brace members. An N joint is a K joint, with one brace perpendicular to the chord. K and N joints can be classified as gapped or overlapped. Joints with brace members attached to the opposite side of the chord can be denoted as an X joint.

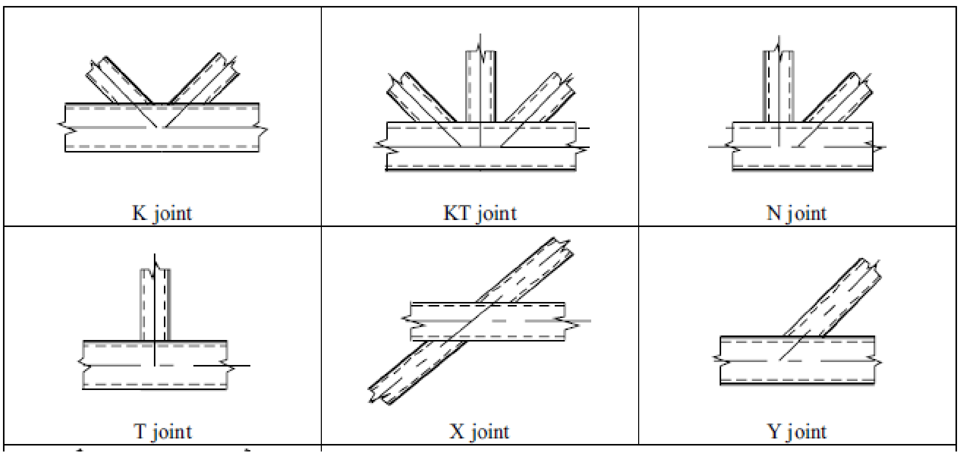

Figure 2-8: Simple uniplanar joints [4]

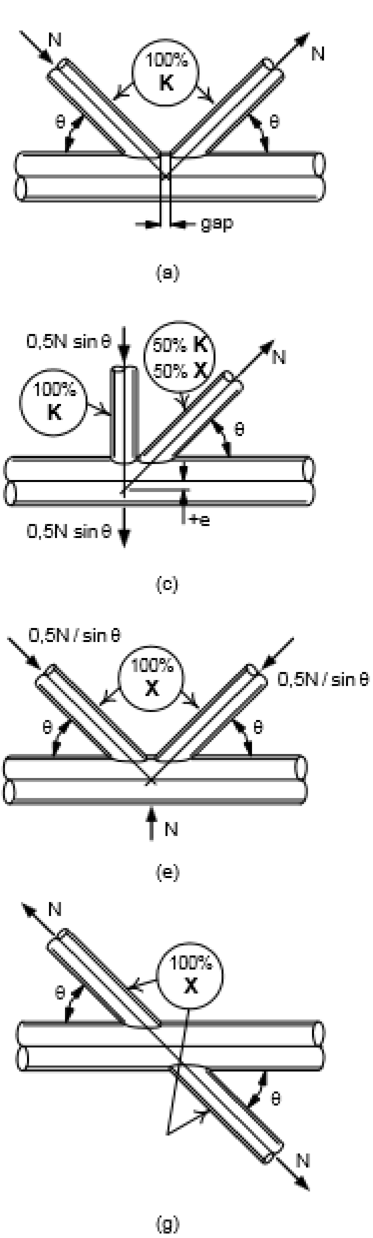

Figure 2-9: Hollow section joint classifications [6]

In the standards, various multiplanar and uniplanar joints between hollow and or open sections are mentioned. In this study, simple uniplanar joints between hollow sections will be discussed. The uniplanar hollow section joint consists of one or more brace members connected to a continuous chord. The classification of the joints is based on the loading which can be seen in **Figure 2-9**. The T and Y joints must have an equilibrium between the shear force in the chord and the force component perpendicular to the chord in the brace member. The forces in both the brace members of K and N joints should be in equilibrium. A margin of 20% is acceptable. K gap joints with a large gap should be considered as two independent Y joints. In an X joint, the force component perpendicular to the chord in both braces should be in equilibrium. A K joint with both brace members in compression or in tension should be considered as an X joint. In **Figure 2-9** various basic joint configurations are shown [4, 6].

Joint Parameters
Figure 2-10 shows the geometry of the members in the joint. For joints with gap or overlap, the following equations can be used to determine the gap and the eccentricity:

$$g = (e + \frac{h_0}{2})\frac{\sin(\theta_1+\theta_2)}{\sin\theta_1 \sin\theta_2} - \frac{h_1}{2\sin\theta_1} - \frac{h_2}{2\sin\theta_2}$$ **Equation 2-8**

$$e = \left(\frac{h_1}{2\sin\theta_1} + \frac{h_2}{2\sin\theta_2} + g\right)\frac{\sin\theta_1 \sin\theta_2}{\sin(\theta_1+\theta_2)} - \frac{h_o}{2}$$ **Equation 2-9**

A positive ‘g’ value indicates a gap and a negative ‘g’ value indicates an overlap. The gap is the distance between the toe of the brace members neglecting the welds. The index i=1 is mostly used for the compression brace and the index i=2 for the tension brace. In an overlap joint, the index i=1 or 2 is used for overlapping brace member and the index ‘j’ is used for the overlapped member[4, 6].

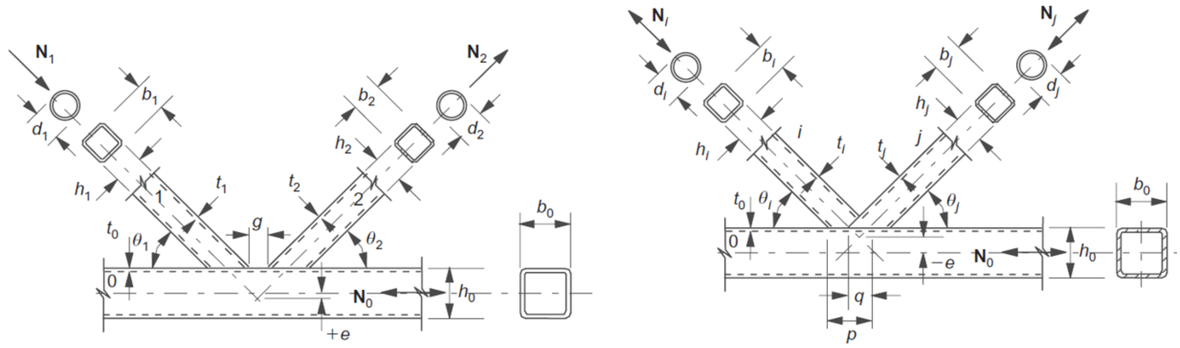

Non-dimensional parameters:

$$\beta = b_1 / b_0 \quad for\ T, Y, X\ joints$$
$$\beta = (b_1 + b_2)/2b_0 \quad for\ K\ and\ N\ joints$$
$$\gamma = b_o / 2t_0$$
$$Overlap = (q/p) \times 100\%$$
$$\eta = h_i / b_0$$

Figure 2-10: K-Joint Geometry of (a) gap K-joint and (b) overlapped K-joint [4]

2.3.2 Range of Validity

The proposed 2020 version of Eurocode 3 part 1-8 [4] provides design equations for joints, which can be applied for joints within the range of validity. Within this range, certain failure modes may occur, which can be used to determine the joints resistance. Joints outside the range are allowed but need a second analysis due to a possible different joint behavior.

Limitation on Material
The recommended design equations can be applied to both cold and hot formed hollow sections made of steel up to S460. The open steel section should be obtained from EN10210 and EN10219. A reduction parameter of 0.9 (material factor) should be applied for the design resistance for steel grade above S355. This limitation takes the low deformation capacity of steel strength above 355 MPa into account. The proposed 2020 version of the

Eurocode 3 part 1-8 [4] recommends using steel up to S700 and a reduction parameter of 0.8 is required. **Table 2-3** and **Table 2-4** summarize the material factors to be included in the design resistance.

Table 2-3: Material factor according to [20]

Steel grade	Material factor
$f_y \leq 355N/mm^2$	$C_f = 1$
$355N/mm^2 < f_y \leq 460N/mm^2$	$C_f = 0.9$

Table 2-4: Material factor according to [4]

Steel grade	Material factor
$f_y \leq 355N/mm^2$	$C_f = 1$
$355N/mm^2 < f_y \leq 460N/mm^2$	$C_f = 0.9$
$460N/mm^2 < f_y \leq 700N/mm^2$	$C_f = 0.8$

Limitation on Geometry

Slender cross sections are susceptible to local buckling and therefore not recommend to use in joints. The joint members in girders are limited to cross section class 1 and class 2. The EN1993-1-1:2006 [16] is used to classify the cross-sections. The minimum nominal thickness of the joint members is limited to 1.5 mm.

Brace Angle (θ)

To fabricate proper welds, the minimum angle between the joint members is limited to 300.

Gap (g) and Overlap (q)

In the joint, the distance between the brace members is the gap. This gap should be larger than the sum of both the brace wall thickness: $g \geq t_1 + t_2$. The minimum gap is necessary to provide sufficient space for the weld and to avoid overlapping of the weld.
In case of an overlap joint, the narrower brace member or the member with the lowest $t_i \times f_{yi}$ should overlap the other brace member. To achieve sufficient force transfer between the brace members, the overlap in an overlap joint should be not less than 25%.

Eccentricity (e)

The joint eccentricity is limited to a range of $-0.55h_o \leq e \leq 0.25h_o$. Within this range, the bending moment can be neglected. Outside this range, the bending moment due to the eccentricity should be included in the joint and member design.

To design rectangular hollow section joints with a gap or an overlap, **Table 2-5** and **Table 2-6** summarizes the range of validity. Additional range of validity for square hollow sections is given in **Table 2-7**. Within the range of validity and the additional range of validity, the joints with square hollow sections can be designed using one failure mode, namely the chord face failure.

Table 2-5: Range of validity for T, Y, X, and K gap joints [4]

General	Gap	$0.5(1-\beta)\leq g/b_o \leq 1.5(1-\beta)$ but minimum $g \geq t_1 + t_2$ (1)
		$b_i / b_o \geq 0.1 + 0.01 b_o / t_o$ $but \geq 0.25$ $-0.55h_o \leq e \leq 0.25h_o$ $\theta \geq 30^0$ $f_y \leq 460MPa$ (2) $f_y \leq 0.8 f_u$, $f_{yi} \leq f_{yo}$ $t_i \leq t_o$
RHS brace	Compression	b_i / t_i and $h_i / t_i \leq 35$ and $class 1\,\&\,2$
	Tension	b_i / t_i and $h_i / t_i \leq 35$
	Aspect ratio	$0.5 \leq h_i / b_i \leq 2$
RHS chord	Compression	b_0 / t_0 and $h_0 / t_0 \leq 35$ and $class 1\,\&\,2$
	Tension	b_0 / t_0 and $h_0 / t_0 \leq 35$

(1) $for\ g/b_o \geq 1.5(1-\beta)$ consider as two seperate Y joints and perfom a chord shear check in the gap with $\alpha = 0$

(2) $for\ f_y \geq 355MPa$, $apply\ reduction\ of$ 0.9

Table 2-6: Range of validity for overlap joints [4]

General		$\lambda_{OV} \geq 25\%$ and $b_i / b_j \geq 0.75$ b_i / b_o and $b_j / b_o \geq 0.25$ θ_i and $\theta_j \geq 30^0$ $-0.55h_o \leq e \leq 0.25h_o$ $t_i \leq t_J$ & $t_i f_{yi} \leq t_j f_{yj}$ t_i and $t_J \leq t_0$ $f_y \leq 460MPa$ (1) $f_y \leq 0.8 f_u$ & f_{yi} and $f_{yj} \leq f_{yo}$
RHS brace	Compression	b_i / t_i and $h_i / t_i \leq 35$ and $class 1\,\&\,2$
	Tension	b_i / t_i and $h_i / t_i \leq 35$
	Aspect ratio	$0.5 \leq h_i / b_i \leq 2$ & $0.5 \leq h_j / b_j \leq 2$
RHS chord	Compression	b_0 / t_0 and $h_0 / t_0 \leq 35$ and $class 1\,\&\,2$
	Tension	b_0 / t_0 and $h_0 / t_0 \leq 35$
	Aspect ratio	$0.5 \leq h_o / b_o \leq 2$

(1) $for\ f_y \geq 355MPa$, $apply\ reduction\ of$ 0.9

Table 2-7: Additional validity range for square hollow section braces [4]

K and N gap joints	$0.6 \leq (b_1 + b_2)/2b_1 \leq 1.3$	$b_o / t_o \geq 15$
T, Y X joints	$b_i / b_o \leq 0.85$	

2.3.3 Failure Modes

Codes and standards [4, 6] provide failure modes that must be considered when designing for rectangular hollow section joints within the range of validity. These are presented in **Figure 2-11**. The location of the failure is determined by the load path, such as the brace, weld, chord face and the chord side-wall. The critical failure modes in each path are determined by the stiffness and the material properties. In the validity range, the width to wall thickness ratios (b/t) of the joint members are limited. Due to these limitations, the local buckling failure doesn't need to be considered in the design. Weld failure and failure due to lamellar tearing are not considered. For all the failure modes, design equations are given by the standards.

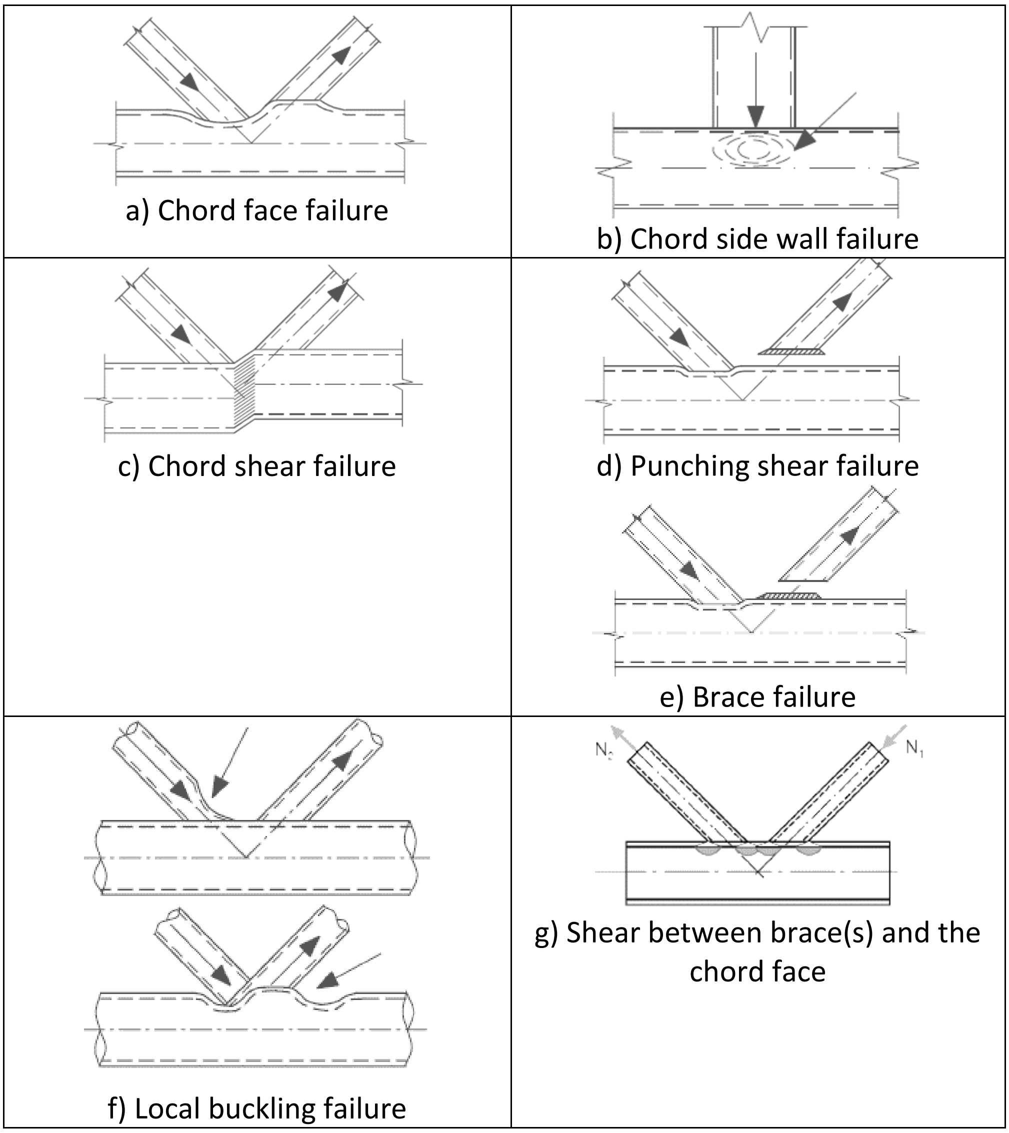

Figure 2-11: Failure modes for joints with RHS loaded by axial forces [4]

The chord face failure has been determine using a simplified yield line model for T, Y and X – joints. K joints the chord face failure has been determined using semi-empirical equations, because of the complex load transfer in the gap zone. Punching shear failure is when the brace is pulled out of the chord. The resistance against this failure is determined using strength of the chord wall and the effective length of the RHS brace perimeter (**Figure 2-7**), which is in case of K joints dependent on the gap size. Brace failure is the resistance of the brace. Due to the uneven stiffness distribution along the RHS brace perimeter at the connection, only certain part is effective to resist the brace load. Chord shear failure may occur for joints with large β-value. This failure occurs in the gap zone due to the complex load transfer (shear load, axial load and bending) [6].

2.3.4 Design Resistance

Chord Stress

The chord stress function is based on the maximum chord load. This function is included in the design resistance for the chord face failure and chord side-wall failure for RHS joints. The chord stress function is consistent for all types of joints. **Table 2-8** describes the chord stress function [4, 6].

Table 2-8: Chord stress[4]

Chord stress	Chord in compression n<0	$Q_f = (1-\lvert n \rvert)^{C1}$ $for\ T, Y, X\ joint: C_1 = 0.6 - 0.5\beta$ $for\ K\ joint: C_1 = 0.5 - 0.5\beta \geq 0.1$
	Chord in tension n>0	$Q_f = (1-\lvert n \rvert)^{C1}$ $C_1 = 0.10$
		$n = \frac{N_{0,Ed}}{A_0 f_{yo}} + \frac{M_{ip,0,Ed}}{W_{ip,pl,0,} f_{yo}} + \frac{M_{op,0,Ed}}{W_{op,pl,0,} f_{yo}}$

Table 2-9 and **Table 2-10** describe all the failure modes that need to be considered for the joints within the range of validity. In the standard, the chord side-wall failure is not critical for the K gap joints and the chord shear failure is not critical for T, Y and X joints. The punching shear failure for the K gap joints and the failure modes to be considered for the T, Y and X joints should be checked for certain β values mentioned in **Table 2-9** and **Table 2-10**. In **Table 2-11** the critical failure mode for square hollow section joints within the range of validity and the additional range of validity is given. The recommended failure modes for the overlap joints are mentioned in **Table 2-12**. The non-uniform stiffness distribution of the joint is through an effective width considered in the failure modes.

Table 2-9: Design resistance for T, Y and X joints with RHS [4]

Chord face failure	$for\ \beta \le 0.85: N_{1,Rd} = \frac{C_f Q_f f_{yo} t_o^2}{\gamma_{m5} \sin\theta_1}\left(\frac{2\eta}{(1-\beta)\sin\theta_1} + \frac{4}{\sqrt{1-\beta}}\right)$
Chord side wall failure	$for\ \beta = 1: N_{1,Rd} = \frac{f_b t_o}{\gamma_{m5} \sin\theta_1}[\frac{2h_1}{\sin\theta_1} + 10t_o]Q_f$ (2) $for\ tension: f_b = f_{yo}$ $for\ compression: f_b = \chi f_{yo}\ (T\ and\ Y\ joint)$ $\& f_b = 0.8\chi f_{yo}\ (X\ joint)$
Punching shear failure	$\beta \le (1-1/\gamma): N_{1,Rd} = \frac{C_f f_{yo} t_o}{\gamma_{m5}\sqrt{3}\sin\theta_1}[\frac{2h_1}{\sin\theta_1} + 2b_{e,p}]$
Brace failure	$N_{1,Rd} = C_f f_{y1} t_1 [2b_{eff} + 2h_1 - 4t_1]/\gamma_{m5}$

(1) For X joints with $\cos\theta_1 > h_1/h_0$ check the design chord shear resistance for K gap joints with $\alpha = 1$

(2) $For\ 0.85 \le \beta = 1$ use linear interpolation between governing resistances at $\beta = 0{,}85\ and\ \beta = 1$

$b_{eff} = \frac{10}{b_0/t_0}\frac{f_{y0}t_0}{f_{y1}t_1}b_1 \le b_i$ & $b_{e,p} = \frac{10}{b_0/t_0}b_i \le b_i$

Table 2-10: Design resistance for K and N joints with gap and RHS [4]

Chord face failure	$N_{i,Rd} = \frac{8.9 C_f \beta \gamma^{0.5} f_{yo} t_o^2 Q_f}{\gamma_{m5}\sin\theta_i}$
Chord shear failure	$N_{1,Rd} = \frac{f_{yo} A_{v,0,gap}}{\gamma_{m5}\sqrt{3}\sin\theta_i}$ $N_{gap,0,Rd} = f_{yo}\left[(A_0 - A_{v,0,gap}) + A_{v,0,gap}\sqrt{1-\left(V_{0,gap,Ed}/V_{0,gap,pl,Rd}\right)^2}\right]/\gamma_{m5}$ $A_{v,0,gap} = (2h_0 + \alpha b_o)t_0\ \&\ \alpha = \sqrt{1/(1+(4g^2/3t_0^2))}$ $V_{pl,0,Rd} = 0.58 f_{yo} A_{v,0,gap}\ \&\ V_{0,gap,Ed} = (N_{i,Ed}\sin\theta_i)_{\max}$
Punching shear failure	$\beta \le (1-1/\gamma): N_{i,Rd} = \frac{C_f f_{yo} t_o}{\gamma_{m5}\sqrt{3}\sin\theta_i}[b_{e,p} + b_i + \frac{2h_i}{\sin\theta_i}]$
Brace failure	$N_{i,Rd} = C_f f_{yi} t_i [b_{eff} + b_i + 2h_i - 4t_i]/\gamma_{m5}$

$b_e = b_{eff} = \frac{10}{b_0/t_0}\frac{f_{y0}t_0}{f_{y1}t_1}b_1 \le b_i\ \&\ b_{e,p} = \frac{10}{b_0/t_0}b_i \le b_i$

Table 2-11: Design resistance for square hollow section joints [4]

Chord face failure	T, Y, X joints $for\ \beta \le 0.75: N_{1,Rd} = \frac{C_f Q_f f_{yo} t_o^2}{\gamma_{m5}\sin\theta_1}\left(\frac{2\eta}{(1-\beta)\sin\theta_1} + \frac{4}{\sqrt{1-\beta}}\right)$
	K and N gap joints $N_{i,Rd} = \frac{8.9 C_f \beta\sqrt{\gamma} f_{yo} t_o^2}{\gamma_{m5}\sin\theta_i}Q_f$

Table 2-12: Design resistance for overlap joints satisfying the range of validity [4]

Overlapping brace failure	$N_{i,Rd} = \dfrac{C_f f_{yi} t_i l_{b.eff}}{\gamma_{m5}}$ (1)
Overlapped brace failure	$N_{j,Rd} = N_{i,Rd}\left(\dfrac{A_j f_{yj}}{A_i f_{yi}}\right)$
Chord member failure	$\left(\left(\dfrac{N_{o,Ed}}{N_{pl,0,Rd}}\right)^C + \dfrac{M_{ip,O,Ed}}{W_{ip,pl,0,Rd}}\right) \le 1$ $with\, C = 1\, for\, RHS\, members$
Brace shear Failure	Should be checked for: $\lambda_{ov,\lim} \le \lambda_{ov}$ (2) $\lambda_{ov,\text{limit}} = 60\%$ if hidden toe is not welded and $c_s = 1$ $\lambda_{ov,\text{limit}} = 80\%\ if\ hidden\, toe\, is\, welded\, and\, c_s = 2$ $N_{i,Ed}\cos\theta_i + N_{j,Ed}\cos\theta_j \le N_{s,Rd}$ $\lambda_{ov,\lim} \le \lambda_{ov} \le 100\%$: $N_{s,Rd} = \dfrac{0.58 f_{yi} t_i}{\gamma_{m5}} \dfrac{f_{ui}}{f_{yi}} \left(\dfrac{\dfrac{100-\lambda_{ov}}{100} 2h_i + 6t_i}{\sin\theta_j}\right) + \dfrac{0.58 f_{yj} t_j}{\gamma_{m5}} \dfrac{f_{uj}}{f_{yj}} \left(\dfrac{2h_j + c_s 6t_j}{\sin\theta_j}\right) t_j$ $\lambda_{ov} = 100\%$: $N_{s,Rd} = \dfrac{0.58 f_{yj} t_j}{\gamma_{m5}} \dfrac{f_{uj}}{f_{yj}} \left(\dfrac{2h_j + b_j + 6t_j}{\sin\theta_j}\right)$

(1) One brace should be in tension and the other brace in tension.

(2) For rectangular hollow section braces with $h_i < b_i\, and\, h_j < b_j$, the connection between the braces and the chord face should be checked for shear.

$b_{e,ov} = \dfrac{10}{b_j / t_j} \dfrac{f_{yj} t_j}{f_{yi} t_i} b_i \le b_i$ & $b_{eff} = \dfrac{10}{b_0 / t_0} \dfrac{f_{y0} t_0}{f_{yi} t_i} b_i \le b_i$

$for\, 25\% \le \lambda_{ov} \le 50\%: l_{b,eff} = \left(\dfrac{\lambda_{ov}}{50}\right) 2h_i + b_{eff} + b_{e,ov} - 4t_i$

$for\, 50\% \le \lambda_{ov} \le 100\%: l_{b,eff} = 2h_i + b_{eff} + b_{e,ov} - 4t_i$

$for\, \lambda_{ov} = 100\%: l_{b,eff} = 2h_i + b_i + b_{e,ov} - 4t_i$

2.4 Secondary Bending Stresses

Design recommendations [4, 6] recommend to perform truss analyses assuming continuous chords and pinned brace members. The eccentricity of the tubular joints is usually taken into account in the design. This will result in axial forces in all the members and bending moments in the chords. This method does not include all the joint parameters and therefore does not represent the real behavior of the truss. Secondary bending stresses may exist in these joints in trusses. The secondary bending moments in hollow section joints are introduced by [6, 21]

- The overall bending stiffness of the joint,
- Local joint flexibility,

- Nodal eccentricity, the centerline of the brace members does not meet the centerline of the chord,
- Large deformations of the truss [5].

The eccentricities are limited to 0.55 and 0.25 times the chord width. Eccentricities in joints outside the validity range may result in large secondary bending stresses and these joints may become critical. Therefore, these secondary stresses need to be included in the design of the joint members in proportion to their stiffness [6].
Welds in lattice girders are practical and commonly applied. The weld introduces additional stiffness in the joints. For RHS brace members, the differences in stiffness between the corners and the center are large, which results in a non-linear stiffness distribution around the perimeter. Because of this, the force transfer is complex. Also, various brace orientations are possible which makes the analyses more difficult. Due to the non-uniform stiffness distribution, some parts of the joint may not have sufficient deformation capacity. The introduced secondary bending moments in the joints can be avoided for joints with sufficient deformation and rotation capacity which is necessary for redistributing the stresses [21]. Current design standards suggest to neglect secondary bending stresses introduced by rotation stiffness for:

- Joints within the validity range,
- Joints within the eccentricity limitations,
- Tubular girders with system length to depth ratio equal to or lower than 6 [4, 20].

For joints within the validity range, these secondary moments are not considered important for static joint resistance. These joints are considered to have sufficient stiffness and ultimate capacity to sustain secondary bending stresses. For joints outside the validity range, the secondary bending stresses needs to be included in the design. For mild-strength steel, this approach, which is recommended by many standards works but for high steel strength the design rules need to be re-analyzed [4, 6].

Professor Wardenier [8] has studied the secondary bending moments in hollow section joints made of mild strength steels. In trusses, next to primary moments secondary bending moments exists. The primary bending moments are needed for the force equilibrium and the secondary bending moments occur due to local deformations or the joint stiffnesses. The relation between the axial load and the secondary bending moment in the brace of a K-joint is shown in **Figure 2-12**. Relatively high secondary bending moments exist in the joint for low axial load. As the axial load increases, the joint stiffness reduces. This will reduce the secondary bending stresses in the joint. At ultimate load resistance, the secondary bending stresses may disappear, due to the redistribution of stresses. The level of secondary bending stresses is dependent on the axial loading and the rotational stiffness capacity. Secondary bending stresses up to 40% to 60% of the axial load has been found in the gap K-joints made of mild-strength steel. Secondary bending moments are neglected for the static design strength but considered important for fatigue design strength.

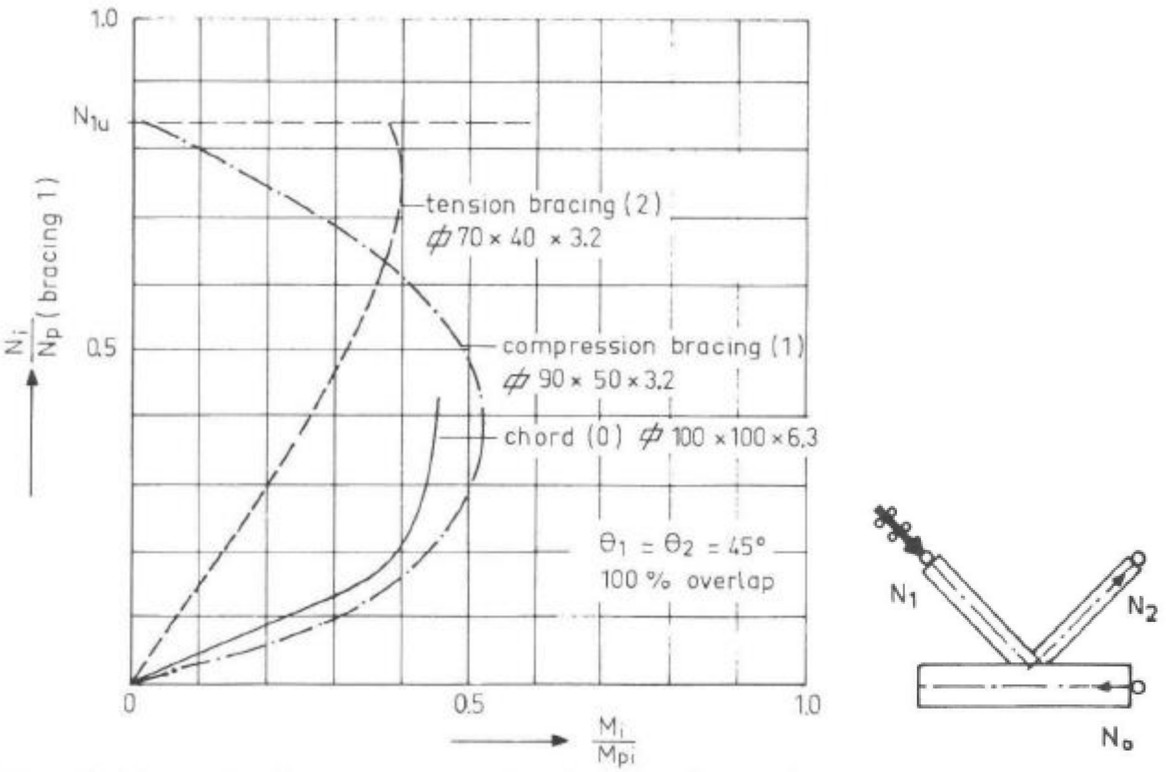

Figure 2-12: Bending stresses in the brace members of a K-joint [8]

2.4.1 Secondary Stresses in Lattice Girders

In 2004, the secondary bending stresses in a lattice girder were investigated by Börger A.J. et al [22]. A numerical analysis was conducted on a tubular truss with circular hollow sections. The impact of the depth of the girder, brace angle (θ), diameter ratio (β), chord diameter to thickness ratio (γ) was investigated. Various finite element models in beam element and shell elements were built. The aim of this study was to describe the structural behavior of each model, study the impact of the parameters on secondary bending stresses and to perform fatigue calculations with the obtained results. For fatigue strength, the secondary stresses are necessary to include. These stresses are determined by multiplying the axial stresses with magnification factors. This simplification is done to avoid the complex calculation of these stresses. Based on the obtained result with respect to the secondary stresses, it is concluded that all the parameters have an impact on the secondary bending stresses. Low secondary stresses were obtained for the numerical model with large girder depth, small brace angle, and small γ. Large β resulted in high secondary bending stresses and low β did not have any impact on these stresses [22].

2.4.2 Secondary Stresses in High Strength Hollow Section Joints

Analytical, experimental and numerical studies were conducted by Björk et al [5] to investigate the secondary bending stresses on the capacity of the K-gap joints. An uneven support-effect (USE) of the brace member on the chord introduces the secondary bending stresses. The asymmetrical support about the neutral axis of the brace member causes this effect (non-uniform joint stiffness). The level of these stresses is based on joint geometry.

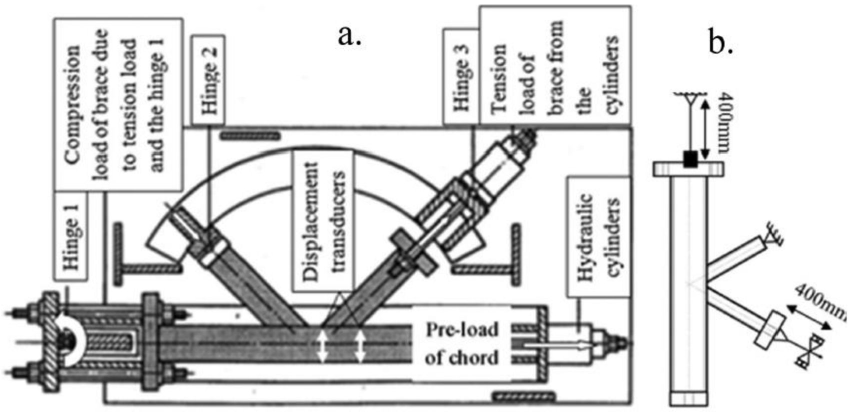

Figure 2-13: Test setup. Preloading of the chord only in K-joint with S960 [5]

The impact of high-strength steel on the secondary bending stresses in joints with various geometry is investigated. Two steel grades, S700 and S960 were used. The test set up is shown in **Figure 2-13**. In both K-joints, one brace member was loaded with tensile load. The nominal stresses were measured in this brace member to determine the secondary bending stresses. A parametric study was performed to investigate the impact of the joint geometry including cross sections, eccentricity and brace angle, on the secondary stresses. The following results were obtained:

- Lower chord thickness results in higher secondary bending stresses
- Larger gap and larger eccentricity result in lower secondary bending stresses
- Lower brace angle results in lower secondary bending stresses
- Lower brace width result in lower secondary bending stresses

According to Björk et al [5], the obtained result proved that secondary bending stresses in high-strength K-joints can be considerably large. This will affect the joint capacity. This is also the case for eccentricities within the recommended limitations. Large deformations occur in the high-strength joints, which influence the secondary stresses. Also mentioned is that the joint geometry has an impact on the uneven support effect [5].

2.5 Yield line method

The yield line theory is an upper bound method to determine the failure load or collapse load. This method is used in many applications from which its application in reinforced concrete plate is well known. During failure it is assumed that plastic deformation is concentrated in numerous yield lines. The bending moment along the yield lines is assumed to be constant and equal to the plastic moment. Parts bounded by yield lines behave like a rigid flat body and because of this the yield lines have to be straight. Yield lines may change direction when intersection another yield line. The elastic deformations are assumed to be negligible compared to the plastic deformations. Using the yield line pattern, the failure load can be determined with the principle of virtual work. In this the external work and the internal work are equated. The external work is the load multiplied by the deflection, while the internal work is the energy dissipated inside the material by yielding [7, 23]. This method is also successfully applied to estimate the strength of the RHS joints. **Figure 2-14** shows the yield line pattern considered by CIDECT [6] for RHS T, Y and X joints loaded by axial force. In this yield line pattern, local strain hardening effects and membrane actions are ignored.

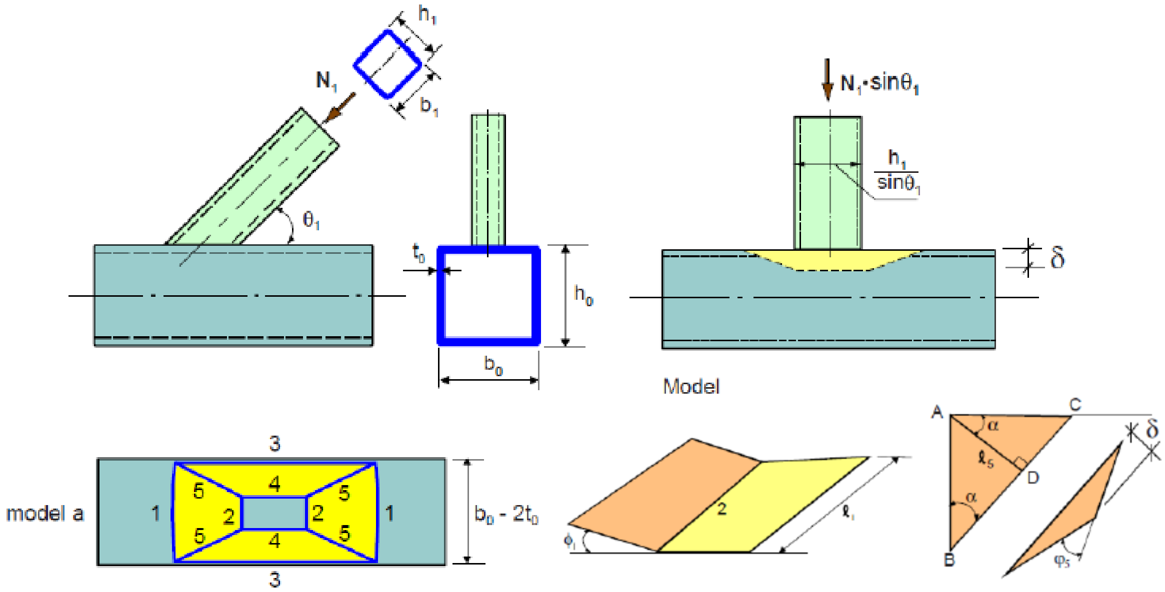

Figure 2-14: Yield line pattern for T, Y and X-joints using RHS members[6]

The work done by the external force and the internal dissipated energy are equated to obtain the chord face plastification capacity of the joints. The external and internal work can be determined using the following equations:

$$W_{external} = N_1 \sin\theta_i \delta \qquad \textbf{Equation 2-10}$$

$$W_{internal} = \Sigma l_i \varphi_i m_p \qquad \textbf{Equation 2-11}$$

where $N_1 \sin\theta_i$ is the vertical component of the axial force, δ is the deflection, l_i yield line length, the parameter φ_i is the rotation angle and the plastic moment, m_p is determined by $m_p = \frac{1}{4} f_y t_o^2$.The internal work is summed up in **Table 2-13**.

Table 2-13: Internal work for each yield line [6]

Line	Internal work:
1	$2\times b_o \times \frac{2\delta}{(b_o - b_1)\cot\alpha} m_p = \frac{4\tan(\alpha)}{(1-\beta)} m_p \delta$
2	$2\times b_1 \times \frac{2\delta}{(b_o - b_1)\cot\alpha} m_p = \frac{4\beta\tan(\alpha)}{(1-\beta)} m_p \delta$
3	$2\times(\frac{h_1}{\sin\theta_i} + \frac{2(b_o - b_1)}{2}\cot\alpha)\frac{2\delta}{(b_o - b_1)} m_p = (\frac{4\eta}{(1-\beta)\sin\theta_i} + 4\cot\alpha) m_p \delta$
4	$2\times(\frac{h_1}{\sin\theta_i})\frac{2\delta}{(b_o - b_1)} m_p = \frac{4\eta}{(1-\beta)\sin\theta_i} m_p \delta$
5	$4l_5 \times (\frac{\delta}{l_5 \tan\alpha} + \frac{\delta}{l_5 \cot\alpha}) m_p = 4(\tan\alpha + \cot\alpha) m_p \delta$

The total internal energy is equal to:

$$W_{internal} = \frac{8m_p\delta}{(1-\beta)}(\tan\alpha + \frac{1-\beta}{\tan\alpha} + \frac{\eta}{\sin\theta_i}) \quad \textbf{Equation 2-12}$$

Finally, the capacity can be determined using the following equation:

$$N_1 = \frac{f_y t_0^{\ 2}}{(1-\beta)\sin\theta_i}(\frac{2\eta}{\sin\theta_i} + 4\sqrt{1-\beta}) \ \text{ with } \tan\alpha = \sqrt{1-\beta} \quad \textbf{Equation 2-13}$$

In this model the thickness of the model and the weld size have not been included. The effect of the chord load has been included by multiplying the equation by the chord stress function (Q_n). Similar simplified yield line models exist to determine the resistance of other type of joints with axial loading or moment loading. For joints with complex load transfer, the standards have used semi-empirical equations to determine the chord face plastification [6]. Bjork [5] has determined a yield line model to estimate the moment capacity for gap K-joints with identical brace members and brace inclination. The yield line pattern for this gap K-joint is shown in **Figure 2-15**. Detailed information has been included in Appendix A.

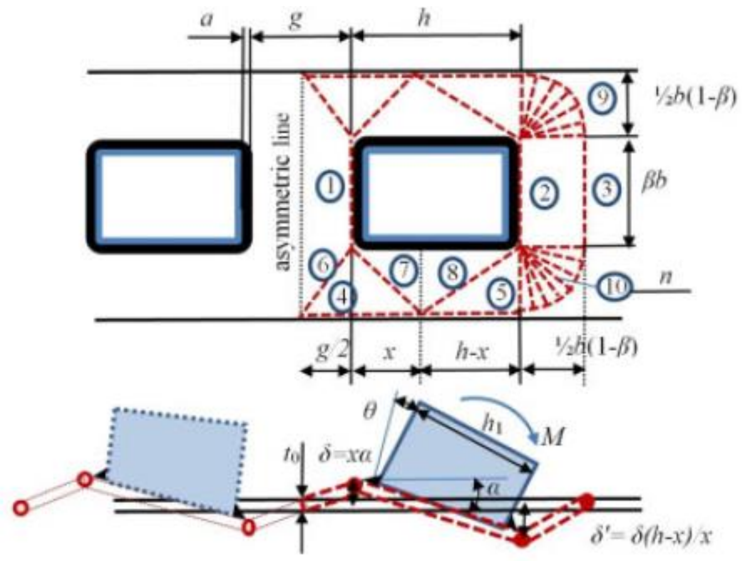

Figure 2-15: Yield line pattern for gap K-joints using RHS members[6]

CHAPTER 3 VALIDATION STUDY

This section describes the development of the finite element model (FEM). Numerical analysis is selected to perform because it provides economical and reliable results. Unlike experimental investigation, various geometrical parameters can be varied in numerical analyses and numerous experiments can be performed. To guarantee the validity of the finite element result, the finite element analysis (FEA) must be carefully calibrated. Earlier experimental tests on a full-scale girder and a T-joint is used to calibrate the finite element models. The dimensions, geometry and material properties of the finite element models are in accordance with the earlier experiment tests[24, 25].

3.1 Validation of a Truss Girder

3.1.1 Previous Experiment of a Truss Girder

In the 1970s tests on welded joint in four girders were performed at the Delft University of Technology and documented in the CIDECT report 5Qg [24]. The main goal of this experiment was to compare the result from the experiment with another experiment, in which individual joints were tested and to investigate the ultimate capacity of the joints in the girders.

3.1.1.1 Geometry and Material Properties

The trusses consisted of K, N and X joints with welded hot finished square hollow sections. These sections were made of mild steel grade RSt.42-2 according to DIN 17100, which is comparable to S275 [26]. The trusses were designed with gap joints and overlap joints. The gap joints had either zero or positive joint eccentricity. The overlap joints were designed with negative joint eccentricity. In the overlap joints, the compression brace member were the overlapping members. From all the four girders, the girder 1 will be investigated in this study. This girder is shown in **Figure 3-1**. The geometry of the joint members and joint parameters are tabulated in **Table 3-1** and **Table 3-2**.

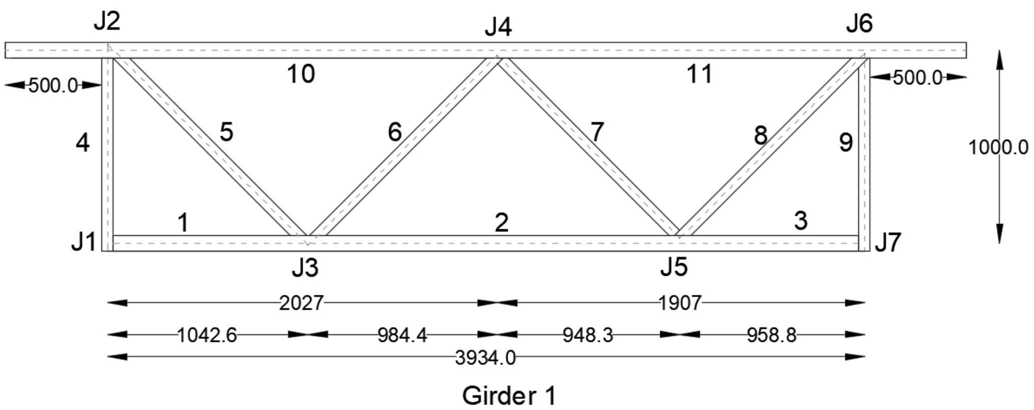

Figure 3-1: Girder 1

Table 3-1: Measured dimensions and material properties

	Member	h, b (mm)	t (mm)	r_i/r_o (mm)	f_y (MPa)	f_u (MPa)	A (mm^2)
Girder 1	10,11	79.8	3.56	3/6	432	490	1083
	1,2,3	79.8	3.56	3/6	432	490	1083
	4,6,7,9	60.2	3.28	3/5	391.5	500	751
	5,8	60	2.96	3/5	417	490	663

Table 3-2: Joint parameters

	joint	$2\gamma=b_0/t_0$ (-)	$\beta=b_1+b_2/(2b_0)$ (-)	θ_1 (^{0})	θ_2 (^{0})	g/b_o (-)	Lap (%)	e (mm)
Girder 1	J2	22.4	0.75	90^0	45^0	0	-	32.3
	J3	22.4	0.75	45^0	45^0	0.2	-	10.3
	J4, J5	22.4	0.75	45^0	45^0	-	50%	-25.8
	J6	22.4	0.75	90^0	45^0	-	50%	-15.3

Welds

The weld geometry, which is described in CIDECT report 5Qg [24] is shown in **Figure 3-2**. Fillet welds and butt welds were used to connect the members and the weld throat thickness was equal to the connected brace member.

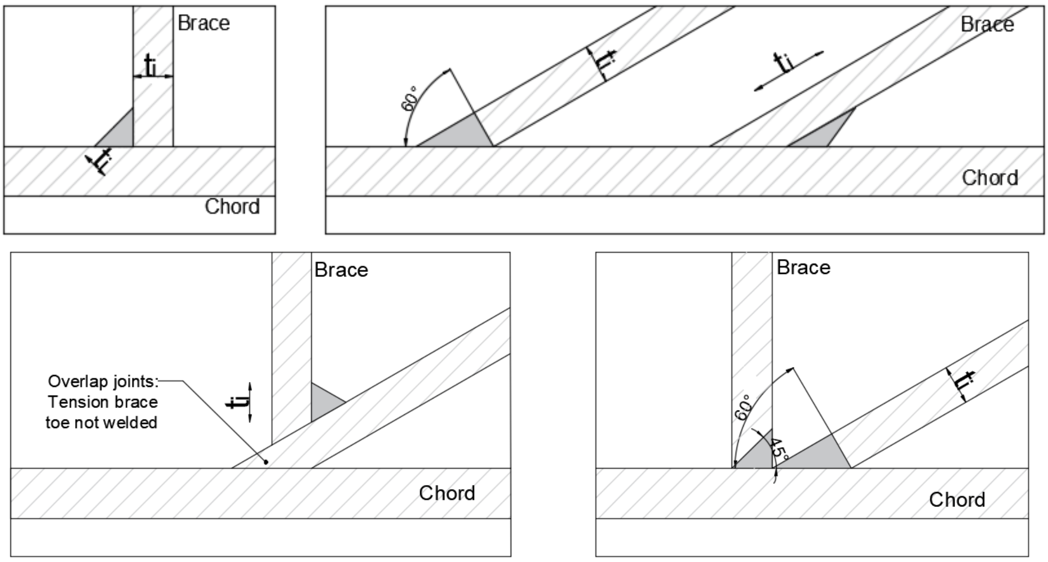

Figure 3-2: Weld geometry

3.1.1.2 Load and Boundary Conditions

The girder has a pin support at one side and a roller support at the other side. The roller support permits the horizontal translation of the girders. The top chord of the truss was horizontally supported to prevent the lateral torsional buckling. The load was applied at the center of the top chord and changed incrementally until failure in a certain joint occurred. After this failure, the girder was unloaded, the joint or the member in yielding or buckling was stiffened, and the girder was reloaded until failure occurred in the following member or joint. These steps were repeated until the ultimate capacity in all joints were obtained.

3.1.2 Finite Element Model of the Truss Girder

3.1.2.1 Geometry

As mentioned before, many girders were tested in the experiment. Girder 1, shown in **Figure 3-1** is selected to perform this numerical study. This girder consists of 7 joints and Joint J6 is selected for the calibrating purpose. The geometry and parameter of the joints are summarized in **Table 3-1** and **Table 3-2**.

3.1.2.2 Analysis with ABAQUS®

ABAQUS® is used for both the calculations and the post-processing. This commercial software has many excellent tools to create parts and to perform linear and nonlinear analyses to predict the structural behavior. An extensive element library exists in ABAQUS® and any combination of elements can be used to create model using constraints [27].

In order to investigate the secondary bending stresses in the hollow section joints, a full-scale girder is modeled in ABAQUS®. Next, to the global behavior, the local behavior in the selected joints is of interest. Solid elements with refined local mesh are suitable to investigate these local stresses. However, creating a truss girder with solid elements is computational expensive. An alternative way is to create a beam-to-solid sub model in which the area of interest is made with solid elements and the rest of the structure is modeled with beam elements. Detailed information of the local behavior in the joints can be obtained using this modeling technique. Also, a variable mesh with fine and coarse mesh can be employed. This sub-model technique is necessary to speed up the simulations. The boundary of the solid elements is located far away from the stress concentrations. After the assembly of the beam and the solid elements, a series of multiple-point constraints (MPC) of type BEAM are used to couple the solid and beam elements [27]. In this way the degree of freedom between the solid and beam elements are related. Initially, all the joints were made with solid elements and the parts in between with beam elements. Due to the long computational time and complexity of the whole girder, the sub model, shown in **Figure 3-3** is selected to analyze the truss.

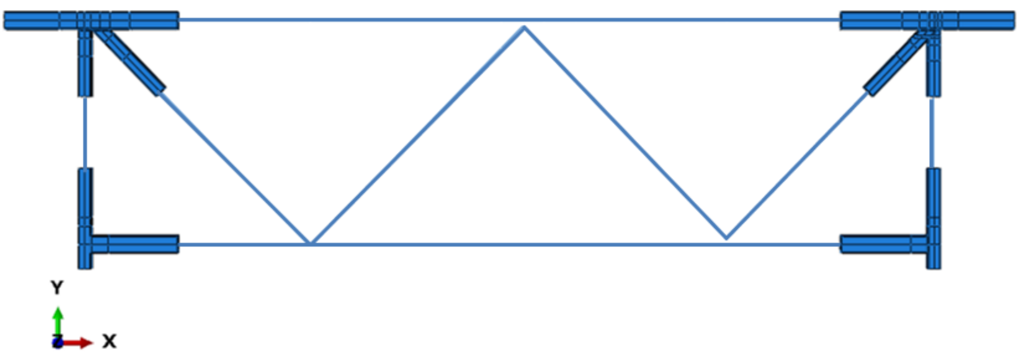

Figure 3-3: Beam-to-solid sub-model

3.1.2.3 Element Type and Finite Element Mesh

The reduced order eight-node linear brick element, C3D8R and a 2-node linear beam, B31 is selected for the solid and beam elements, respectively. Meshing has a great influence on computational time. The finer the mesh the better results will be, but the computational time will be higher. Therefore, a variable mesh is applied to the solid-to-beam sub model. A fine mesh of 3 mm in the area of interest and a coarse mesh of 8 mm outside the joint zone is applied. The variable mesh in the solid element is shown in **Figure 3-4**. To ensure the accuracy of the analyses a four-layered mesh is used. Multiple meshing techniques are available in ABAQUS®. The structured and sweep meshing techniques have been used during the mesh generation of the model. The sweep meshing technique is used to mesh the complex solid regions. For a regularly shaped region, the mesh can be generated by use of the structured meshing technique. Additionally, the assembled solid model is partitioned into several parts to generate the mesh.

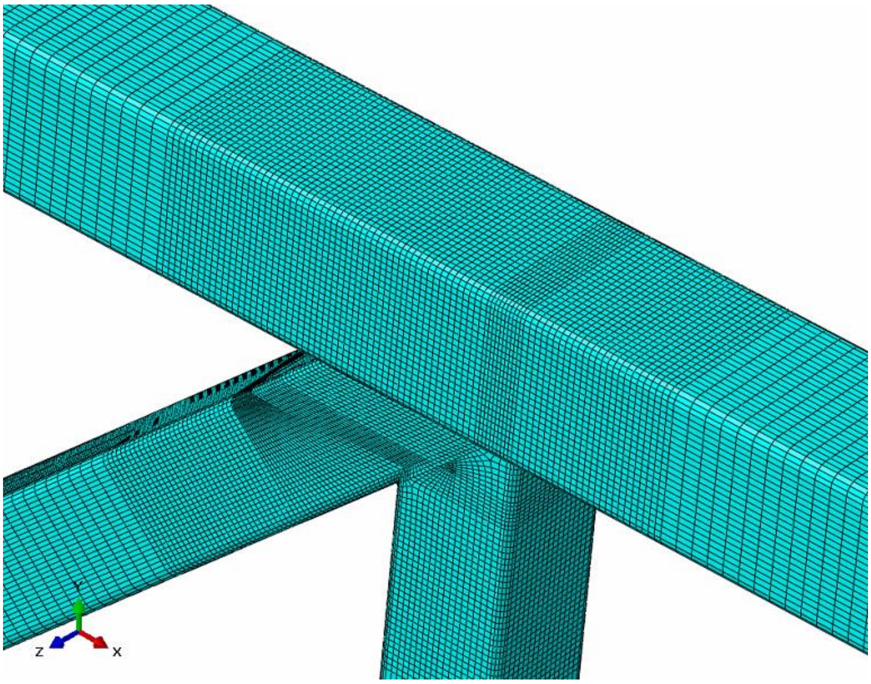

Figure 3-4: The variable mesh in the solid element

3.1.2.4 Material Properties

All material properties are adopted from the document of the earlier experiment [24]. This document describes the measured elongation, the measured yield strength and the measured ultimate strength of the joint members. These properties are used to develop the material model.

Material Model
Based on the available material properties a simplified material model, the tri-linear stress-strain model is assumed for the stress-strain relation. This model, shown in **Figure 3-5** considers the main parameters including yield stress (f_y), ultimate stress (f_u), yield strain (ε_y), strain hardening (ε_{sh}) and ultimate strain (ε_u). The recommended value for the strain hardening modulus is 2%E and for strain hardening is around $10\varepsilon_y$ [28]. **Table 3-3** shows the

stress and strain values of the steel material. The Young's Modulus and Poisson's ratio in the elastic stage are 210 GPa and 0.3, respectively [16].

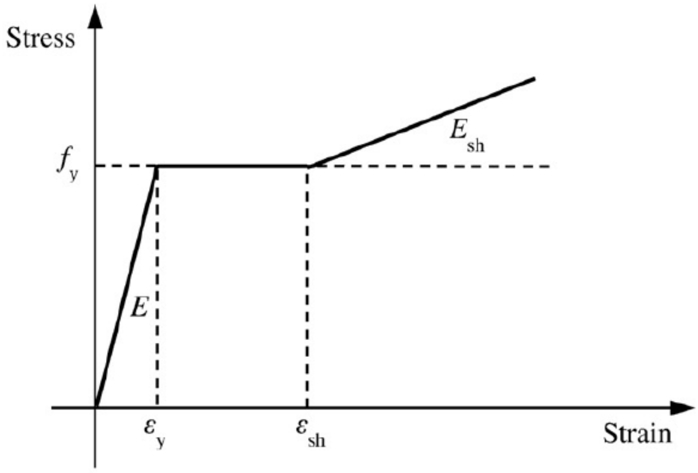

Figure 3-5: Tri-linear material model [28]

Table 3-3: Engineering material properties of the steel sections

f_y (MPa)	f_u (MPa)	ε_y (-)	ε_{sh} (-)	ε_u (-)
432	490	0.002057	0.02057	0.485
391.5	500	0.001864	0.01864	0.454
417	490	0.0019857	0.019857	0.464

True Stress-True Strain Relation

A non-linear analysis is performed by use of the material and geometrical non-linearity. The employed non-linearity requires the true stress and true strain values of the material, which is obtained from the engineering stress and strain using the following equations:

$$\varepsilon_{true} = \ln(1+\varepsilon_{eng}) \quad \textbf{Equation 3-1}$$

$$\sigma_{true} = \sigma_{eng}(1+\varepsilon_{eng}) \quad \textbf{Equation 3-2}$$

where ε_{eng} and σ_{eng} are engineering strain and engineering stress, respectively and ε_{true} is the true strain and σ_{true} is the true stress [29]. **Figure 3-6** shows the measured stress strain and the converted true stress-strain relation for all the members in the joint.

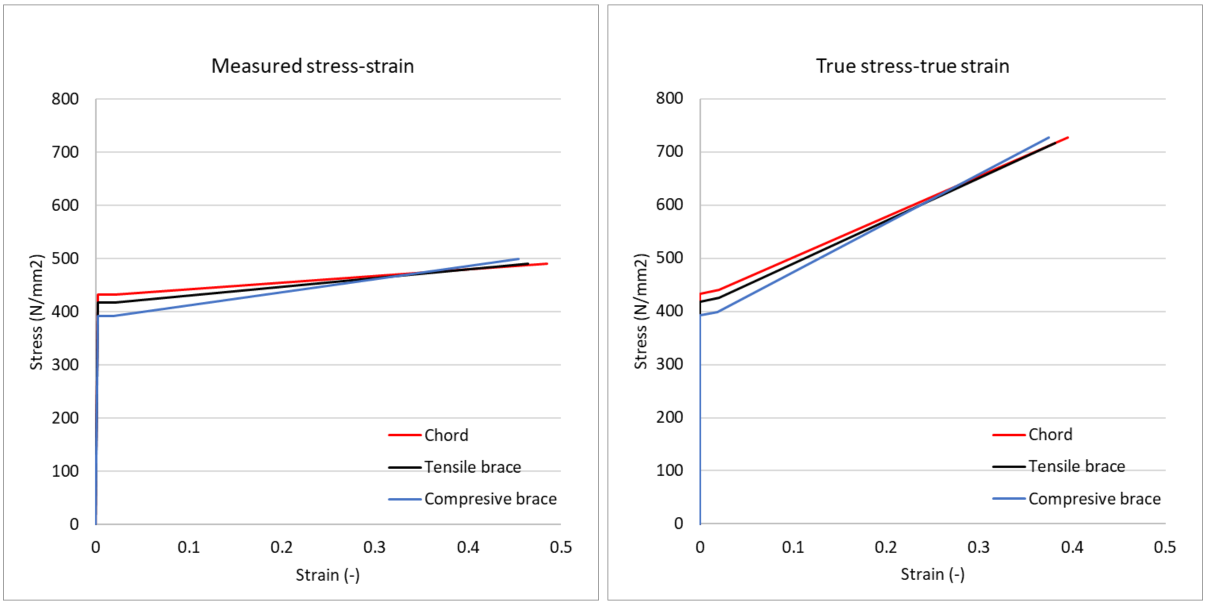

Figure 3-6: Measured stress-strain and the true stress – strain curves

3.1.2.5 Profile of the Weld

The joint members in the experiment are connected using fillet and butt welds. The fillet welds are designed with a weld throat thickness equal to the connected brace member. The fillet welds are considered in the analyses, because of its contribution to the joint resistance [30]. The weld profile in the analyses are made with solid elements and is simplified as a triangle with a throat thickness equal to the thickness of the connected member. The weld strength in this study is considered equal to the strength of the brace member. In the real hollow section joints, a gap opening between the chord and brace members exists. To take the influence of this gap opening in the numerical analyses into account a gap of 0.15 mm is considered. In **Figure 3-7** the profile of the weld and the meshed weld is shown.

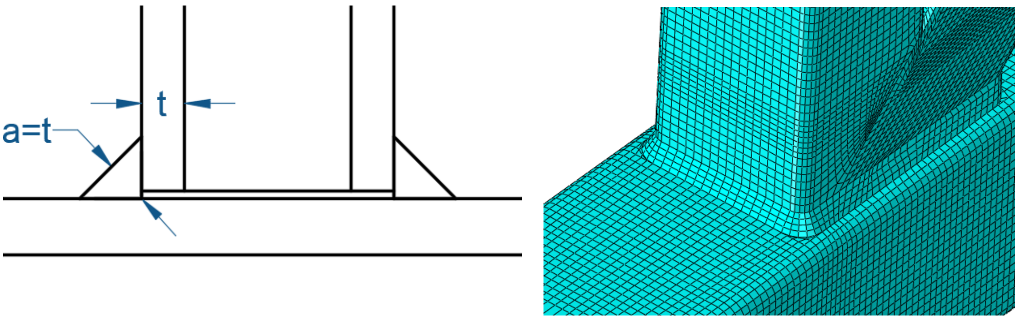

Figure 3-7: The weld throat thickness

3.1.2.6 Boundary and Load Condition

The real girder is pinned at the left side and roller supported at the right side and the top chord is supported against lateral torsional buckling. These boundary conditions are used in the finite element model. Kinematic constraints are used to simulate these boundary conditions. The out-of-plane translations and rotations are restrained. The finite element model consists of solid and beam elements. In order to simulate the real behavior of the girder, the solid and the beam models are coupled using MPC – constraints. All the joint members in solid elements have a length of approximately 5 times the member's width. This is done to avoid any influence from the supports, constraints and the loading [31]. During the analysis, a prescribed force is applied at the center of joint J4. This force is applied in small increments until the prescribed value is reached.

3.1.2.7 Stiffening

Since the position, dimensions and method of the stiffening are not mentioned in the report, the stiffening procedure of the finite element model is difficult and time-consuming. Therefore, it is chosen to make these joints with beam elements. The beam elements are stiffened by increasing the cross-sections.

3.1.3 Validation of the Numerical Model of the Truss

3.1.3.1 Load displacement relation

Comparisons with the experimental results are made to validate the numerical model. The experimental test data included the load-deflection diagram, load-displacement diagram, and the member forces at failure. Joint J6 is chosen to validate the numerical model. This joint is an overlap N-joint and is shown in **Figure 3-1**.

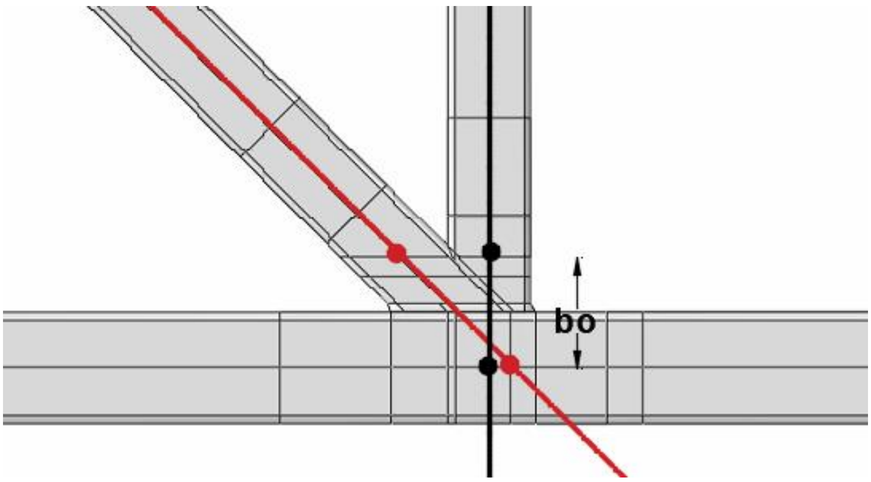

Figure 3-8: The points to determine the displacement

To reproduce the load-deflection curve for the numerical model, the applied load at the midspan of the top chord is plotted against the deflection of the midspan of the bottom chord. The load – displacement curve is obtained by plotting the applied load against the displacement of both the tensile and compressive brace members. The displacement, shown in Figure 3-8 is the distance between two points, one is located at the centerline of the chord and the other is located at the brace centerline. The initial vertical distance between the two points is equal to the width of the chord member. During loading the distance between these two points changes. The load-deflection figure and the load-displacement figure are shown in **Figure 3-9** and **Figure 3-10**, respectively. Looking at both the figures, it can be said that the numerical model predicted the joint behavior roughly OK. In the experiment, the joint J6 behaves linearly up to 350 kN and the joint fails shortly hereafter. The maximum load for which the joint J6 fails is 370.5 kN with a deflection of 13.9

mm. For the numerical analysis, the linear part is up to 300 kN. And the deflection corresponding to the experimental ultimate load resistance is around 12.8 mm, which is 8% lower. For a given load, the numerical model shows lower deflection. Maximum difference of 19% in the deflection is observed.

Comparing both the load-displacement curves not much similarities can be found. For both the analyses, the ultimate capacity of the joint occurred before the *3%bo* deformation limit. In the numerical analysis, the compressive brace member deformed more than the experimental one, whereas the opposite can be observed for the tensile member. At failure load differences of 29% and 121% in the displacement for the diagonal and vertical member, respectively are observed. The numerical and experimental obtained member forces are compared in **Figure 3-11**. It can be noticed that lower member forces are obtained with the numerical analysis. Differences up to 12.1% are obtained. Appendix A includes the joint resistance. The joint resistance for Joint J6 is 266 kN. The experimental failure load and the failure load determined with the standard match well. Also, variations in the boundary conditions are made in order to match the experimental and numerical results. Neglectable improvements are obtained using this variation.

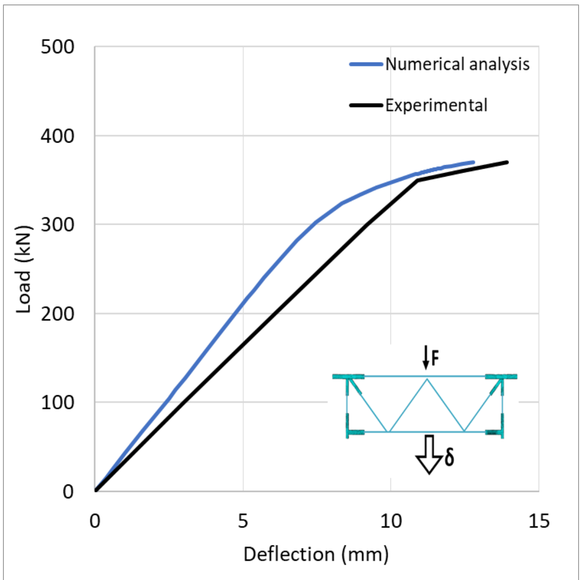

Figure 3-9: Load deflection relation

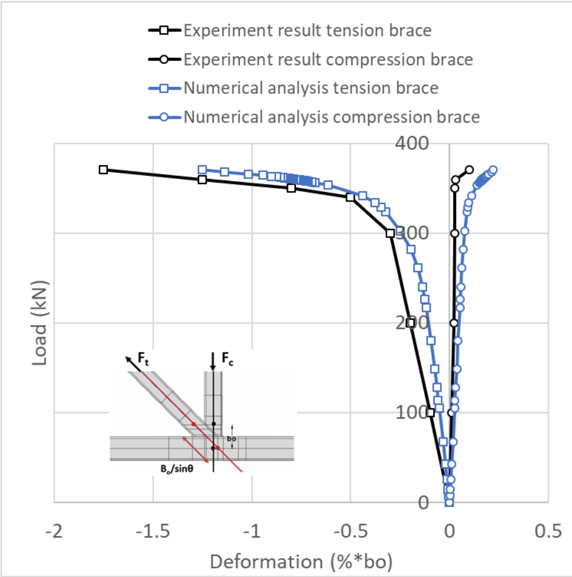

Figure 3-10: Load displacement relation

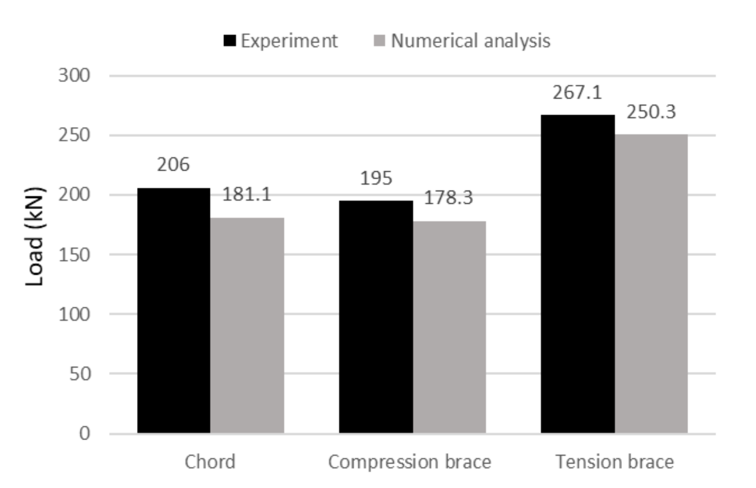

	Chord	Compression brace	Tension brace
Experiment	206	195	267.1
Numerical analysis	181.1	178.3	250.3
Difference [%]	-12.1	8.54	6.30

Figure 3-11: Comparison of the member forces

3.1.3.2 Strain and Stress Distribution

To obtain more knowledge in the joint behavior of the numerical model, the local stresses from the FEA are studied. **Figure 3-12** shows the deformation and the mises stresses in the girder. **Figure 3-13** shows the plastic strain in the joint J6. Maximum plastic strain of 0.011 is obtained in the joint. Local yielding occurs in the joint members. Also, the stresses in the girder exceeds the measured ultimate strength of the material.

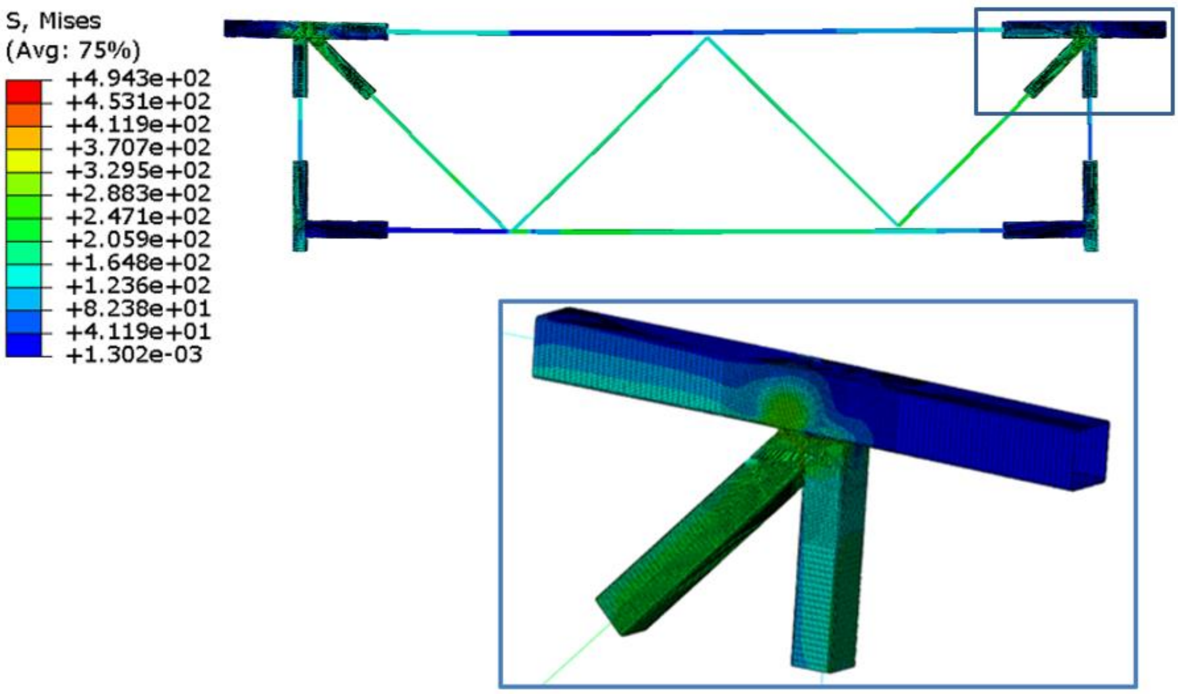

Figure 3-12: Mises stresses in the girder (scale 2)

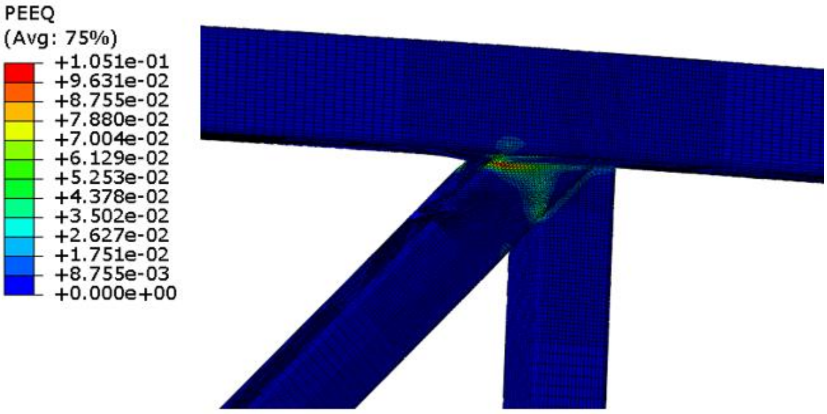

Figure 3-13: Plastic strain in the joint J6

3.1.3.3 Secondary bending stress

The secondary bending moments in the compressive brace of the N-joints are obtained from the uneven stress distribution at the cross-section as shown in **Figure 3-14**. This section is around 60 mm away from the meeting point between the chord face and the system line of the compressive brace. The secondary bending moment is integrated via a free body cut with element set and node set shown in before mentioned figure. The secondary bending stress is calculated based on FE secondary bending moment and moment inertia. The average stress and the secondary bending stress in this section are used to determine the level of secondary bending stress. The secondary bending moment and the level of secondary bending moments in the FEM is shown in **Figure 3-15**.

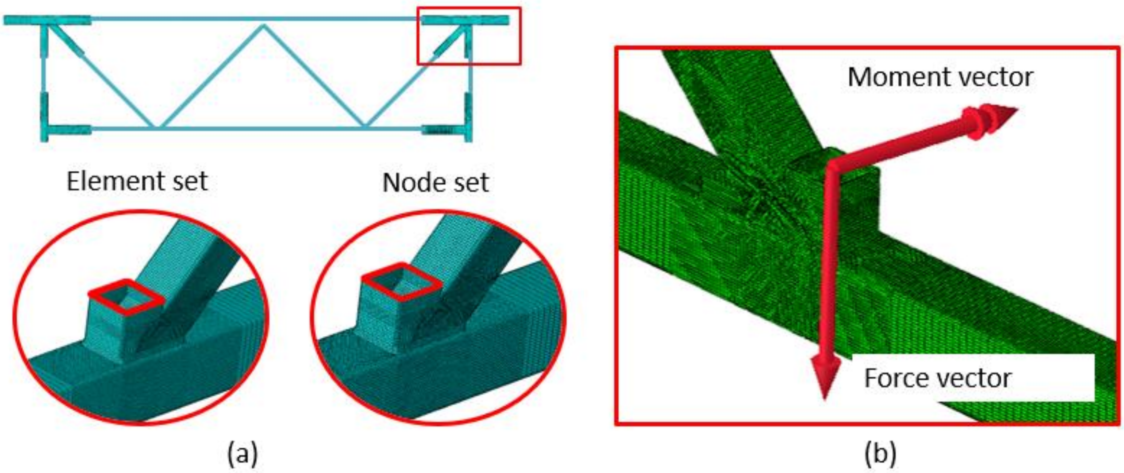

Figure 3-14: (a) Element set and node set (b) moment and force vector overlap N-joint

The secondary bending stresses in the overlap N-joint is maximum $0.1f_y$ at axial load of $0.4f_y$. For axial load larger than $0.4f_y$, the level of secondary bending stresses decreased rapidly and at failure this stress is zero and lower. Also, the level of secondary bending stresses, shown in **Figure 3-15(b)** are negative at failure. This is mainly due to the large deformation of the truss and stresses in the other joints. **Table 3-4** summarizes the level of secondary bending stresses in the N-joint. The highest level of secondary bending stresses is obtained for axial load up to $0.5f_y$.

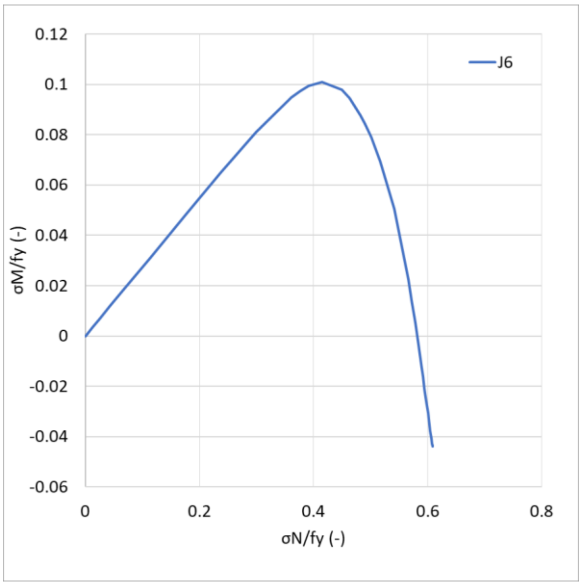

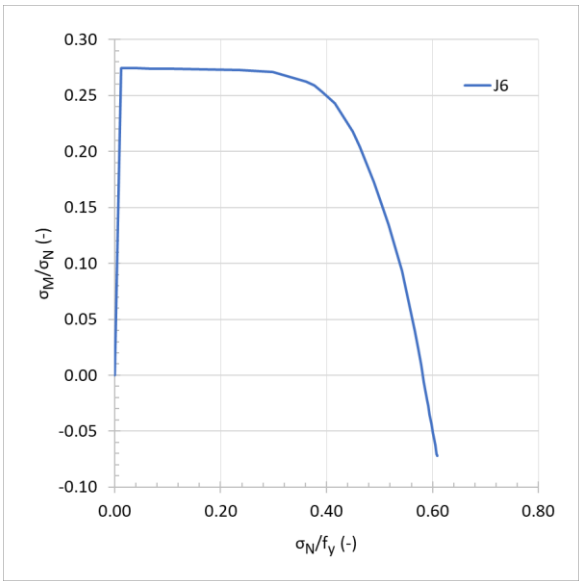

Figure 3-15: (a) Secondary bending stresses (b) and the level of secondary bending stresses

Table 3-4: Level of secondary bending stresses

σ_N/f_y	σ_M/f_y	σ_M/σ_N
0	0	0
0.05	0.01	0.27
0.1	0.03	0.27
0.2	0.05	0.27
0.3	0.08	0.27
0.4	0.10	0.25
0.5	0.08	0.16
0.6	-0.03	-0.05
0.61	-0.04	-0.07

3.2 Validation of a T-joint

Another validation study on an individual T-joint is performed. The T-joint is taken from an ongoing investigation (at the time of writing this report) in weld type and size effect on resistance of hollow section joints [25]. Multiple T-joint subjected to axial or moment loading are tested in this experiment. For this validation study, a T-joint loaded in axial force is selected.

3.2.1 Finite element model

3.2.1.1 Geometry and mesh

The selected T-joint consists of square hollow sections and is connected by but welds. **Figure 3-16** and **Table 3-5** show the geometry, dimensions and the material properties of the joint members. The H-section, which is used to support the T-joint, is assumed to have a height of 300 mm, width of 300 mm and a thickness of 20 mm. Four plates, each with a dimension of 100 mm × 50 mm × 10 mm are welded to the sides of the chord. Also, two thin plates are observed between the T-joint and the H-section. In ABAQUS®, a solid-to-solid sub-model is created. The interaction between the T-joint and the H-section is done by a general contact. The hard contact and a friction coefficient of 0.4 are included.

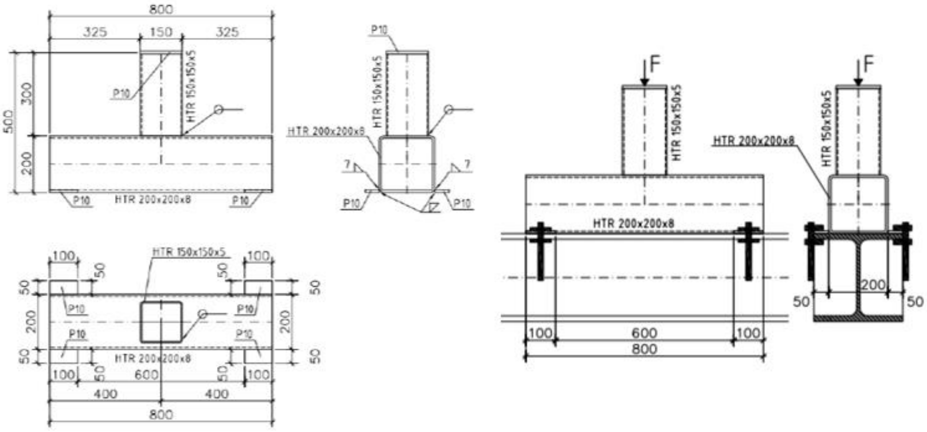

Figure 3-16: Geometry and the loading of the T-joint [25]

Table 3-5: T-Joint geometry

Model	Chord profile	Brace profile	Steel	Weld	Loading
TC.1.A	HTR 200×200×8	HTR 150×150×5	S355	Butt weld	Axial

Mesh

The 8-node brick elements for the joint and the H-profile are suitable for accurate/reliable and economical prediction of the T-joint. In the direction of the wall thickness of the joint, 4-layer mesh is used. Fine mesh of 5 mm is applied in the joint zone and a coarse mesh of 8 mm and 12 mm is chosen in the remaining regions. **Figure 3-17** shows the meshed finite element model in which the variable mesh is seen.

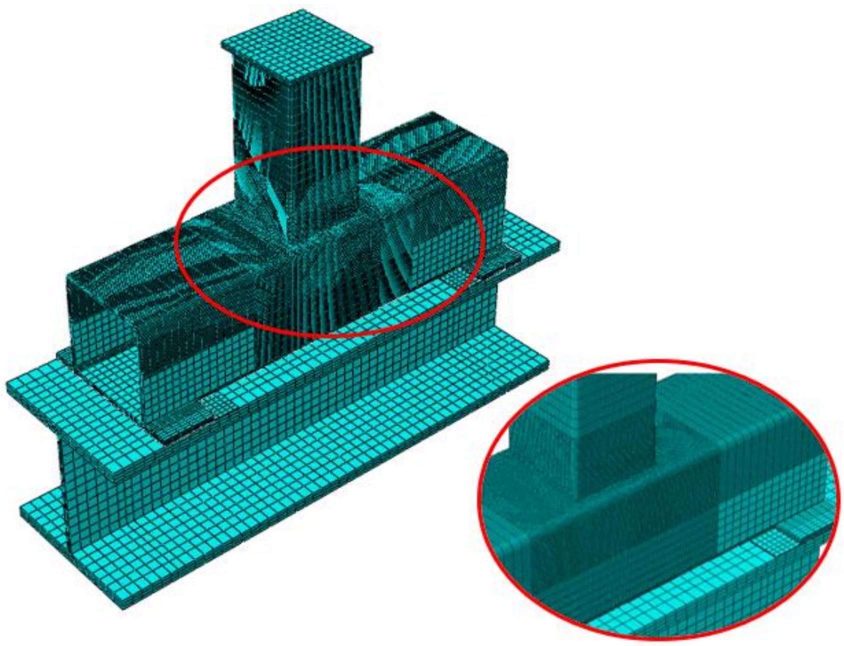

Figure 3-17: Finite element mesh of the T-joint

3.2.1.2 Boundary and loading conditions

According to the report, the T-joint is supported along its entire bottom surface of the chord. The four welded plates are clamped, to avoid body rigid movement of the joint. Furthermore, two plates between the T-joint and the H-section are observed in **Figure 3-18**. The axial load is applied to the loading plate at the brace end. Boundary condition used in the experiment is also applied to the finite element model. The thin plates in FEM are 300 mm long, 150 mm wide and 10 mm thick.

Figure 3-18: Experimental test T-joint [25]

3.2.1.3 Material properties

All the joint members are made of steel S355. Coupon test are carried out to obtain the material properties of all the members. In this test, the chord member has a yield strength of 429 N/mm^2 and and ultimate strength of 513 N/mm^2. The yield and ultimate strength of the brace member are 420 N/mm^2 and 530 N/mm^2, respectively. The stress-strain relation obtained by the coupon test together with the converted true stress-true strain relation are shown in the **Figure 3-19**. The material properties of the H-section are considered similar as the chord member.

Figure 3-19: Nominal and true stress-strain curve for the members in the T-joint

3.2.2 Experimental and Finite Element Results

In the experiment, deformations are measured using linear variable differential transformers (LVDT). The position of these instruments is given in the **Figure 3-20**. In the FEM, the deformation at the similar location are measured.

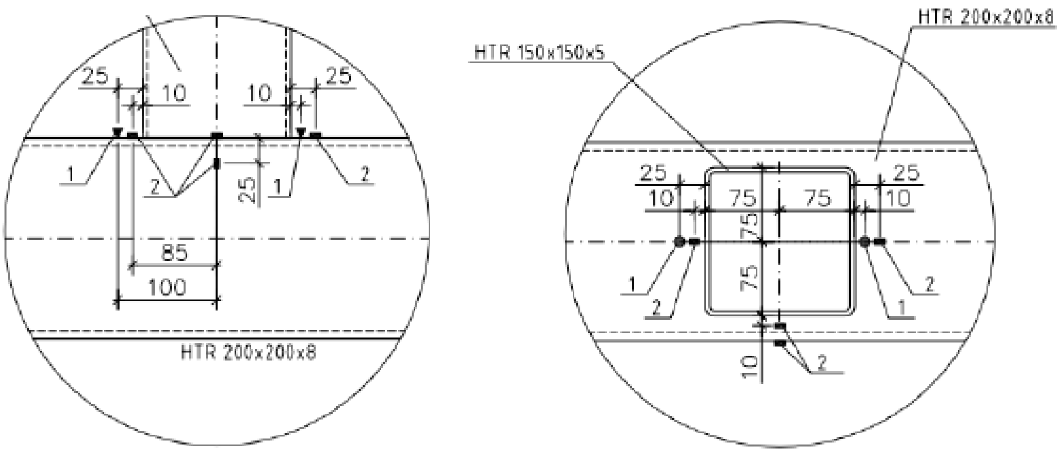

Figure 3-20: Position of the LVDT's and strain gauges [25]

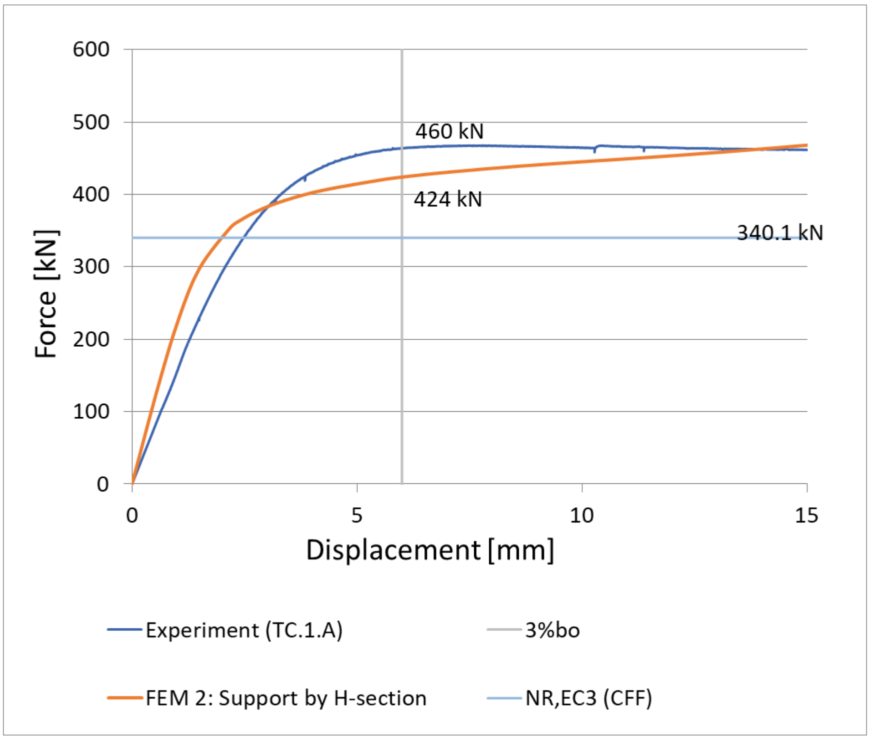

Figure 3-21: Load displacement curve for the experiment and the FEM

The load deformation curve for the experiment and the FEM is shown in the **Figure 3-21**. Comparing both curves, it can be concluded that the FEM has a larger initial stiffness and approximately 10% lower ultimate strength was obtained. The deformation and the von mises stresses at *3%b₀* deformation (6 mm) are shown in the **Figure 3-22**. The axial stresses and strain in the brace are shown in **Figure 3-23**. The maximum obtained axial strain in the brace was 0.064. Von Misses stresses of around 581 N/mm^2 and axial stresses of 635 N/mm^2 are obtained in the joint. Due to the discontinuity at the joint zone larger stresses occurred in the model.

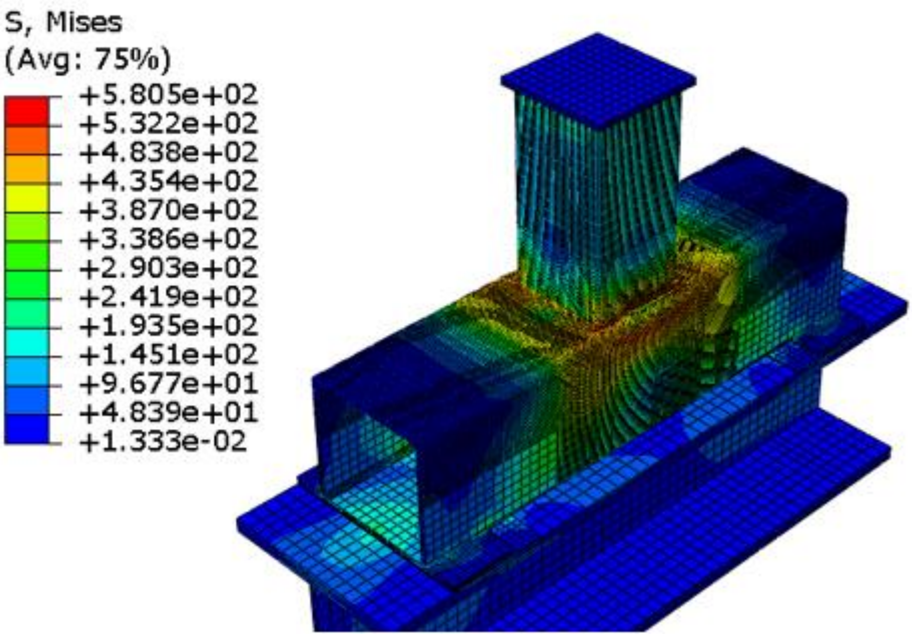

Figure 3-22: v. Mises stresses in the T-joint at $3\%b_o$ deformation (scale factor 2)

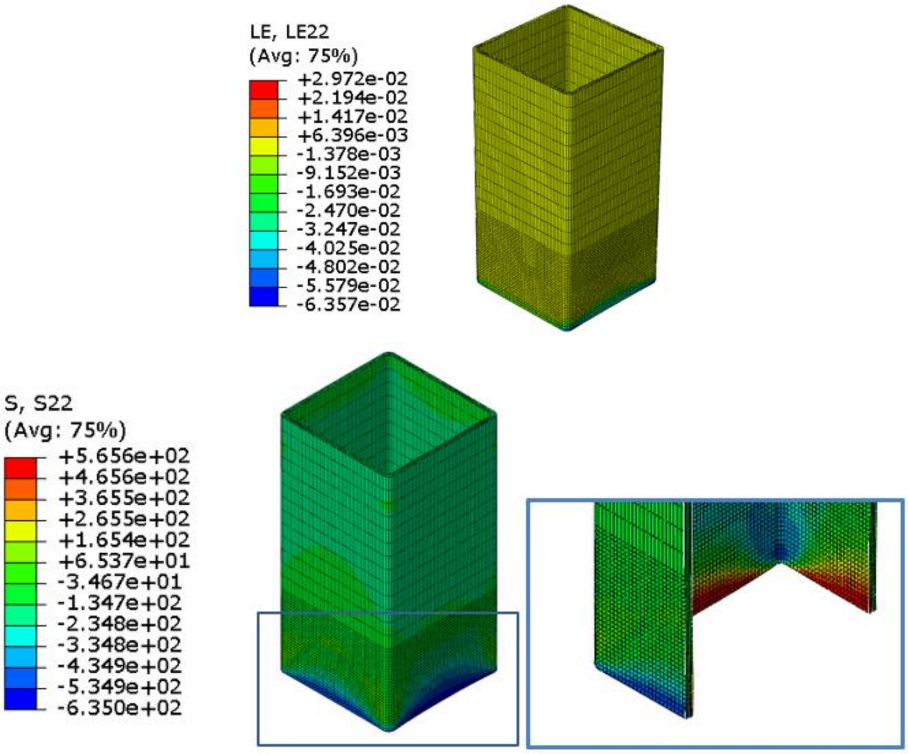

Figure 3-23: (a) Axial strain and (b) axial strain in the brace at *3%b_o* deformation

Secondary bending stresses

The secondary bending moments in the brace of the T-joints are obtained from the uneven stress distribution at the cross-section as shown in **Figure 3-24**. This section is around 20 mm away from the chord face. The secondary bending moment is integrated via a free body cut with element set and node set shown in before mentioned figure. The secondary bending stress is calculated based on FE secondary bending moment and moment inertia. The axial stress and the secondary bending moment in this section are used to determine the level of secondary bending stress.

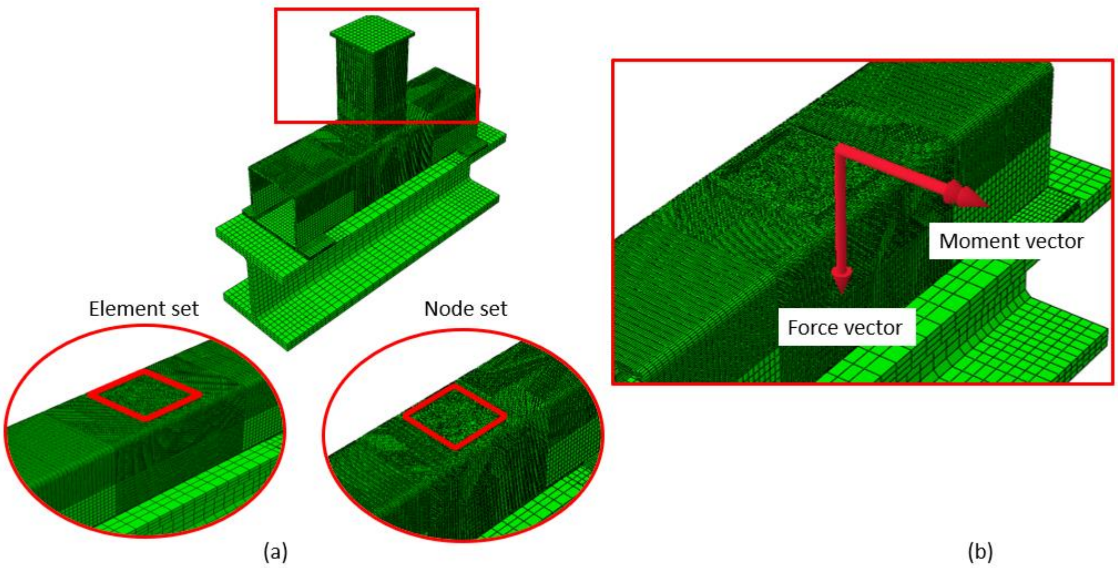

Figure 3-24: (a)Element set and node set (b) moment and force vector T-joint

The secondary bending moment development in the FEM is shown in **Figure 3-25**. Up to failure the secondary bending stresses and the level of secondary bending stresses are less than $0.0002f_y$ and 0.0002, respectively. Compared to the yield strength, these secondary bending stresses in the butt-welded T-joint are small and therefore neglectable.

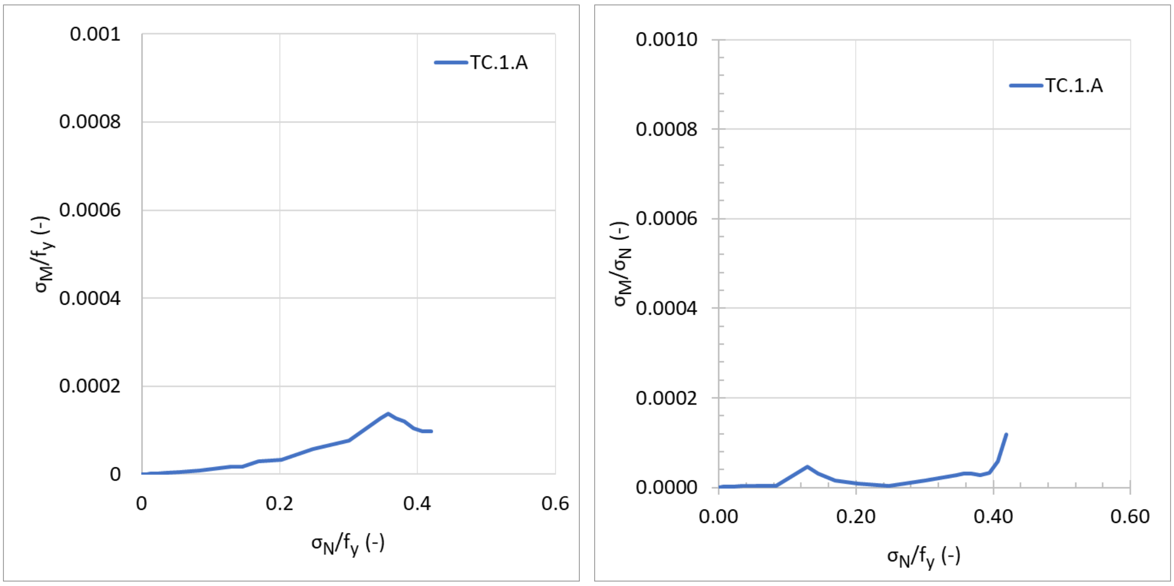

Figure 3-25: (a)Secondary bending stress (b) and the level of secondary bending stress

3.3 Summary

In this section, a truss girder is verified. The geometry, material properties, dimensions, boundary and loading conditions from an earlier experiment are applied to the FEM. The FEM was based on an initially undeformed girder without the consideration of the previous loading. Based on the available data a tri-linear material model is assumed in the analysis. The local behavior of the joint J6 is investigated. The numerical and experimental obtained results are compared with each other. Lower member forces, lower deflections different stress distribution and different joint behavior were obtained using FEM in ABAQUS. Variations in the boundary conditions are done in order to get better comparable results, but neglectable improvements are obtained. The nominal yield strength of the members is much lower than measured material properties. Due to this the FEM behaved in the elastic stage stiffer than the experimental one.
Due to the complexity of the FEM it is difficult to find the origin of the differences. Many factors, such as the material properties, dimensions, geometry might influence the numerical obtained results. The verification study of the truss is roughly good.
Also, the level of the secondary bending moment in this joint is investigated. High level of secondary bending stresses is present in the joint for low axial load. As expected at failure the level of secondary bending stresses is low when compared to the axial stresses and the yield strength.

Another validation study of a RHS T-joint has been performed. An accurate FEM is built using the geometry, material properties, boundary and loading condition obtained from an experimental result. The numerical obtained results are compared to the experimental data. The only available data is the load deflection curve. The experimental and numerical

obtained ultimate load resistance are 35% and 25% larger than the joint resistance. This is due to the additional stiffness and strength introduced by the support of the girder at the bottom surface. Moreover, the numerical analysis results in 10% lower failure load than the experimental one. The nominal yield strength of the material is 355 N/mm^2 and through coupon tests yield strength of around 420 N/mm^2 was obtained. The coupon tests resulted in much higher yield and ultimate strength and this may have influenced the higher initial stiffness of the FEM. In the FEM, at the joint zone locally larger stresses occurred at ultimate load resistance. The joint capacity of the FEM is roughly good predicted using the FEM.
Due to the lower non-uniform stress distributions, the secondary bending stresses and the level of secondary bending stresses in the butt-welded T-joint are low and therefore neglectable.

CHAPTER 4 PARAMETRIC STUDY

In this chapter a parametric study on an individual gap K – joint made of square hollow sections is described. The boundary and loading condition of the individual K-joint have been adopted from [32]. The numerical analyses are performed in ABAQUS®. With this study the behavior of the high-strength hollow section K-joints with respect to the secondary bending stresses and the joint behavior is investigated.

4.1 Parameters

The proposed 2020 version of the Eurocode 3 part 1-8 [4] provides design equations for hollow section joints up to S700. These equations, which are initially validated for the mild-strength steels and a certain range of parameters are adopted for high-strength steels by including material reduction factors 'C_f'. In this parametric study, the impact of the material properties on the hollow section joints is investigated. Four material properties ranging from S355 to S960, the gap size, the brace to chord width ratio (β) and the weld type are varied. All other parameters, such as thickness chord, thickness brace, brace thickness to chord thickness ratio (τ), brace angle (θ), chord width to chord thickness ratio(2γ), are kept constant. **Table 4-1** gives the parameters for the parametric study.

Table 4-1: The parameters

Parametric values	
Steel grade	S355, S460, S700, S960
Gap, g	G0=25mm, G1=40mm
Beta, β	β1=0.50, β2= 0.571, β3=0.64
Weld	Butt and fillet weld

Gap (G) and brace width to chord ratio (β)
The gap in a K-joint is the distance between the braces. The gap size has a certain impact on the joint strength and stiffness, since the gap area is subjected to normal and shear and bending stresses. The gap area has a larger stiffness in case of a low gap size (for β up to a medium value) and as the gap size increases the stiffness decreases. Two gap sizes are selected to vary. Another parameter which has an impact on the stiffness and strength of the joint, is the brace width to chord width ratio (β). The initial stiffness and strength increase with increasing β-value. To study the impact of this parameter on the secondary bending stresses, three β values are varied. [6]

Weld
The impact of the butt weld and the fillet weld on the strength and the stiffness is different. In case of the butt-welded joints, the edges of the hollow sections are usually beveled. For this study a full penetrated butt weld with size equal to the thickness of the brace is considered. Secondary bending stresses may occur due to the joint geometry and the uneven stiffness distribution of the RHS member. The fillet weld in RHS joins are single sided welds which introduces a local eccentricity which might increase the local stresses and the

secondary bending stresses. The fillet welds have a throat thickness equal to or larger than the thickness of the connected brace. The level of secondary bending stresses is obtained for the butt and fillet welded joints of similar joint geometry.

4.2 Finite Element Model

4.2.1 Geometry

The dimensions and the joint geometry of the gap K-joint are taken from the girder validated in the previous chapter. In order to satisfy the validity range, many joint geometries and parameter are adjusted. The parameters for the gap K-joint is shown in **Figure 4-1** and the joint geometry is summarized in **Table 4-2**. The length of each member is set to 5 times the member's width, b_i to ensure that the stresses at the joint zone are not influenced by the boundary conditions. Both brace members are made with the same cross section and have the same inclination θ_i=30^0. The parameter β is the brace width to chord width ratio, whereas the modified β_{mod} is the ratio of the brace width including the weld over the chord width. According to [4], for the joint members of cross-section class 3 and class 4, the plastic section modulus of chord member should be replaced by the elastic section modulus $W_{el,0}$.

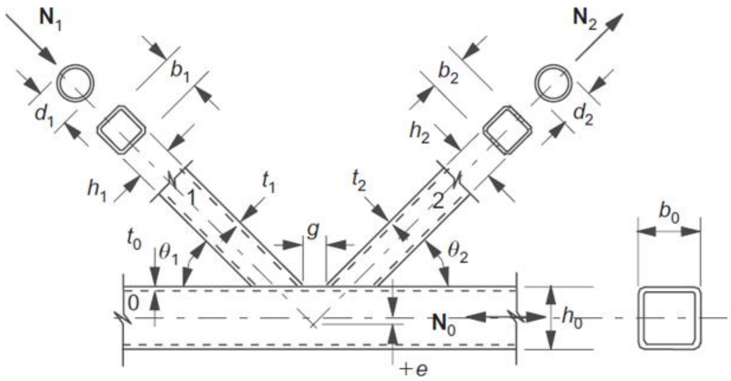

Figure 4-1: Gap K-joint parameters

Table 4-2: Joint geometry for the parametric study

Geometry	b_o	t_o	b_i	t_i	g	θ_i	e	β	Weld
	(mm)	(mm)	(mm)	(mm)	(mm)	(°)	(mm)	(-)	
1	120	5	80	5	40	30	-2.3	0.67	Fillet
2	120	5	80	5	25	30	-6.6	0.67	Fillet
3	140	6.3	70	5	40	30	-18	0.5	Fillet
4	140	6.3	80	5	40	30	-12.3	0.57	Fillet
5	140	6.3	90	5	40	30	-5.5	0.67	Fillet
3	140	6.3	70	5	40	30	-18	0.5	Butt
6	140	6.3	80	5	40	30	-12.3	0.57	Butt
7	140	6.3	90	5	40	30	-6.5	0.53	Butt

Fillet weld geometry
Fillet welds and butt welds are included in the finite element model. The butt welds are full penetrated of thickness equal to the thickness of the brace. The throat thickness of the fillet weld a_w is dependent on the brace thickness and the nominal yield strength of the material. The minimum weld size used in this study is summarized in **Figure 4-2**. A gap or opening of 0.15 mm between the chord and brace members is also considered in the analyses.

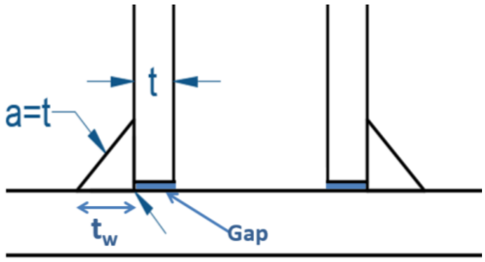

Steel grade	a	Weld size
$f_y \le 500MPa$	$a \ge t_i$	$t_w \ge 1.4 \times t_i$
$500MPa < f_y < 700MPa$	$a \ge 1.2t_i$	$t_w \ge 1.69 \times t_i$
$700 < f_y \le 960MPa$	$a \ge 1.4t_i$	$t_w \ge 1.98 \times t_i$

Figure 4-2: The weld throat thickness

4.2.2 Mesh

The K-joint including the welds are modelled with eight-node linear brick element C3D8. Numerical model with solid elements can be time consuming and therefore a variable mesh is used. The finite element mesh is illustrated in **Figure 4-3**. Near the joint zone, a fine mesh of 3 mm and a coarse mesh of 9 mm outside the joint zone is used. Four layers of elements is considered through the thickness of each member. The numerical model is partitioned into several faces to generate the variable mesh.

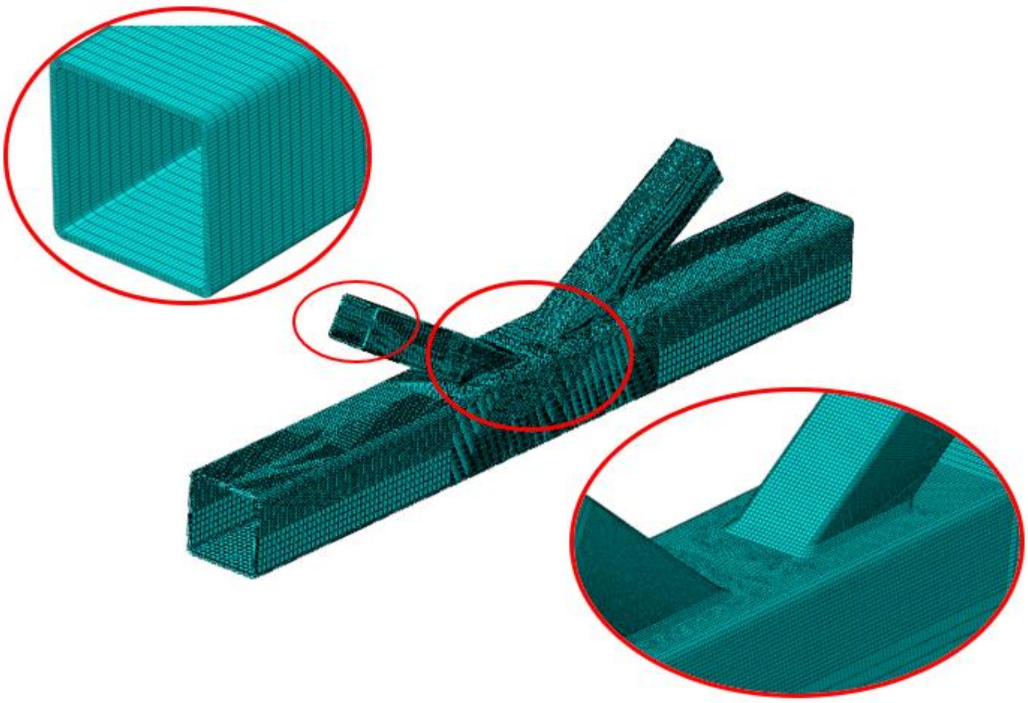

Figure 4-3: Finite element mesh of the K joint

4.2.3 Boundary and Loading Conditions

The mechanical boundary conditions of the K-joint are illustrated in **Figure 4-4**. One chord end and one brace end are translational fixed whereas the second chord end is free. Moreover, the other brace end is translational fixed in two direction and the load is applied in the axial direction. This boundary condition is taken from [32]. The length of the members is 5 times the member width b_i to ensure that the stresses at the joint zone are not influenced by the boundary conditions. The boundary condition and the load are applied using the MPC constrain where the center of the member is the reference point and the chord end surface is the slave surface. The displacement-controlled load is applied in small increments using the implicit finite element simulation in ABAQUS®.

Figure 4-4: Boundary and loading condition

4.2.4 Material Parameters

To study the impact of the material on the K-joints various steel grades including mild-strength and high strength steels is used. The steel grade varying from S355 to S960 are shown and listed in **Table 4-3** and shown in **Figure 4-5** [14]. These stress-strain curves are obtained by the coupon test. All the materials have a modulus of elasticity of 210 GPa and a Poisson's ratio of 0.3. The material and the geometrical non-linearity are also included in the analyses. **Figure 4-5** shows both the true stress-strain curves and the nominal stress-strain curves for the materials.

Table 4-3: Material properties

Material	f_y (N/mm^2)	f_u (N/mm^2)	f_u/f_y (-)	ε_u (%)	ε_f (%)
S355	390	521	1.34	0.15	0.3
S460	460	575.5	1.25	0.15	0.23
S700	700	835	1.19	0.05	0.146
S960	960	1175	1.22	0.035	0.086

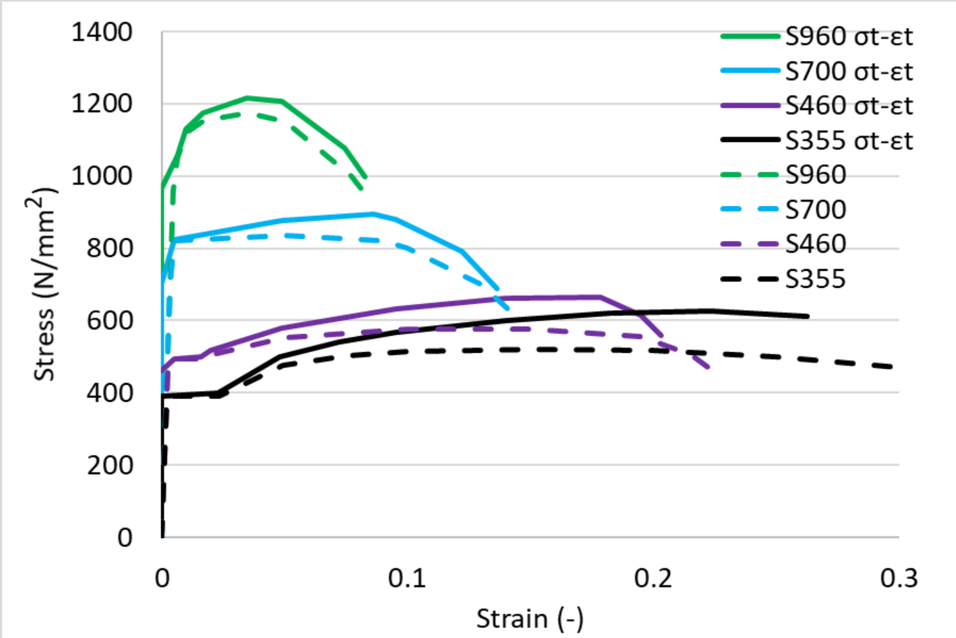

Figure 4-5: Nominal and true stress-strain relation

4.3 Finite Element Results

4.3.1 Effect of the gap between chord and brace

The effect of the assumed gap between the chord and the brace (see **Figure 4-2**) on the ultimate strength is investigated. Two finite element models, one with and the other without a gap between the chord and the brace are built. The ultimate capacity is determined using the load displacement behavior of the joints. The displacement is defined as the displacement of the brace member minus the displacement of the chord member at the intersection of the brace and the chord center line. This displacement is measured along the corresponding brace. The initial distance between these two points is equal to $b_o/\sin\theta$ (see **Figure 4-6**). The strength of the joint is defined as the peak load or the corresponding load at the $3\%b_o$ deformation limit. The $3\%b_o$ deformation limit is used to determine the strength of the joint that do not exhibit a peak load. **Table 4-4** summarizes the FEM used in this study.

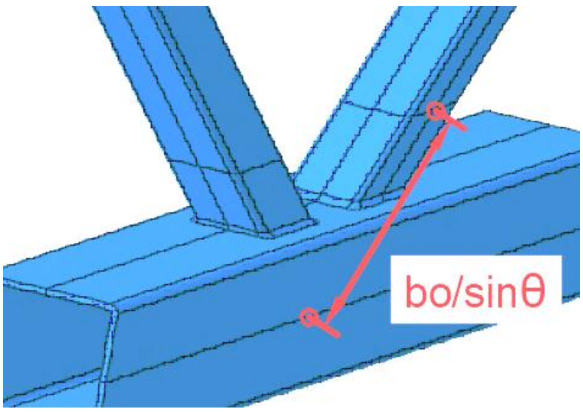

Figure 4-6: Displacement brace member

Table 4-4: The joint geometry for both the FE models

Model	b_o	t_o	b_i	t_i	θ_i	e	g	β	β_{mod}	gap opening
	(mm)	(mm)	(mm)	(mm)	(°)	(mm)	(mm)	(-)	(-)	(mm)
G1-S355	120	5	80	5	30	-2.3	40	0.67	0.82	0
G1-S355	120	5	80	5	30	-2.3	40	0.67	0.82	0.15

Figure 4-7 shows the load displacement curve for the FE model of the joints. The assumed gap is 0.15 mm. Less differences are obtained between both the load-displacement curves. At *3%b_o* deformation limit, the difference between the ultimate load resistance for both the FE models is around 1.30%. **Figure 4-8** shows the displacement around the gap between the brace and the chord in both the models. Similar displacement distribution is observed in both the models. The displacements in both cases are around 11.6 mm at the brace toe side and around 8.55 mm at the brace heel side. The gap between the brace and the chord has a little influence on the local displacement. The stress distribution in the area of interest is shown in **Figure 4-9**. For the model with a gap between the brace and chord, a larger stress distribution in the welds are observed. Furthermore, locally the stresses in the brace are lower compared to the model without a gap between the chord and the brace. Locally similar stress range are obtained for the FE models. Comparing both the FE models, a good agreement is found between both the FE models. A "numerical" gap between the brace and the chord of 0.15 mm is considered in the analyses.

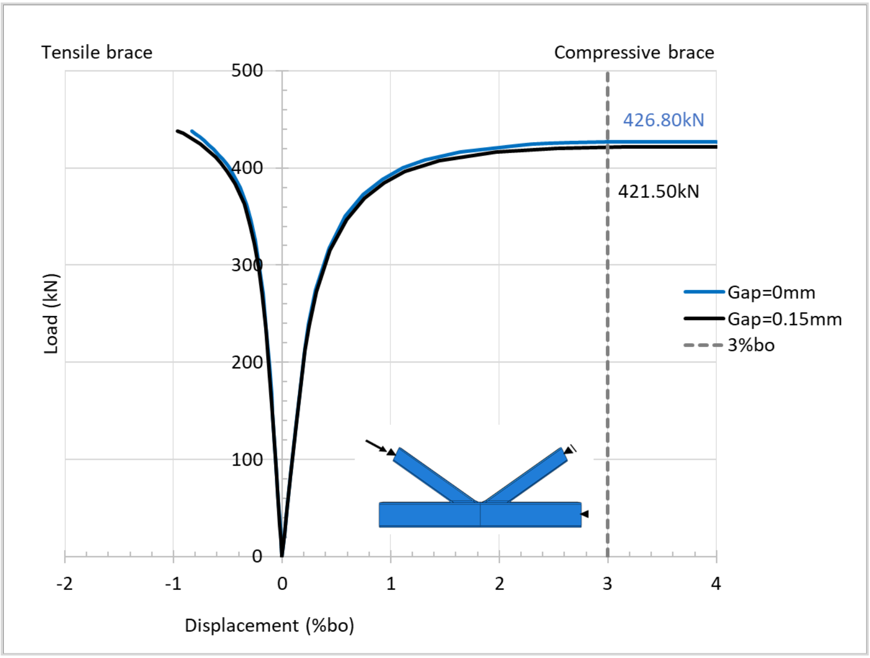

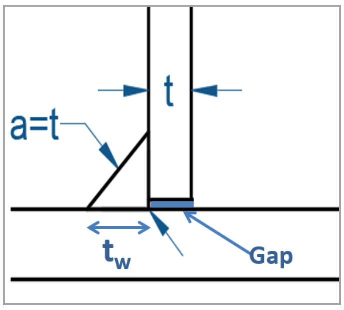

Figure 4-7: Load displacement curve for FE models with and without gap

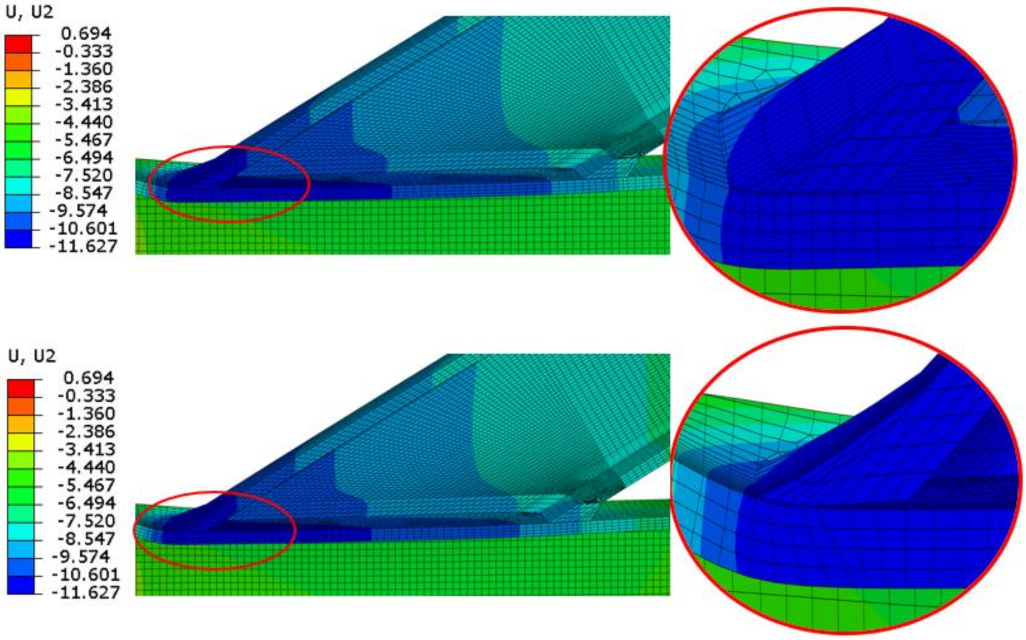

Figure 4-8: Displacement in FEM (a) with and (b) without gap between brace and chord

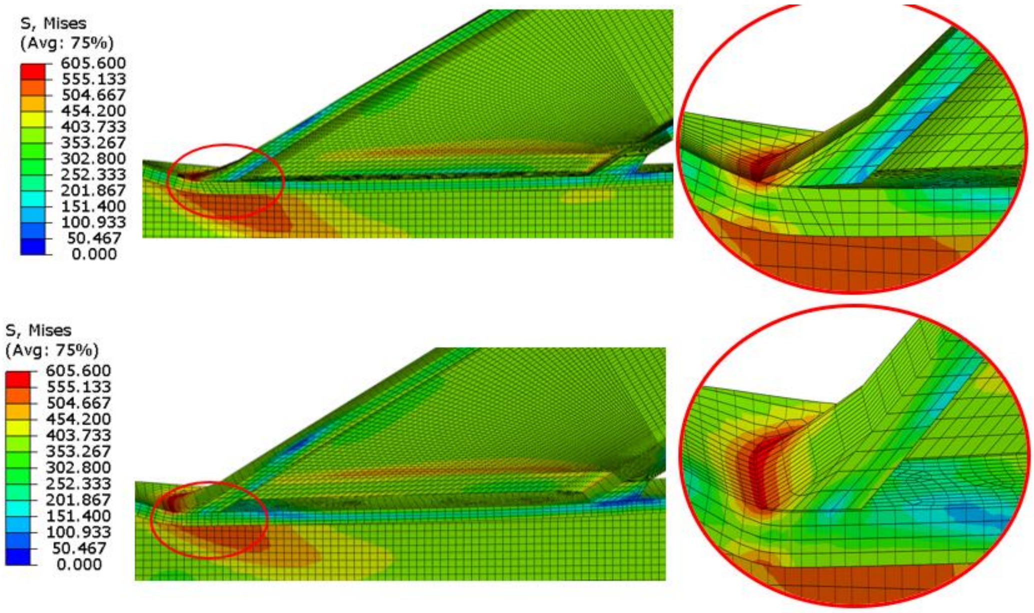

Figure 4-9: Stress distribution in FEM (a) with (b) without gap between brace and chord

4.3.2 Effect of the material properties

Material properties is varied in order to study the impact of these properties on the RHS joints. Similar joint geometry has been used for this study. **Table 4-5** shows the joint geometry for the various steel grades. Each model is given an identification, in which the parameter and the steel grade are described.

Table 4-5: The joint geometry for various steel grades

Geometry	b_o	t_o	b_i	t_i	θ_i	E	g	β	β_{mod}
	(mm)	(mm)	(mm)	(mm)	(°)	(mm)	(mm)	(-)	(-)
G1-S355	120	5	80	5	30	-2.3	40	0.67	0.78
G1-S460	120	5	80	5	30	-2.3	40	0.67	0.78
G1-S700	120	5	80	5	30	-2.3	40	0.67	0.81
G1-S960	120	5	80	5	30	-2.3	40	0.67	0.83

4.3.2.1 Ultimate load resistance

Figure 4-10 shows the load displacement behavior for the models. In this study, the compressive brace is investigated. Due to the similar geometry, identical initial stiffness is observed in the first stage of the curve. The load corresponding to the *3%b₀* deformation limit is considered as the ultimate capacity of the joints. The ultimate capacity of the joints depends mostly on the geometry and the nominal yield strength. Obviously, joints with higher yield strength will result in higher ultimate capacity. The highest ultimate capacity of 1019 kN is obtained for the FE G1-S960 and the lowest failure load of 421.5 kN is obtained for FE G1-S355. Joints with steel grade S460, S700 and S960 resulted in 20%, 83% and 142% larger resistance compared to joint with steel grade S355.

The proposed 2020 version of Eurocode 3 part 1-8 [4] provides design equations to determine the design resistance of the hollow section joints. **Table 4-6** summarizes the design resistance without considering the material factor (C_f) and the partial safety factor (γ_{m5} = 1.0). The material factor is dependent on the steel grade and is summarized in **Table 2-3** and **Table 2-4**. The governing failure mode is the chord face failure (CFF). **Table 4-7** compares the design joint resistance with the FE results. The resistance for the FE, G1-S960, G1-S700 and G1-S460 are 14%, 2% and 4% larger than the ultimate load resistance. For joints with yield strength larger than 460 N/mm^2 larger resistance is predicted. Compared to FEA, a reduction factor 0.8, 0.8, 0.9 and 1.00 are considered for G1-S960, G1-S700, G1-S460 and G1-355. These reductions are consistent with the material reduction factors shown in **Table 2-2**.

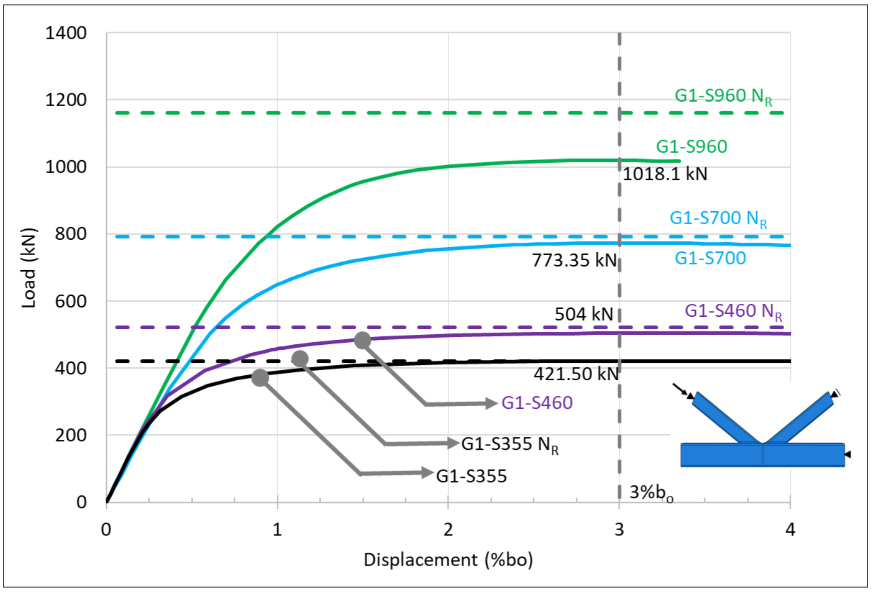

Figure 4-10: Load displacement relation

Table 4-6: Design resistance without the material factors

Model	CFF (kN)	CSF (kN)	BF (kN)	PSF (kN)	Failure mode
G1-S355	420.69	569.48	494.00	975.72	CFF
G1-S460	522.17	671.69	582.67	1150.85	CFF
G1-S700	777.29	957.89	830.93	1641.21	CFF
G1-S960	1162.36	1372.59	1190.67	2351.74	CFF

Table 4-7: Ratio resistance over failure load

Model	N_{FEA} (kN)	N_R (kN)	N_R/N_{FEA} (-)	$N_{R,Cf}/N_{FEA}$ (-)
G1-S355	421.49	420.69	1.00	1.00
G1-S460	503.99	522.17	1.04	0.93
G1-S700	773.35	792.41	1.02	0.82
G1-S960	1018.81	1162.36	1.14	0.91

4.3.2.2 Secondary bending moment in the brace members

The secondary bending moment are obtained from the uneven stress distribution in the compression brace at the cross-section as shown in **Figure 4-11**. This section is around 95 mm away from chord rectangular to the compressive brace. The secondary bending moment is integrated via a free body cut with element set and node set shown in before mentioned figure. The secondary bending stress is calculated based on FE secondary bending moment and moment inertia. The average stress or nominal stress ($\sigma_n=\sigma_{average}=N_{FEA}/A$) is determined using the obtained FE axial force and the cross-sectional area.

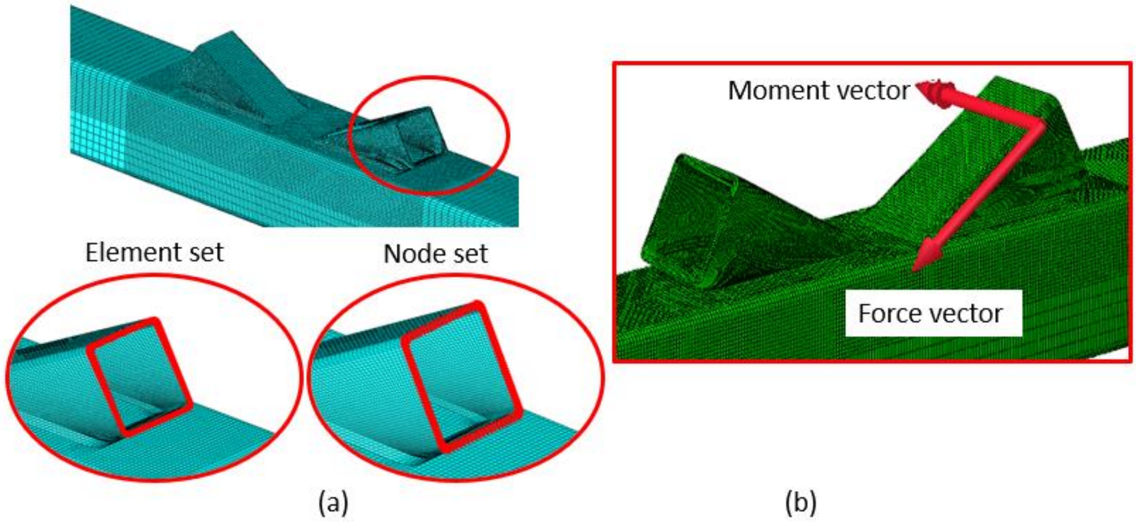

Figure 4-11: (a)Element set and node set and (b) moment and force vector K-joint

To evaluate and compare the secondary bending stress and the average stress for various steel grades, the obtained stresses from the before mentioned cross-section are divided by the yield strength. The ratio secondary bending stress to yield strenght (σ_m/f_y) is plotted against the ratio average stress to yield strenght (σ_n/f_y) in **Figure 4-12**(a). With axial load increasing, the secondary bending moment increases in the beginning and decreases later after the secondary bending stress reaches to the peak. As mentioned before, the secondary bending moment in a joint is dependent on the axial loading and the remaining rotational stiffness in the joint. The initial stiffness of the joints is for low axial load the largest and decreases with the increasing axial load. With the decrease of the rotational capacity, the stresses redistribute, and secondary bending stresses reduces.

For the models G1-S355 and G1-S460 the largest secondary bending moment is $0.22f_y$. The FE models G1-S700 and G1-S960 have secondary bending moment 23% and 30% larger than the models with mild-strength steels. At ultimate load resistance the average stresses (N_{FEA}/A) for joints with HSS varies from $0.73f_y$ to $0.75f_y$ and the secondary bending stresses from $0.04f_y$ to $0.06f_y$.

The level of secondary bending stress ($\sigma_m/\sigma_{average}$), which is the ratio of secondary bending stress over the average stress is plotted against the the ratio average stress over the yield strength ($\sigma_{average}/f_y$) in **Figure 4-12(b)**. The $\sigma_m/\sigma_{average}$ ratio is for low axial load the largest. As the average stress increases, the $\sigma_m/\sigma_{average}$ ratio decreases rapidly until the ultimate load resistance is reached. **Table 4-8** summarizes the secondary bending stresses and the $\sigma_m/\sigma_{average}$ ratios. For all the models the maximum $\sigma_m/\sigma_{average}$ ratio is varied from 53% to 56%. In the FE models, large $\sigma_m/\sigma_{average}$ ratio is obtained in the joint for average stresses up to $0.5f_y$.

At ultimate load resistance the $\sigma_m/\sigma_{average}$ ratio is 5% and 8% for the models G1-S700 and G1-S960, respectively. For the models G1-S355 and G1-S460 the secondary bending stresses disappears at failure.

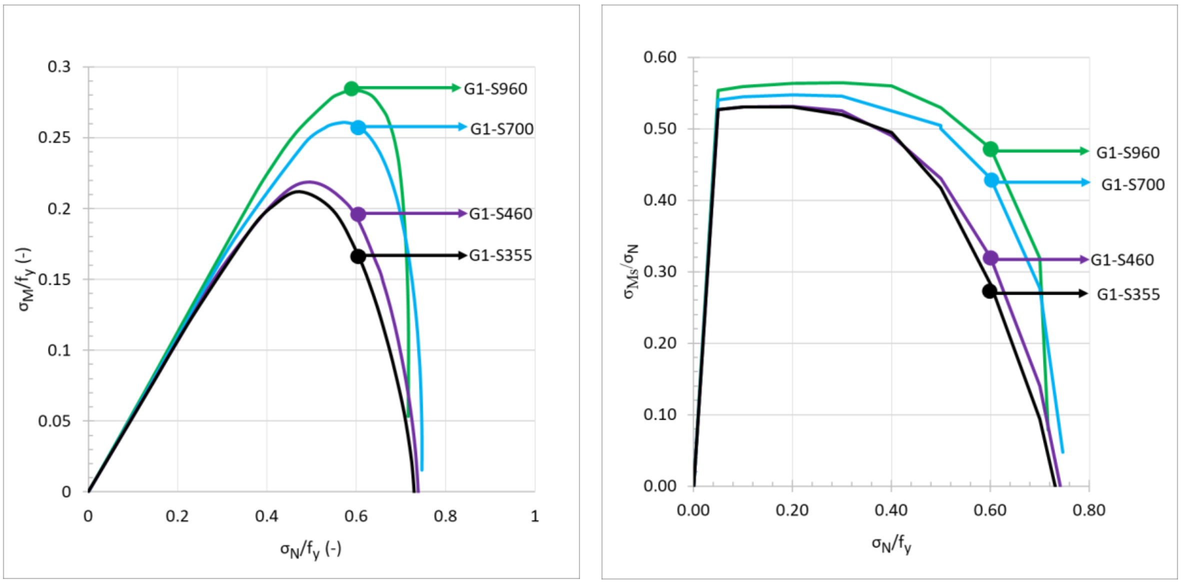

Figure 4-12: (a) Secondary bending stress and (b) the level of secondary bending stress

Table 4-8: Average stresses and the level of secondary stresses in the joints

G1-S355			G1-S460			G1-S700			G1-S960		
σ_N/f_y	σ_M/f_y	σ_M/σ_N	σ_N/f_y	σ_M/f_y	σ_M/σ_N	σ_N/f_y	σ_M/f_y	σ_M/σ_N	σ_N/f_y	σ_M/f_y	σ_M/σ_N
0	0	0	0	0	0	0	0	0	0	0	0
0.05	0.03	0.53	0.05	0.03	0.53	0.05	0.03	0.54	0.05	0.03	0.55
0.10	0.05	0.53	0.10	0.05	0.53	0.10	0.05	0.54	0.10	0.06	0.56
0.20	0.11	0.53	0.20	0.11	0.53	0.20	0.11	0.55	0.20	0.11	0.56
0.30	0.16	0.52	0.30	0.16	0.53	0.30	0.16	0.55	0.30	0.17	0.56
0.40	0.20	0.49	0.40	0.19	0.49	0.50	0.25	0.50	0.40	0.22	0.56
0.50	0.21	0.42	0.50	0.21	0.43	0.50	0.25	0.50	0.50	0.26	0.53
0.60	0.17	0.28	0.60	0.19	0.32	0.60	0.26	0.43	0.60	0.28	0.47
0.70	0.07	0.09	0.70	0.10	0.14	0.70	0.19	0.28	0.70	0.22	0.32
0.73	0	0	0.74	0	0	0.75	0.04	0.05	0.72	0.06	0.08

Figure 4-13 shows the axial stresses in the compressive brace at the maximum secondary bending stress. The maximum secondary bending stresses for joints with steel grade S355, S460, S700 and S960 occur at a deformation of around 0.31%b_o, 0.36%b_o, 0.80%b_o, 1.10%b_o. At this deformation level the average stresses (σ_n=σ_{averge}) are around 0.48f_y, 0.47f_y, 0.58f_y, and 0.58f_y for joints with steel grade S355, S460, S700 and S960. At this load level the secondary bending stresses starts to decrease due to the redistribution of stresses. The peak axial stresses in the compressive brace which occurs in the weld region are evaluated. The peak axial stress in the mild-strength joints is approximately equal to the yield strength. The corresponding axial strain in these braces in FE G1-S355 and G1-S460 are around 0.004606 and 0.003977. For the high-strength joints, the peak axial stress in the compressive brace is around 125%f_y. The corresponding axial strain in the brace of the FE G1-S700 and G1-S960 are 0.006256 and 0.001276.
The high peak axial stress in joints with HSS can be explained by the shorter or missing lower yielding plateau in the stress-strain curve for HSS. Due to this the strain hardening starts immediately after the yield stress. The strain and the stresses in the strain hardening stage increases significantly. Whereas for the mild-strength steel, after the yield stress has

reached a clear low yield plateau is present. In this stage the strain increases without a significant change in the stress. **Figure 4-14** shows the corresponding axial strain the compressive brace.

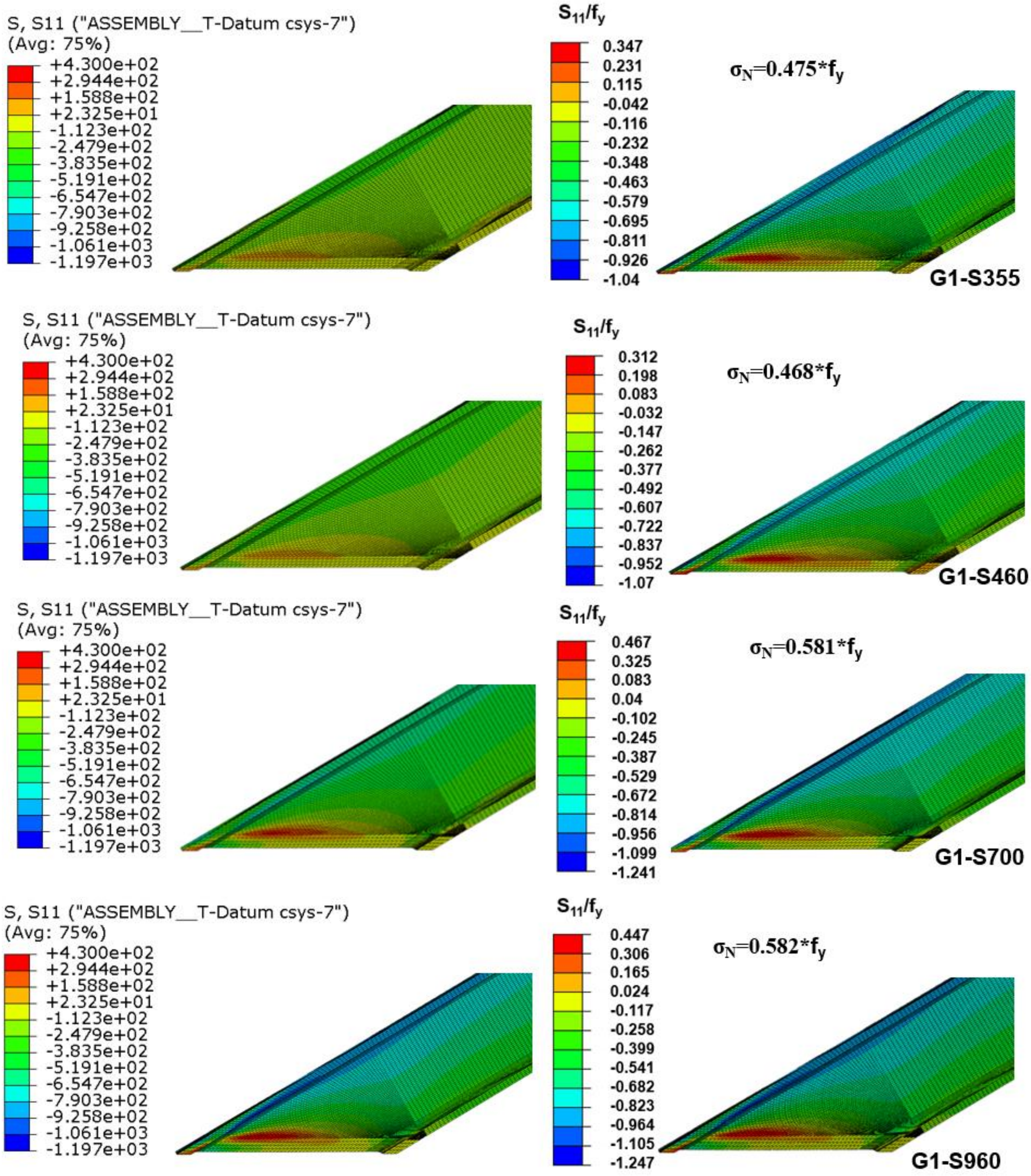

Figure 4-13: Axial stress at maximum secondary bending stress

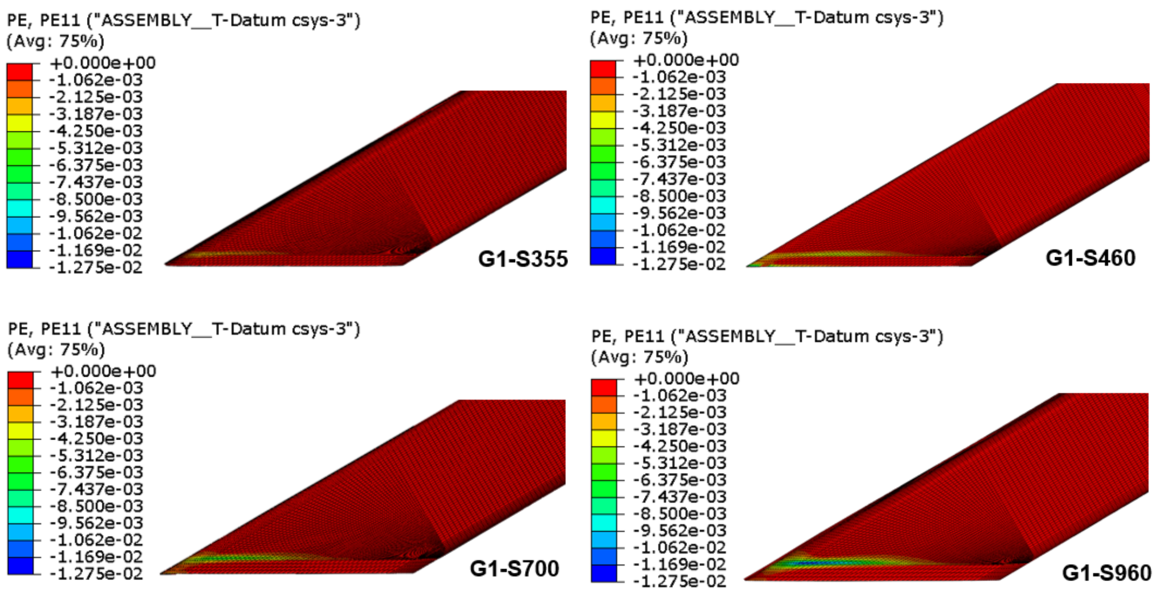

Figure 4-14: Axial strain at maximum secondary bending stress

4.3.2.3 Stress and strain distribution at ultimate load resistance

Von Misses stress distribution at ultimate load resistance

The stress distribution and the deformation at *3%*b_o deformation limit in the FE models is shown in **Figure 4-15**. At ultimate load resistance, which is the load corresponding to the *3%*b_o deformation limit, the chord is deformed, which is clearly visible in the figure. In the weld zone, the stresses can be higher than the nominal yield strength. For the models G1-S355 and G1-S460 the mises stresses are approximately 55% and 44% larger. In high strength joints this percentage is 27%. Compared to the joints with mild strength steel, lower stresses occur in the high-strength joints, when the weld thickness is assumed as shown in **Figure 4-2**.

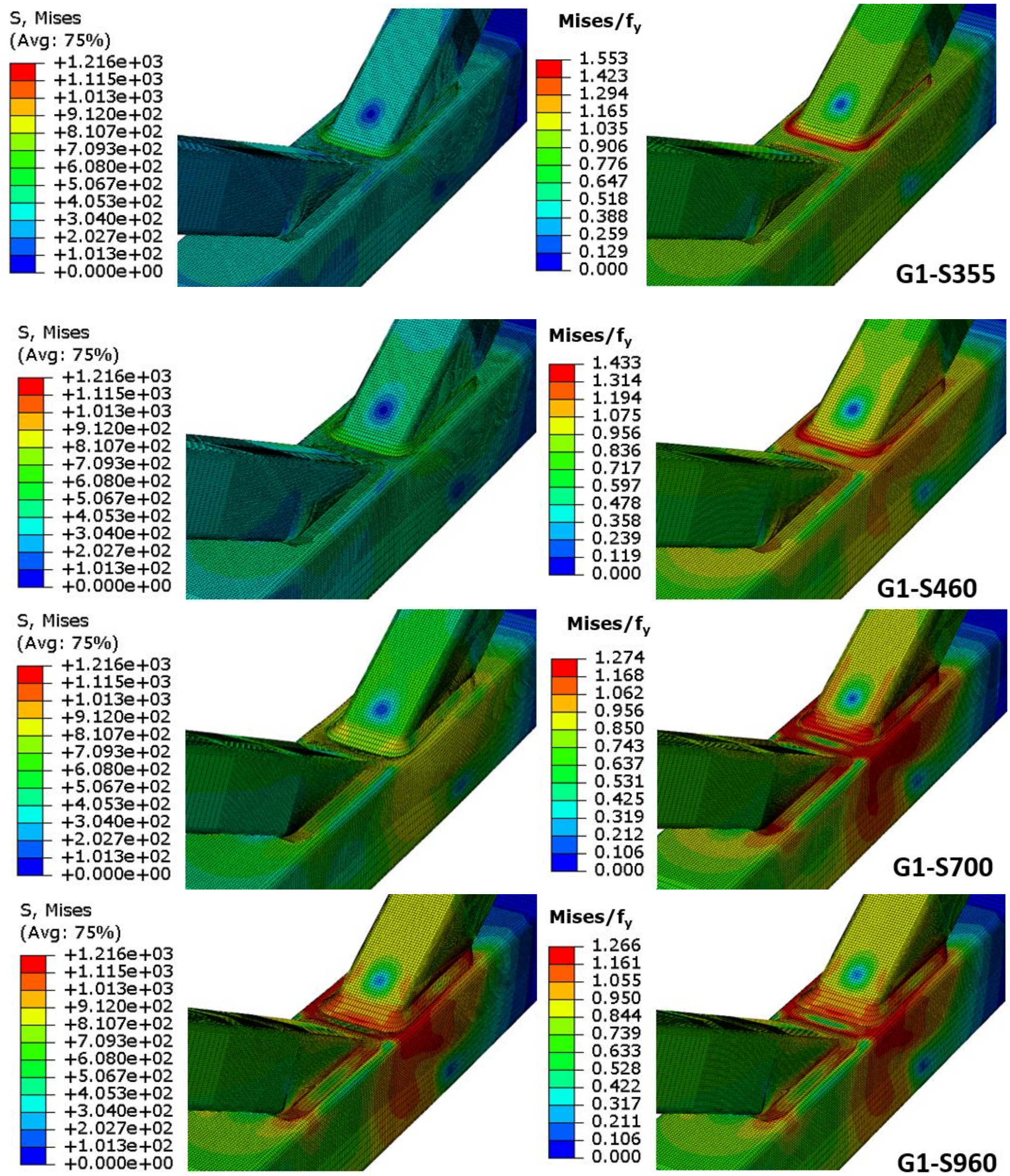

Figure 4-15: Von Mises stresses at ultimate load resistance (scale factor 1)

The axial stress and strain distribution in the compressive brace are shown in **Figure 4-16** and **Figure 4-17**. In the FE G1-S960 the maximum axial stresses are 49% larger than the yield strength. This percentage is around 70% for FE G1-S355. The stresses vary along the length and through the thickness of the member. Large stresses occur in the weld and near the welded joint. **Table 4-9** summarizes the maximum axial stress and axial strain in the compressive brace. The average stress is the stress due to the applied load in the brace without the considering the effect of the weld effect and the geometry. The ratio maximum axial stress to average stress ($\sigma/\sigma_{average}$) varies from 2.00 to 2.30 and the ratio axial stress over yield strength (σ/f_y) from 1.49 to 1.70. The lowest ratio is obtained the FE G1-S960 and the largest ratio is obtained for the FE models with mild-strength steel. Joints with HSS have obtained lower σ/f_y ratio and $\sigma/\sigma_{average}$ ratio when compared to joints with mild-strength steels. The axial strain at ultimate load resistance are around 0.0633 and 0.0655 for mild-strength joints. For high strength joints, G1-S700 and G1-S960 the axial strain is around 0.0444 and 0.03318. The stress and strain distribution in high-strength joints at ultimate load resistance are lower compared to the mild-strength joints.

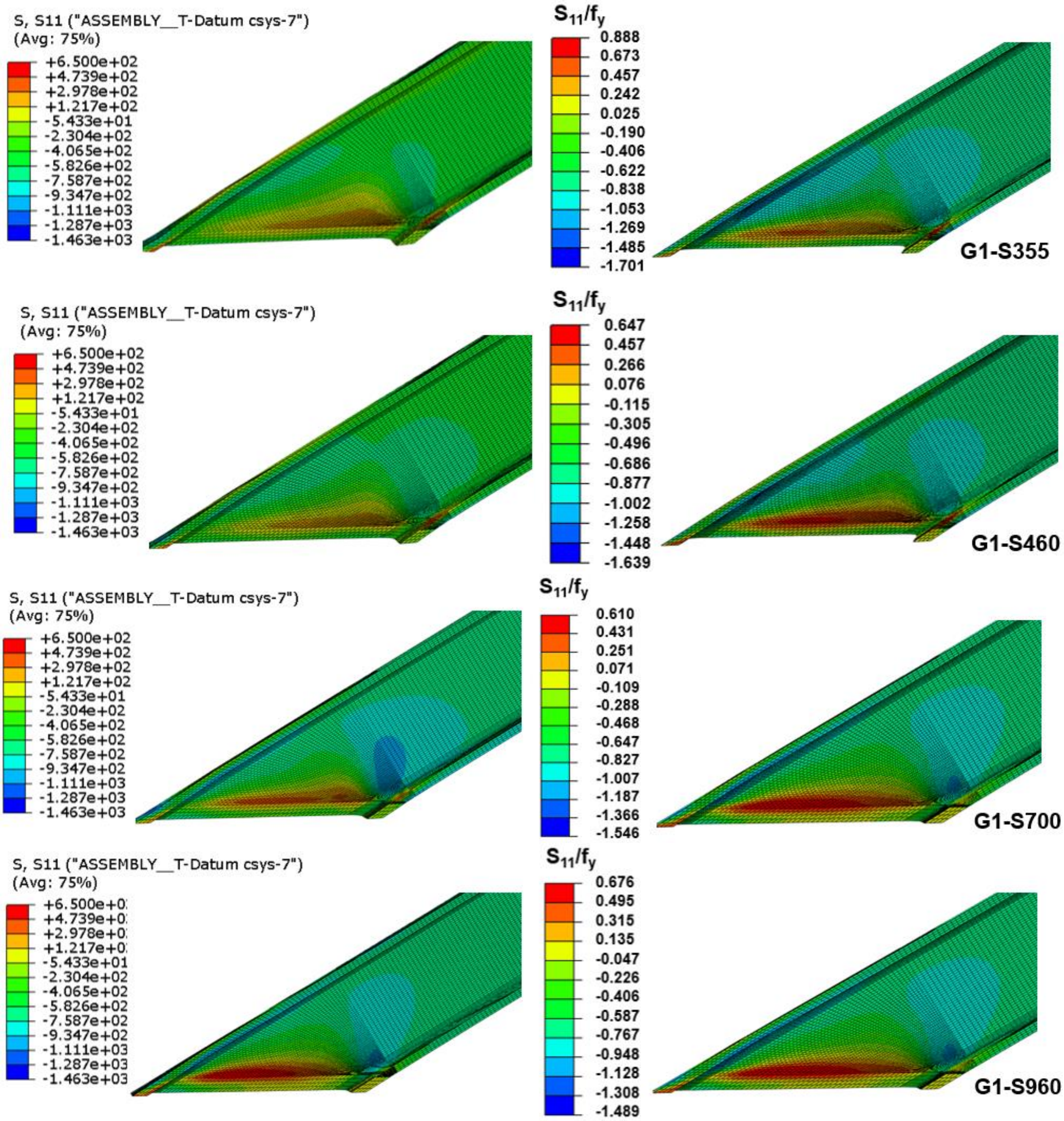

Figure 4-16: Axial stress distribution brace at ultimate load resistance

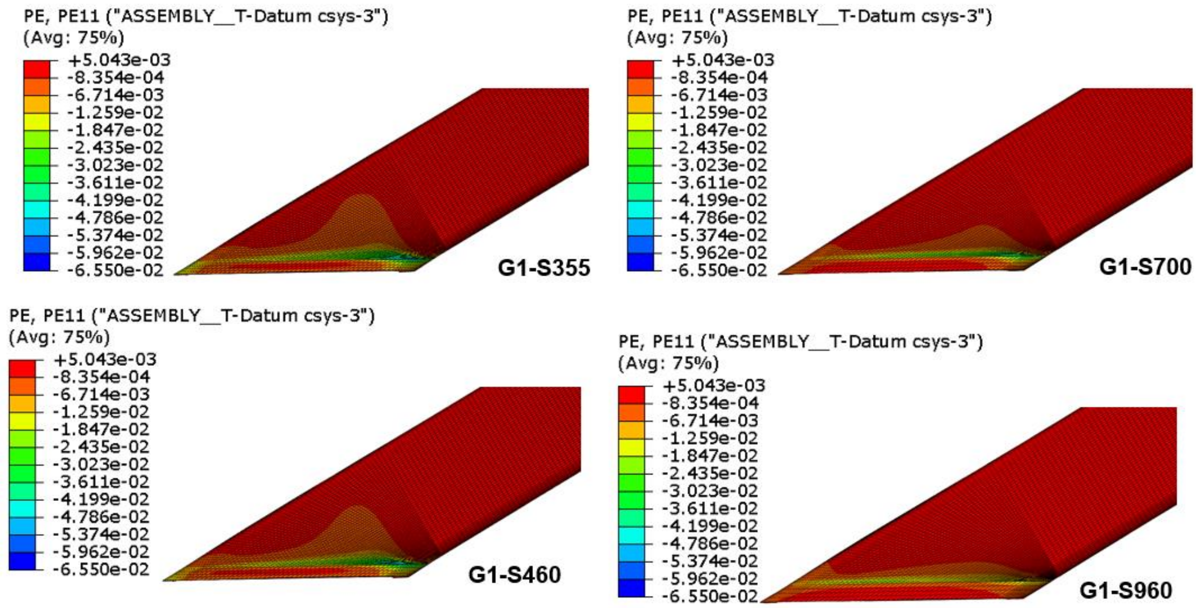

Figure 4-17: Axial strain distribution at ultimate load resistance

Table 4-9: Stress and strain in compressive brace at ultimate load resistance

Model	Stress σ_{max}	Strain ε	Nominal stress σ_{nom}	Yield stress f_y	$\sigma_{max}/\sigma_{nom}$	σ_{max}/f_y
	(N/mm^2)	(-)	(N/mm^2)	(N/mm^2)	(-)	(-)
G1-S355	-663.50	-0.0633	-286.73	390	2.31	1.70
G1-S460	-753.90	-0.0671	-342.85	460	2.20	1.64
G1-S700	-1082	-0.0481	-544.61	700	1.99	1.55
G1-S960	-1463	-0.00409	-717.47	960	2.03	1.52

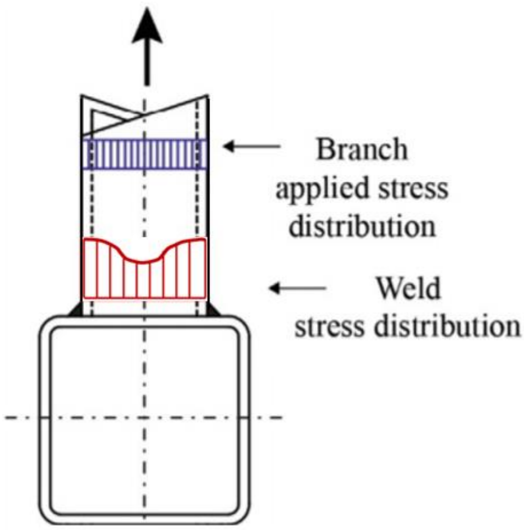

Figure 4-18: Non-uniform stress distribution in RHS joints in the weld region

In the weld and in the area close to the weld, considerably large stresses are present. **Figure 4-18** shows the theoretical shape of the non-uniform stress distribution due to the welded connection. At the corner the stresses are larger than the stresses in the flat sides. The stress distribution depends on the type of loading, joint type and geometry of the connection. Axial stresses are investigated in two cross-sections near the weld toe, one in the brace and the other in the chord (see **Figure 4-19**). **Figure 4-20** shows the non-uniform stress distribution through the thickness of the brace at the weld toe for FE G1-S355 and G1-S960. Stresses vary through the thickness and in the corners larger stresses are observed. Furthermore, the stresses in the brace toe and corners are larger than the stresses in the brace heel side. This is due to the stiffness differences along the brace perimeter. **Figure 4-21** and **Figure 4-22** shows the axial stress distribution at ultimate load resistance in position 2 – 8 and 10 – 16 in the middle line of both the cross sections. For axial stress and strain distribution for FE G1-S355, G2-S460, G1-S700 and G1-S960 reference is made to Appendix C.3.

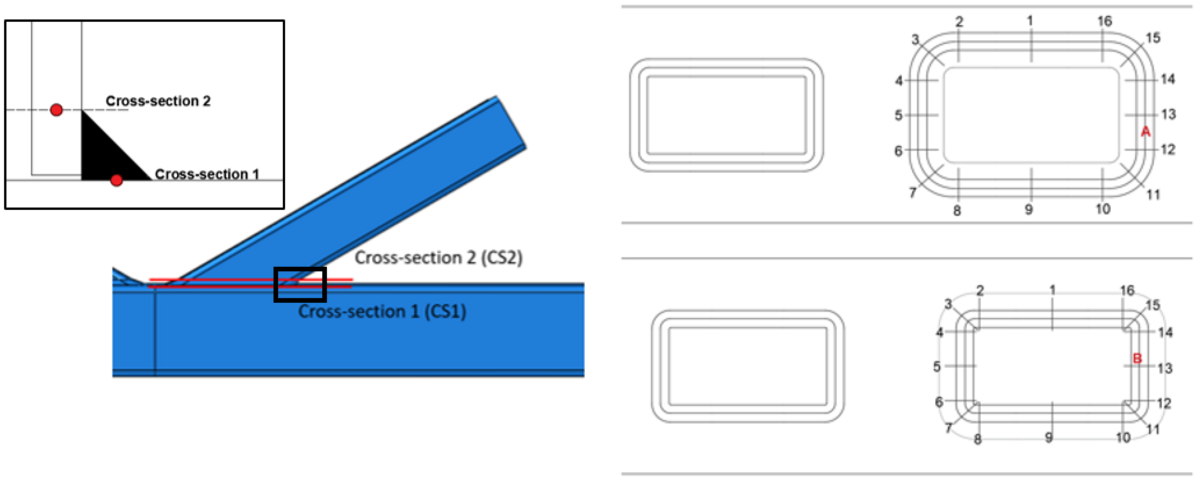

Figure 4-19: Cross-sections to investigate stress distribution

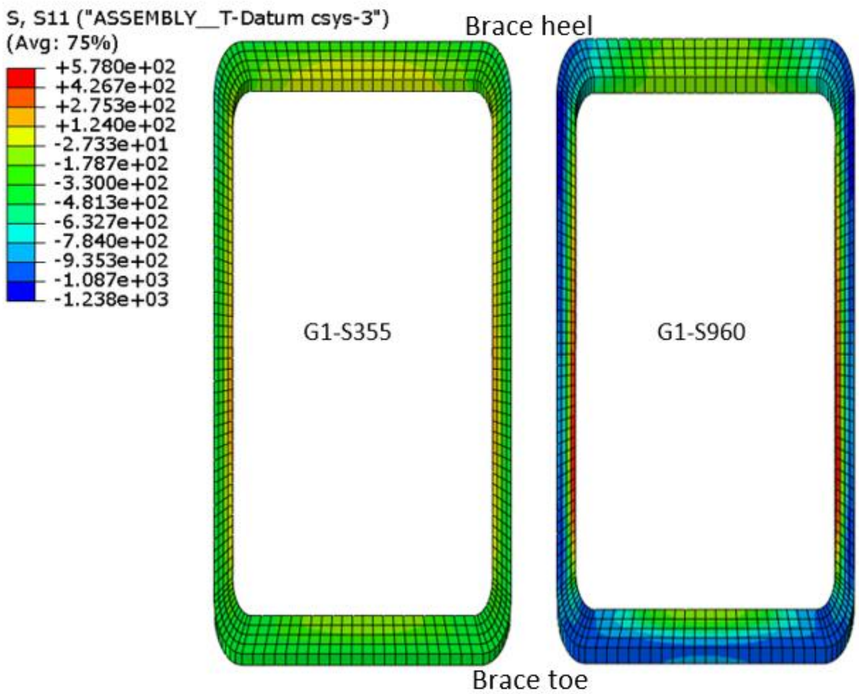

Figure 4-20: Stress distribution in cross-section 2 for model (a) G1-S355 (b) G1-S960

Comparisons are made between the FE models in order to investigate the behavior of the high strength steels. The compressive axial stresses in the joint are larger than the nominal yield strength. The combination of secondary bending stress and the average stress at *3%b₀* deformation is also plotted in the figures. Due to neglectable secondary bending stress at ultimate load resistance, little difference is observed between before mentioned stress and the average stress. The ratio axial stress in the positions to the average stress of the FE model is given in **Table C-14** and **Table C-15** (see Appendix C.3). This ratio is the largest for FE model G1-S355 and the lowest for FE models with high-strength steel.

Joint with HSS resulted in lower σ/f_y ratio and $\sigma/\sigma_{average}$ ratio when compared to joints with mild-strength steels. The can be explained to the low f_u/f_y ratio. **Table 4-3** summarizes the f_u/f_y ratio. Ratios between 1.22 and 1.34 are obtained for the material properties used in this study. The lowest ratio is obtained for steel grades S960 and S700 and the largest for steel grade S355. The difference between the yield strength and the ultimate strength decreases for the increasing yield strength. Therefore, the maximum stresses in high-strength joints are lower when compared to the joints with mild-strength steel.

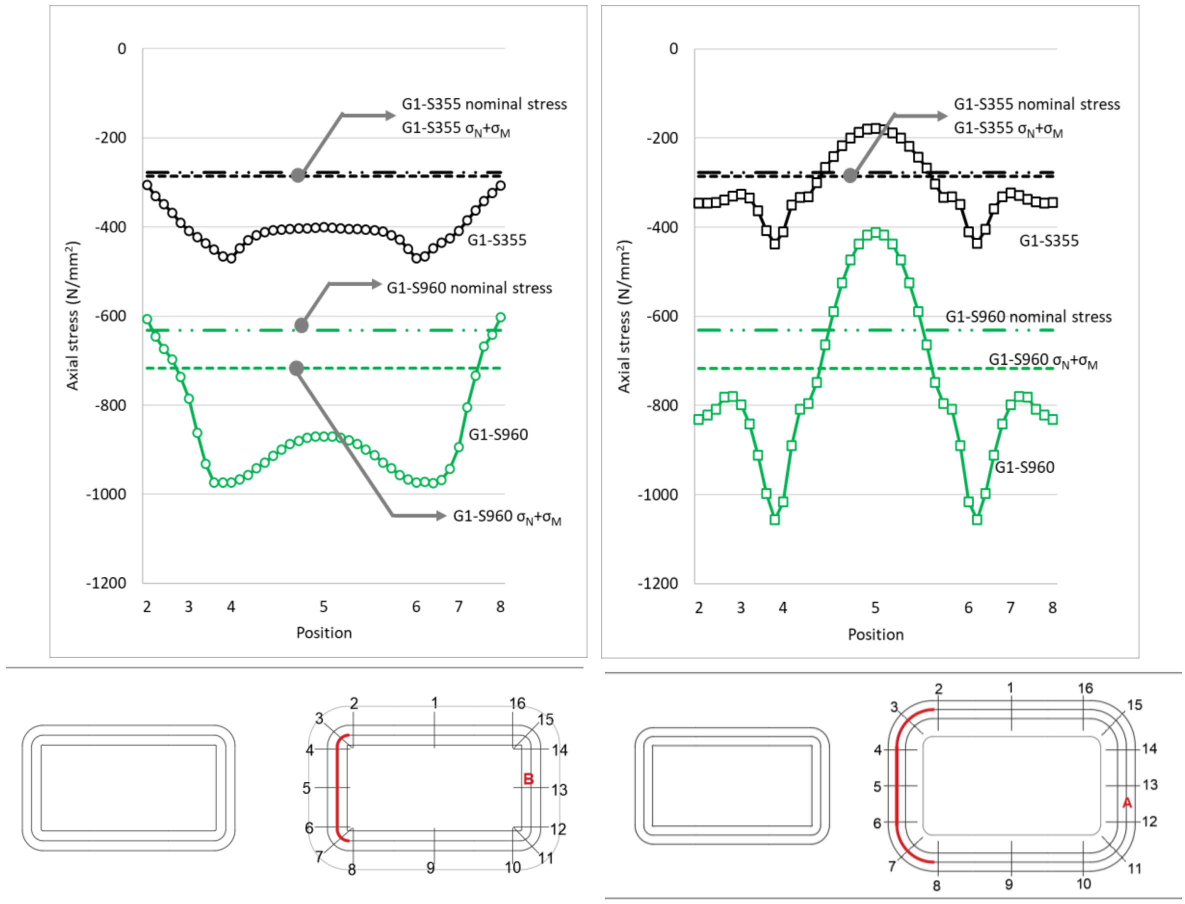

Figure 4-21: Stress distribution in position 2-8 (a)cross-section 1 and (b) cross-section 2

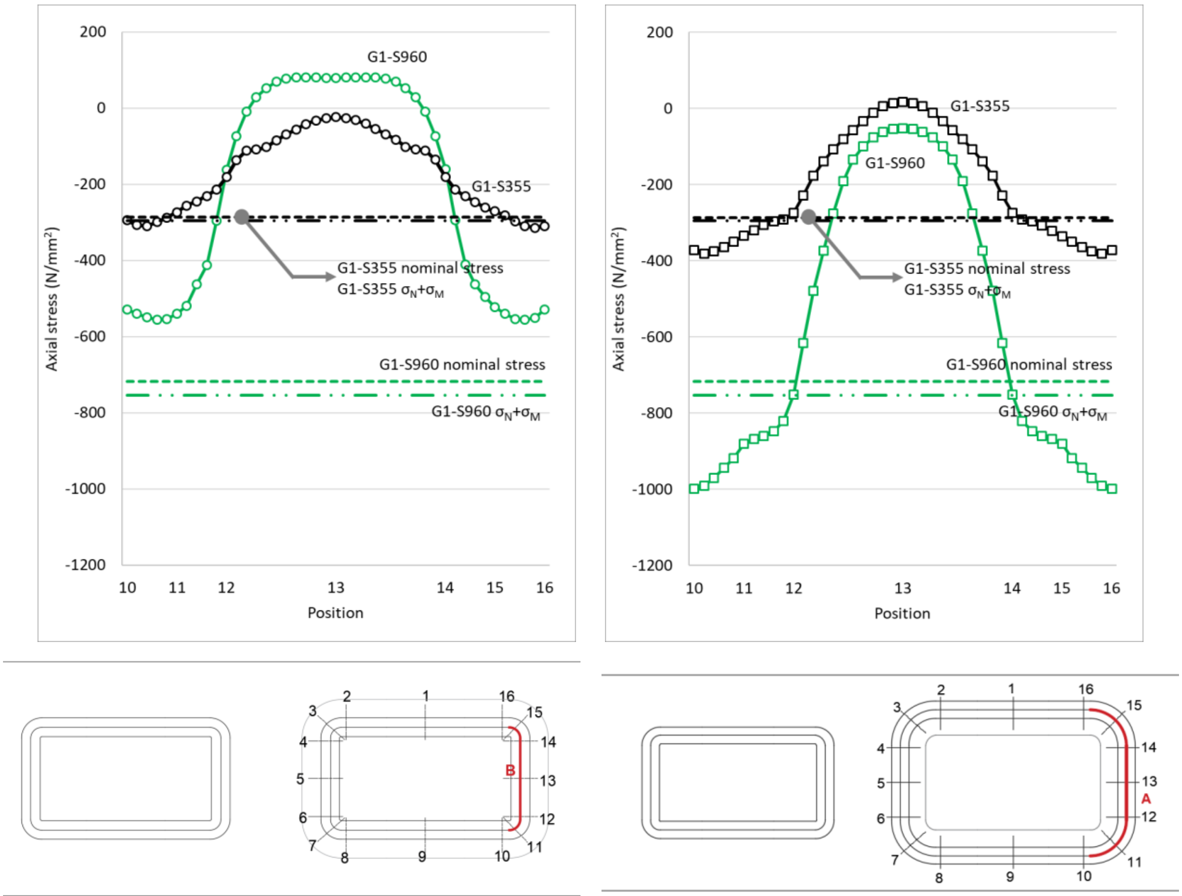

Figure 4-22: Stress distribution in cross-section 1 and 2 in the positions 10-16

.

4.3.3 Effect of the gap size

FE models with similar joint geometry, but different gap size is studied to investigate the impact of the gap on the high-strength hollow section joints (see **Table 4-10**). Two gap sizes, minimum gap size of 25 mm (G0) and an average gap of 40 mm (G1) are chosen to perform the numerical analysis.

Table 4-10: The joint geometry for two gap sizes

Geometry	b_o (mm)	t_o (mm)	b_i (mm)	t_i (mm)	θ_i (°)	e (mm)	g (mm)	β (-)	β_{mod} (-)
G0-S355	120	5	80	5	30	-6.60	25	0.67	0.78
G0-S460	120	5	80	5	30	-6.60	25	0.67	0.78
G0-S700	120	5	80	5	30	-6.60	25	0.67	0.81
G0-S960	120	5	80	5	30	-6.60	25	0.67	0.83
G1-S355	120	5	80	5	30	-2.26	40	0.67	0.78
G1-S460	120	5	80	5	30	-2.26	40	0.67	0.78
G1-S700	120	5	80	5	30	-2.26	40	0.67	0.81
G1-S960	120	5	80	5	30	-2.3	40	0.67	0.83

4.3.3.1 Ultimate load resistance

The load displacement curve for both joint geometries with different gap sizes are shown in **Figure 4-23**. As mentioned before, joints with lower gap sizes have larger stiffness and therefore higher resistance. This is also noticed in **Figure 4-23**. The FE models with the lower gap size result in larger ultimate load resistance. Moreover, the impact of lower gap size on the joint resistance increases with the yield strength. The ultimate load resistance for the FE model with steel grade G1-S355 is 421 kN and for G0-S355 445 kN. The model with the lower gap size, G0-S355 result in 6% larger ultimate load resistance than the model G1-S355. This percentage is also 6% for S460, 9% for S700 and 12% for S960.

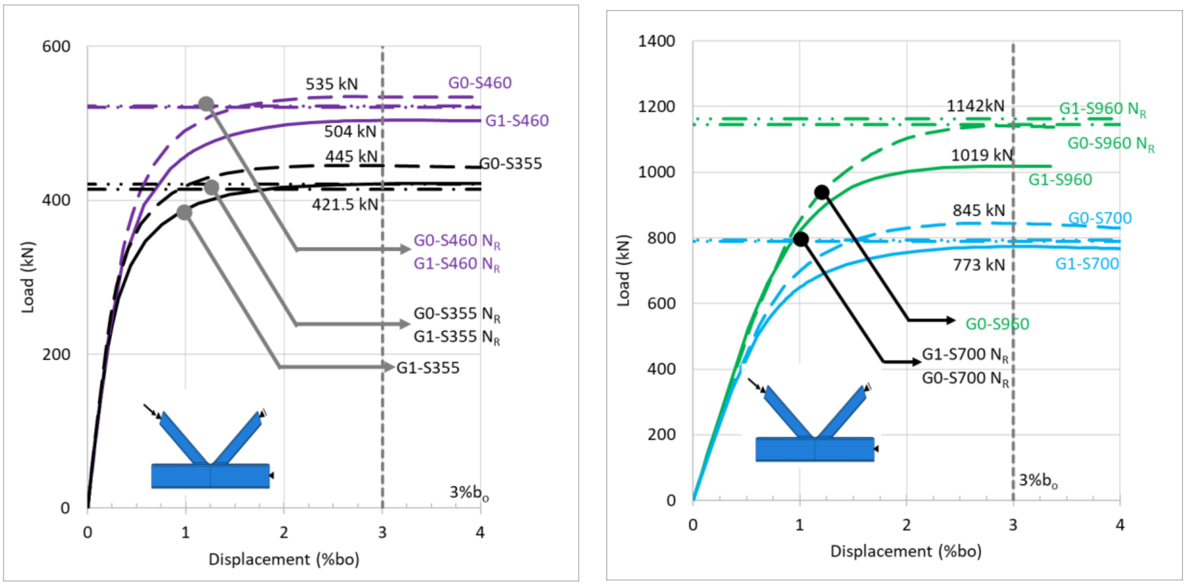

Figure 4-23: Load displacement relation for two gap sizes

Table 4-11: Joint resistance N_R without the material factors

Model	CFF (kN)	CSF (kN)	BF (kN)	PSF (kN)	Failure mode
G0-S355	414.48	586.51	494.00	975.72	CFF
G0-S460	520.92	691.78	582.67	1150.85	CFF
G0-S700	790.14	1004.59	846.13	1671.24	CFF
G0-S960	1144.66	1413.65	1190.67	2351.74	CFF
G1-S355	420.69	569.48	494.00	975.72	CFF
G1-S460	522.17	671.69	582.67	1150.85	CFF
G1-S700	792.41	975.42	846.13	1671.24	CFF
G1-S960	1162.36	1372.59	1190.67	2351.74	CFF

The resistance of the RHS gap K-joints is determined using the standard [4].**Table 4-11** summarizes the design resistance without considering the material reductions C_f and the partial safety factor γ_{m5}. **Table 4-12** compares the joint resistance with the FEA. The resistance for FE G1-S460, G1-S700 and G1-S960 is 2%-14% larger than the ultimate load resistance. The resistance for FE models with lower gap size (G0) is smaller or equal to the ultimate load resistance. The reduction factor (C_f) summarized in **Table 2-4** are considered to compare the design resistance with the ultimate load resistance. For FEM with steel grade above S700, a reduction factor of 0.8 is applied.

Table 4-12: Ratio resistance over failure load

Model	N_{FEA} (kN)	N_R (kN)	N_R/N_{FEA} (-)	$N_{R,Cf}/N_{FEA}$ (-)
G0-S355	445.11	414.48	0.93	0.93
G0-S460	534.74	520.92	0.97	0.88
G0-S700	845.17	790.14	0.93	0.75
G0-S960	1141.92	1144.66	1.00	0.80
G1-S355	421.49	420.69	1.00	1.00
G1-S460	503.99	522.17	1.04	0.93
G1-S700	773.35	792.41	1.02	0.82
G1-S960	1018.81	1162.36	1.14	0.91

4.3.3.2 Secondary bending moment in the brace member

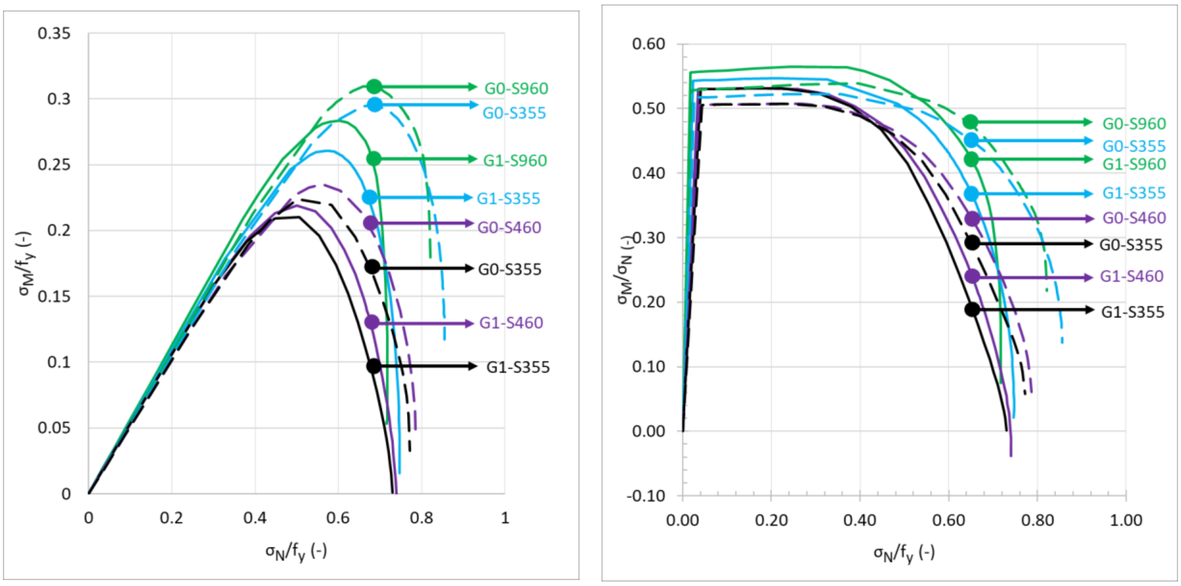

Figure 4-24: (a) Secondary bending stress and (b) level of the secondary bending stress

The secondary bending moment values for the different gap size is shown in **Figure 4-24**(a). As already mentioned, the FE models with high yield strength result in 23% to 30% higher secondary bending stresses. For each steel grade, the secondary bending stresses for the FE models with smaller gap size (G0) are higher than that of the models with larger gap size. The maximum secondary bending stress for the model G1-S960 is $0.28f_y$ and for G0-S960 is $0.31f_y$. Comparing both the gap sizes, the FE models with the smaller gap size result in 7% – 15% larger secondary bending moment. The largest percentage is obtained for joints with HSS and the lowest for joints with S355.

At ultimate load resistance the average stresses are $0.77f_y$ – $0.86f_y$ and $0.72f_y$ – $0.75f_y$ for joints with G0 and G1, respectively. The secondary bending stresses are maximum $0.06f_y$ for joints with mild strength steel. For joints with S700 and gap size G1 and G0, the secondary bending stresses are around $0.04\ f_y$ and $0.12f_y$, respectively. These stresses are around 0.06

f_y and $0.14f_y$ for FE G1-S960 and G0-S960, respectively. Joints with the smaller gap size (G0) and HSS, exhibit larger secondary bending stresses at ultimate load resistance.

Figure 4-24(b) shows and **Table 4-13** and **Table 4-14** summarize the level of secondary bending stresses ($\sigma_m/\sigma_{average}$) for all the models. Compared to the model with gap G1, the models with G0 result in lower $\sigma_m/\sigma_{average}$ ratio for low average stress and as the average stress increases the opposite was observed. Maximum $\sigma_m/\sigma_{average}$ ratio is around 53% – 56% for joints with larger gap size (G1) and 50%-54% for joints with lower gap size (G0). The models with larger gap G1 resulted in maximum 5% larger $\sigma_m/\sigma_{average}$ ratio when compared to FE models with smaller gap, G0. The largest percentage is obtained for joints with HSS. High $\sigma_m/\sigma_{average}$ ratio are obtained for average stresses up to $0.4f_y – 0.7f_y$.
At ultimate load resistance, for the FE models with S355 and S460 the $\sigma_m/\sigma_{average}$ ratio decreases to 5%. For the models G1-S700 and G0-S700, the $\sigma_m/\sigma_{average}$ ratio decreases to 5% and 14%, respectively. The largest $\sigma_m/\sigma_{average}$ ratio at failure is observed for the FE G0-S960 with 22%. At ultimate load resistance, larger $\sigma_m/\sigma_{average}$ ratio are obtained for joints with higher yield strength and lower gap size.

Table 4-13: Level of secondary stresses in the joints with gap size G0

G0-S355			G0-S460			G0-S700			G0-S960		
σ_N/f_y	σ_M/f_y	σ_M/σ_N	σ_N/f_y	σ_M/f_y	σ_M/σ_N	σ_N/f_y	σ_M/f_y	σ_M/σ_N	σ_N/f_y	σ_M/f_y	σ_M/σ_N
0	0	0	0	0	0	0	0	0	0	0	0
0.05	0.03	0.51	0.05	0.03	0.51	0.05	0.03	0.52	0.05	0.03	0.53
0.10	0.05	0.51	0.10	0.05	0.51	0.10	0.05	0.52	0.10	0.06	0.53
0.20	0.10	0.51	0.20	0.10	0.51	0.20	0.10	0.52	0.20	0.11	0.53
0.30	0.15	0.50	0.30	0.15	0.50	0.30	0.16	0.52	0.30	0.16	0.54
0.40	0.20	0.49	0.40	0.19	0.48	0.40	0.21	0.52	0.40	0.22	0.54
0.50	0.22	0.45	0.50	0.23	0.46	0.50	0.25	0.50	0.50	0.26	0.52
0.60	0.21	0.36	0.60	0.23	0.39	0.60	0.28	0.47	0.60	0.30	0.50
0.70	0.15	0.22	0.70	0.19	0.27	0.70	0.30	0.39	0.70	0.31	0.44
0.77	0.03	0.04	0.79	0.04	0.05	0.80	0.27	0.24	0.80	0.27	0.28
						0.86	0.12	0.14	0.82	0.18	0.22

Table 4-14: Level of secondary stresses in the joints with gap size G1

G1-S355			G1-S460			G1-S700			G1-S960		
σ_N/f_y	σ_M/f_y	σ_M/σ_N	σ_N/f_y	σ_M/f_y	σ_M/σ_N	σ_N/f_y	σ_M/f_y	σ_M/σ_N	σ_N/f_y	σ_M/f_y	σ_M/σ_N
0	0	0	0	0	0	0	0	0	0	0	0
0.05	0.03	0.53	0.05	0.03	0.53	0.05	0.03	0.54	0.05	0.03	0.55
0.10	0.05	0.53	0.10	0.05	0.53	0.10	0.05	0.54	0.10	0.06	0.56
0.20	0.11	0.53	0.20	0.11	0.53	0.20	0.11	0.55	0.20	0.11	0.56
0.30	0.16	0.52	0.30	0.16	0.53	0.30	0.16	0.55	0.30	0.17	0.56
0.40	0.20	0.49	0.40	0.19	0.49	0.50	0.25	0.50	0.40	0.22	0.56
0.50	0.21	0.42	0.50	0.21	0.43	0.50	0.25	0.50	0.50	0.26	0.53
0.60	0.17	0.28	0.60	0.19	0.32	0.60	0.26	0.43	0.60	0.28	0.47
0.70	0.07	0.09	0.70	0.10	0.14	0.70	0.19	0.28	0.70	0.22	0.32
0.73	0	0	0.74	0	0	0.75	0.04	0.05	0.72	0.06	0.08

4.3.4 Effect of the parameter β

To study the impact of the β on the high-strength hollow section joints, the parameter β is varied. (see **Table 4-15**). The three β values are 0.50, 0.57 and 0.64.

Table 4-15: The joint geometry for three β values

Geometry	b_0	t_0	b_i	t_i	θ_i	e	g	β	β_{mod}
	(mm)	(mm)	(mm)	(mm)	(°)	(mm)	(mm)	(-)	(-)
β1-S355	140	6.3	70	5	30	-18.04	40	0.5	0.60
β1-S460	140	6.3	70	5	30	-18.04	40	0.5	0.60
β1-S700	140	6.3	70	5	30	-18.04	40	0.5	0.62
β1-S960	140	6.3	70	5	30	-18.04	40	0.5	0.64
β2-S355	140	6.3	80	5	30	-12.26	40	0.57	0.67
β2-S460	140	6.3	80	5	30	-12.26	40	0.57	0.67
β2-S700	140	6.3	80	5	30	-12.26	40	0.57	0.69
β2-S960	140	6.3	80	5	30	-12.26	40	0.57	0.71
β3-S355	140	6.3	90	5	30	-6.49	40	0.64	0.74
β3-S460	140	6.3	90	5	30	-6.49	40	0.64	0.74
β3-S700	140	6.3	90	5	30	-6.49	40	0.64	0.76
β3-S960	140	6.3	90	5	30	-6.49	40	0.64	0.78

Ultimate load resistance

The load displacement curves for the three joint geometries with different β values are plotted in **Figure 4-25**. Joints with β_2 and β_3 obtained around 15% – 18% and 34% – 40% larger resistance when compared with joint with β_1. Largest difference is obtained for joints with steel grade S355 and the lowest for joints with S960. For all the steel grades, for the increasing β value, the ultimate load resistance increases. However, the effect of the large β-value on high-strength joints, are lower when compared to the joints with mild-strength steels.

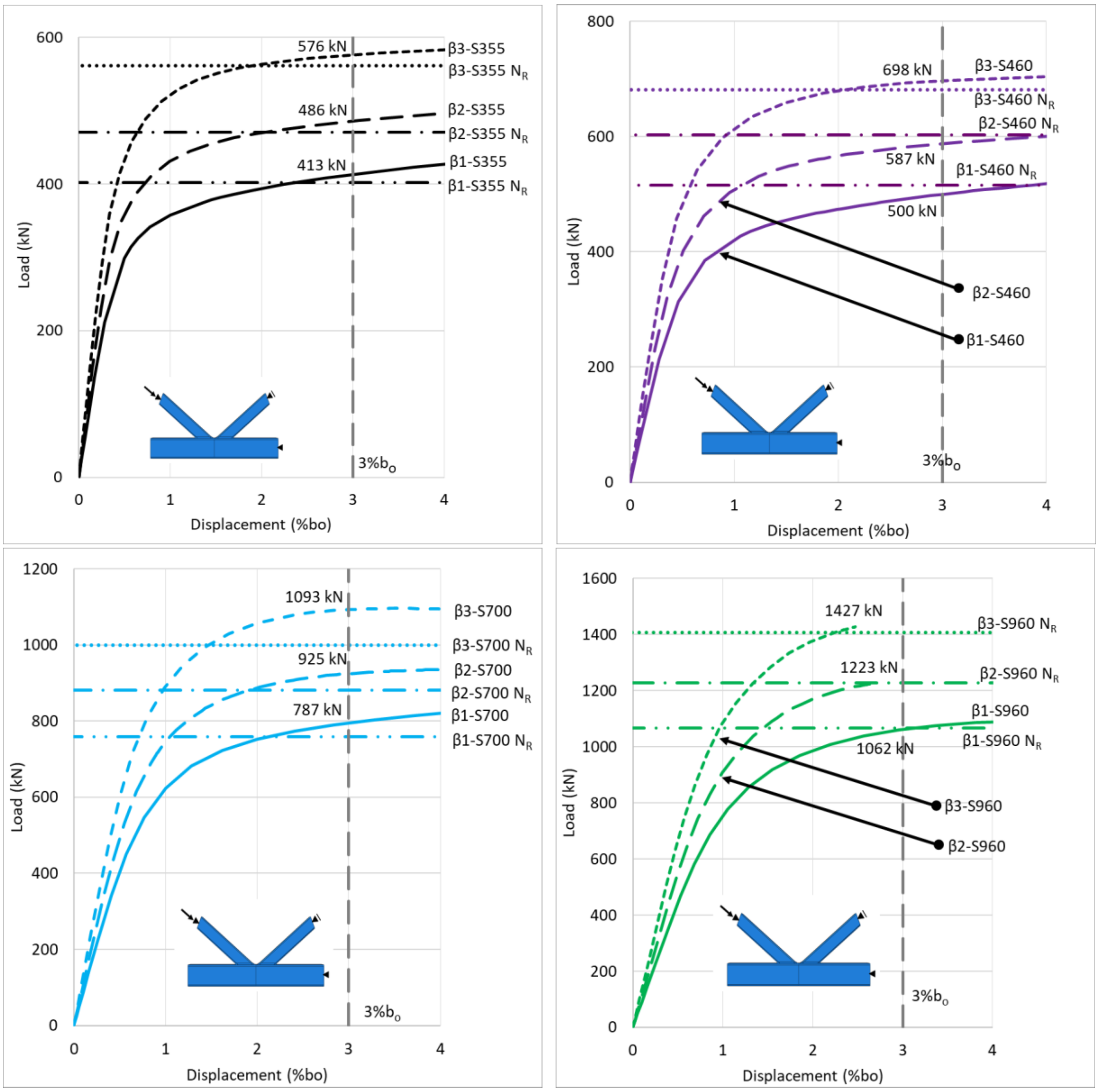

Figure 4-25: Load displacement curve for (a) S960, (b) S700, (c) S460 and (d) S355

Table 4-16 summarizes the joint resistance without considering the reductions. For each steel grade, larger β-values result in larger joint resistance. Chord face failure is the governing failure mode. The ratio between the joint resistance and the ultimate load resistance is summarized in **Table 4-17**. For the FE models with S355 the ratios are lower than 1.0. For the FE models with steel grade above S460, the ratios vary between 0.94 and 1.03. Compared to FEA, reduction factor summarized in **Table 2-4** are considered for the FEM. For FEM with steel grade S960, a reduction factor of 0.8 is applied. The reduced joint resistance is equal or lower than the numerical obtained ultimate load resistance.

Table 4-16: Joint resistance N_R without the material factors

Model	CFF (kN)	CSF (kN)	BF (kN)	PSF (kN)	Failure mode
β1-S355	402.25	848.07	447.90	1082.35	CFF
β1-S460	514.92	1000.28	528.29	1276.62	CFF
β1-S700	759.20	1452.59	767.16	1853.88	CFF
β1-S960	1067.22	2044.06	1079.54	2608.75	CFF
β2-S355	470.87	848.07	517.45	1236.98	CFF
β2-S460	602.69	1000.28	610.33	1459.00	CFF
β2-S700	881.43	1452.59	886.30	2118.72	CFF
β2-S960	1226.50	2044.06	1247.19	2981.43	CFF
β3-S355	561.48	848.07	587.01	1391.60	CFF
β3-S460	681.49	1000.28	692.37	1641.37	CFF
β3-S700	999.57	1452.59	1005.44	2383.56	CFF
β3-S960	1407.28	2044.06	1414.84	3354.11	CFF

Table 4-17: Ratio resistance over failure load for three β parameter

Model	N_{FEA} (kN)	N_R (kN)	N_R/N_{FEA} (-)	$N_{R.Cf}/N_{FEA}$ (-)
β1-S355	413.03	402.25	0.97	0.97
β1-S460	499.99	514.92	1.03	0.93
β1-S700	786.92	759.20	0.96	0.77
β1-S960	1061.02	1067.22	1.01	0.80
β2-S355	486.35	470.87	0.97	0.97
β2-S460	587.24	602.69	1.03	0.92
β2-S700	925.00	881.43	0.95	0.76
β2-S960	1223.20	1226.50	1.00	0.80
β3-S355	576.15	561.48	0.97	0.97
β3-S460	697.57	681.49	0.98	0.88
β3-S700	1092.94	999.57	0.91	0.73
β3-S960	1427.38	1407.28	0.99	0.79

4.3.4.1 Secondary bending moment in the brace members

The secondary bending moment values for different β values is shown in **Figure 4-26**. For each steel grade, larger β-values result in larger secondary bending moments. The maximum secondary bending moment for the models β_1-S355 was 0.16f_y, β_2-S355 is 0.19f_y and β_3-S355 was 0.23f_y. For the models β_1-S960, β_2-S960 and β_3-S960 the maximum secondary bending moments are 0.22f_y, 0.26f_y and 0.30f_y respectively. For each steel grade, compared to joins with β_1 larger secondary bending moment in the range of 14% – 28% and 33% – 41% are obtained for joints with β_2 values and β_3 values, respectively. The lowest percentage is obtained for S960 and the largest is obtained for S355. The impact of larger β-value on the secondary bending stresses in high-strength joints is lower when compared to mild-strength steel.

At ultimate load resistance the average stresses vary from 0.84f_y to 0.98f_y. At this load, the joints with mild-strength steel have obtained maximum 0.06f_y secondary bending stresses.

The secondary bending stresses are between $0.09f_y - 0.19f_y$ for joints with HSS. The largest is obtained for the FE β3-S960. Joints with HSS and larger β-value result in larger secondary bending stresses at ultimate load resistance.

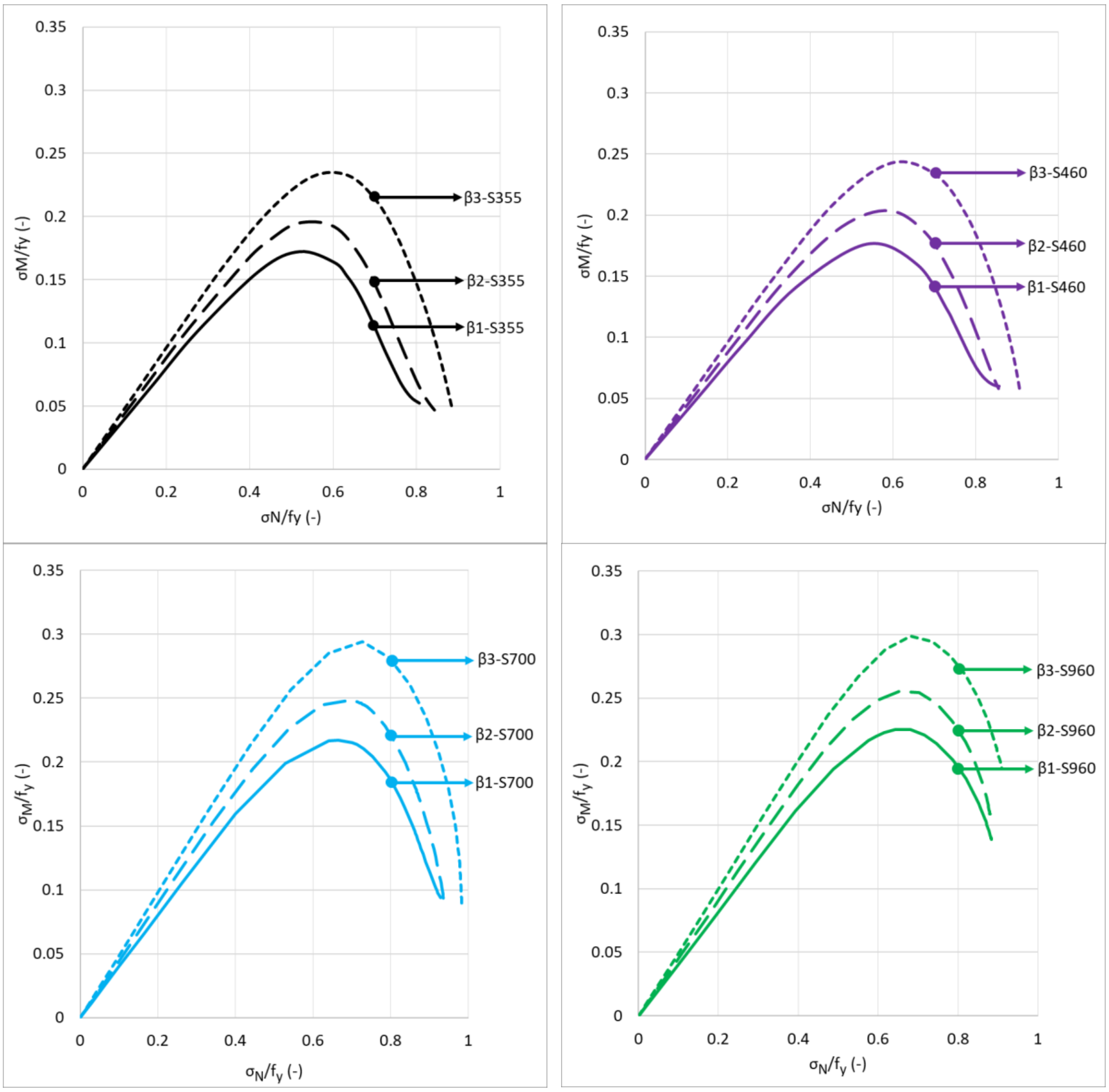

Figure 4-26: Secondary bending stress for (a) S355, (b)S460, (c)S700 and (d)S960

The level of secondary bending stress ($\sigma_m/\sigma_{average}$) for each steel grade is plotted in **Figure 4-27** and summarized in **Table 4-18** and **Table 4-20**. Up to the ultimate load resistance, the FE models with larger β-values result in larger level of secondary bending stresses. The maximum $\sigma_m/\sigma_{average}$ ratio is around 40%-41% for joints with β_1, around 42% – 44% for joints with β_2 and 48% – 50% for joints with β_3. Large values are obtained for joints with HSS and low values for joints with S355. Compared to joints with β_1, the maximum $\sigma_m/\sigma_{average}$ ratio for joints with β_2 and β_3 is around 10% – 13% and 20% – 23% larger. The lowest percentage is obtained for the joints with mild strength steel. Large $\sigma_m/\sigma_{average}$ ratios are obtained for average stresses up to $0.7f_y$.

At Ultimate load resistance, the $\sigma_m/\sigma_{average}$ ratio is maximum 6% for joints with S355, maximum 7% for joints with S460 and maximum 10% for joints with S700. The $\sigma_m/\sigma_{average}$ ratio is around 16% for β_1-S960, 18% for β_2-S960 and 21% for β_3-S960. For joints with steel grade S700 and S960 and larger β-value, large $\sigma_m/\sigma_{average}$ ratios at ultimate load resistance are observed.

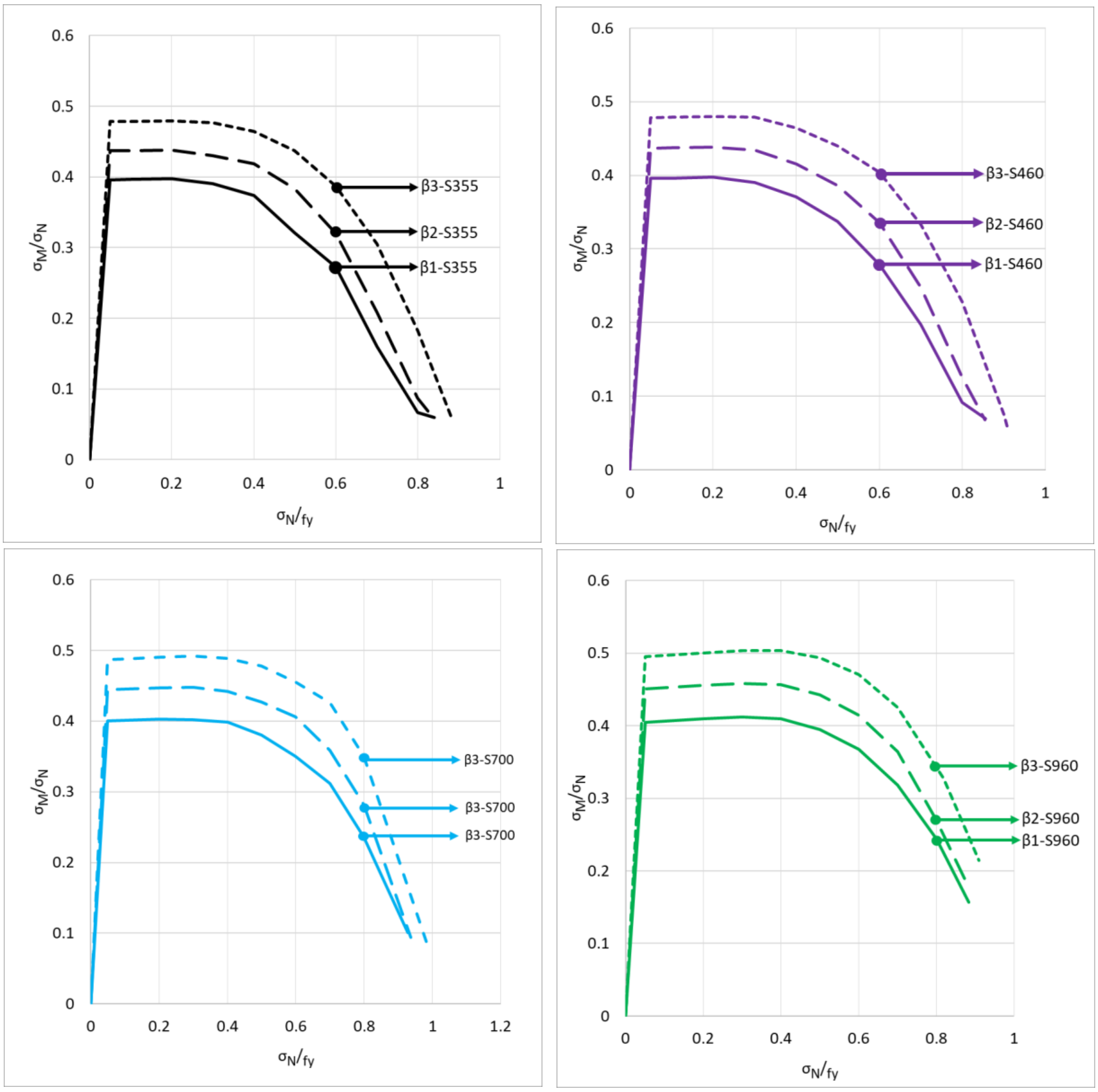

Figure 4-27: Level of secondary bending stress for (a)S355, (b)S460, (c)S700 and (d)S960

Table 4-18: Level of secondary bending stress for the FE models with β_1

β1-S355			β1-S460			β1-S700			β1-S960		
σ_N/f_y	σ_M/f_y	σ_M/σ_N	σ_N/f_y	σ_M/f_y	σ_M/σ_N	σ_N/f_y	σ_M/f_y	σ_M/σ_N	σ_N/f_y	σ_M/f_y	σ_M/σ_N
0	0	0	0	0	0	0	0	0	0	0	0
0.05	0.02	0.40	0.05	0.02	0.40	0.05	0.02	0.40	0.05	0.02	0.40
0.10	0.04	0.40	0.10	0.04	0.40	0.10	0.04	0.40	0.10	0.04	0.41
0.20	0.08	0.40	0.20	0.08	0.40	0.20	0.08	0.40	0.20	0.08	0.41
0.30	0.12	0.39	0.30	0.12	0.39	0.30	0.12	0.40	0.30	0.12	0.41
0.40	0.15	0.37	0.40	0.15	0.37	0.40	0.16	0.40	0.40	0.16	0.41
0.50	0.16	0.32	0.50	0.17	0.34	0.50	0.19	0.38	0.50	0.20	0.39
0.60	0.16	0.27	0.60	0.17	0.28	0.60	0.21	0.35	0.60	0.22	0.37
0.70	0.11	0.16	0.70	0.14	0.20	0.70	0.22	0.31	0.70	0.22	0.32
0.80	0.05	0.07	0.80	0.07	0.09	0.80	0.19	0.24	0.80	0.20	0.24
0.84	0.05	0.06	0.86	0.06	0.07	0.93	0.09	0.10	0.88	0.14	0.16

Table 4-19: Level of secondary bending stress for the FE models with β2

β2-S355			β2-S460			β2-S700			β2-S960		
σ_N/f_y	σ_M/f_y	σ_M/σ_N	σ_N/f_y	σ_M/f_y	σ_M/σ_N	σ_N/f_y	σ_M/f_y	σ_M/σ_N	σ_N/f_y	σ_M/f_y	σ_M/σ_N
0	0	0	0	0	0	0	0	0	0	0	0
0.05	0.02	0.44	0.05	0.02	0.44	0.05	0.02	0.44	0.05	0.02	0.45
0.10	0.04	0.44	0.10	0.04	0.44	0.10	0.04	0.45	0.10	0.05	0.45
0.20	0.09	0.44	0.20	0.09	0.44	0.20	0.09	0.45	0.20	0.09	0.46
0.30	0.13	0.43	0.30	0.13	0.43	0.30	0.13	0.45	0.30	0.14	0.46
0.40	0.17	0.42	0.40	0.17	0.42	0.40	0.18	0.44	0.40	0.18	0.46
0.50	0.19	0.38	0.50	0.19	0.39	0.50	0.21	0.43	0.50	0.22	0.44
0.60	0.19	0.32	0.60	0.20	0.34	0.60	0.24	0.41	0.60	0.25	0.41
0.70	0.15	0.21	0.70	0.17	0.25	0.70	0.25	0.36	0.70	0.26	0.36
0.80	0.07	0.09	0.80	0.10	0.13	0.80	0.23	0.28	0.80	0.22	0.27
0.84	0.05	0.06	0.85	0.06	0.07	0.94	0.09	0.09	0.88	0.16	0.18

Table 4-20: Level of secondary bending stress for the FE models with β_3

β3-S355			β3-S460			β3-S700			β3-S960		
σ_N/f_y	σ_M/f_y	σ_M/σ_N	σ_N/f_y	σ_M/f_y	σ_M/σ_N	σ_N/f_y	σ_M/f_y	σ_M/σ_N	σ_N/f_y	σ_M/f_y	σ_M/σ_N
0	0	0	0	0	0	0	0	0	0	0	0
0.05	0.02	0.48	0.05	0.02	0.48	0.05	0.02	0.49	0.05	0.02	0.50
0.10	0.05	0.48	0.10	0.05	0.48	0.10	0.05	0.49	0.10	0.05	0.50
0.20	0.10	0.48	0.20	0.10	0.48	0.20	0.10	0.49	0.20	0.10	0.50
0.30	0.14	0.48	0.30	0.14	0.48	0.30	0.15	0.49	0.30	0.15	0.50
0.40	0.19	0.46	0.40	0.19	0.46	0.40	0.20	0.49	0.40	0.20	0.50
0.50	0.22	0.44	0.50	0.22	0.44	0.50	0.24	0.48	0.50	0.25	0.49
0.60	0.23	0.39	0.60	0.24	0.40	0.60	0.27	0.46	0.60	0.28	0.47
0.70	0.21	0.31	0.70	0.23	0.33	0.70	0.30	0.43	0.70	0.30	0.42
0.80	0.15	0.18	0.80	0.18	0.23	0.80	0.28	0.35	0.82	0.27	0.33
0.88	0.05	0.05	0.90	0.07	0.07	0.98	0.09	0.09	0.91	0.19	0.21
			0.91	0.05	0.06						

4.3.5 Effect of the weld

To study the impact of the weld on the high-strength hollow section joints, the weld type (fillet weld and butt weld) is varied. Three joint geometries are used to study the impact of the weld on high-strength RHS joints (see **Table 4-21** to **Table 4-23**).

Table 4-21: The joint geometry for β1

Geometry	b_0	t_0	b_i	t_i	θ_i	e	g	β	β_{mod}
	(mm)	(mm)	(mm)	(mm)	(°)	(mm)	(mm)	(-)	(-)
β1-S355	140	6.3	70	5	30	-18.04	40	0.5	0.60
β1-S460	140	6.3	70	5	30	-18.04	40	0.5	0.60
β1-S700	140	6.3	70	5	30	-18.04	40	0.5	0.62
β1-S960	140	6.3	70	5	30	-18.04	40	0.5	0.64
β1-S355B	140	6.3	70	5	30	-18.04	40	0.5	
β1-S460B	140	6.3	70	5	30	-18.04	40	0.5	
β1-S700B	140	6.3	70	5	30	-18.04	40	0.5	
β1-S960B	140	6.3	70	5	30	-18.04	40	0.5	

Table 4-22: The joint geometry for β_2

Geometry	b_0	t_0	b_i	t_i	θ_i	e	g	β	β_{mod}
	(mm)	(mm)	(mm)	(mm)	(°)	(mm)	(mm)	(-)	(-)
β2-S355	140	6.3	80	5	30	-12.26	40	0.57	0.67
β2-S460	140	6.3	80	5	30	-12.26	40	0.57	0.67
β2-S700	140	6.3	80	5	30	-12.26	40	0.57	0.69
β2-S960	140	6.3	80	5	30	-12.26	40	0.57	0.71
β2-S355B	140	6.3	80	5	30	-12.26	40	0.57	
β2-S460B	140	6.3	80	5	30	-12.26	40	0.57	
β2-S700B	140	6.3	80	5	30	-12.26	40	0.57	
β2-S960B	140	6.3	80	5	30	-12.26	40	0.57	

Table 4-23: The joint geometry for β_3

Geometry	b_0	t_0	b_i	t_i	θ_i	e	g	β	β_{mod}
	(mm)	(mm)	(mm)	(mm)	(°)	(mm)	(mm)	(-)	(-)
β3-S355	140	6.3	90	5	30	-6.49	40	0.64	0.74
β3-S460	140	6.3	90	5	30	-6.49	40	0.64	0.74
β3-S700	140	6.3	90	5	30	-6.49	40	0.64	0.76
β3-S960	140	6.3	90	5	30	-6.49	40	0.64	0.78
β3-S355B	140	6.3	90	5	30	-6.49	40	0.64	
β3-S460B	140	6.3	90	5	30	-6.49	40	0.64	
β3-S700B	140	6.3	90	5	30	-6.49	40	0.64	
β3-S960B	140	6.3	90	5	30	-6.49	40	0.64	

4.3.5.1 Effect of the weld for parameter β1

Ultimate load resistance

The load displacement curves for similar joint geometry with different weld types are plotted in **Figure 4-28**. Noticeable is the strength difference between the FE models with butt and fillet welds. The fillet-welded joints result in approximately 37% for S960, 28% for S700, 20% for S460 and 18% for S355 larger ultimate load resistance than the butt-welded joints. This is due to the additional stiffness introduced by the fillet welds. The largest difference is obtained for the models with high strength steel S960.

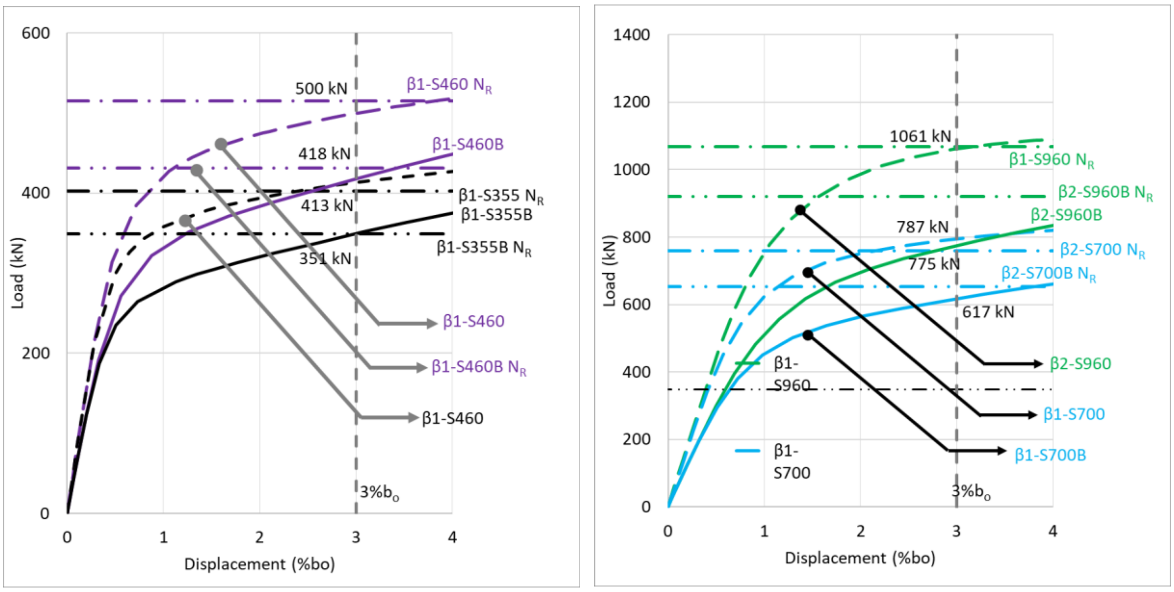

Figure 4-28: Load displacement curve for FE models with β_1

Table 4-24: Joint resistance N_R for joints with β_1

model	CFF (kN)	CSF (kN)	BF (kN)	PSF (kN)	Failure mode
β1-S355	402.25	848.07	447.90	1082.35	CFF
β1-S460	514.92	1000.28	528.29	1276.62	CFF
β1-S700	759.20	1452.59	767.16	1853.88	CFF
β1-S960	1067.22	2044.06	1079.54	2608.75	CFF
β1-S355B	348.93	848.07	447.90	1082.35	CFF
β1-S460B	431.33	1000.28	528.29	1276.62	CFF
β1-S700B	653.34	1452.59	767.16	1853.88	CFF
β1-S960B	920.66	2044.06	1079.54	2608.75	CFF

Table 4-24 summarizes the design resistance without considering the reductions recommended by the standard [4]. The governing failure mode is the chord face failure. The design resistance and the ultimate load resistance is summarized in **Table 4-25**. Compared to the fillet-welded joints, high ratios are observed for the butt-welded joints.
The resistance for β1-S460 and β1-S460B is 3% larger than the ultimate load resistance. The resistance for β1-S700B and β1-S960B is 6% and 19% larger than the ultimate load resistance. Reduction factors summarized in **Table 2-4** are considered for the FEM. For FEM

with steel grade S960, a reduction factor of 0.8 is applied. These material reductions parameters are consistent with the material reduction parameters recommended by the proposed 2020 version of the Eurocode 3 part 1-8 [4]. Also, the additional recommendation for the yield strength ($f_y \leq 0.8f_u$) is considered in the design resistance. Due to these reductions, the design resistance is smaller or equal to the ultimate load resistance

Table 4-25: Ratio resistance over failure load for joints β_1

Model	N_{FEA} (kN)	N_R (kN)	N_R/N_{FEA} (-)	$N_{R.Cf}/N_{FEA}$ (-)
β1-S355	413.03	402.25	0.97	0.97
β1-S460	499.99	514.92	1.03	0.93
β1-S700	786.92	759.20	0.96	0.77
β1-S960	1061.02	1067.22	1.01	0.80
β1-S355B	351.16	348.93	0.99	0.99
β1-S460B	418.20	431.33	1.03	0.93
β1-S700B	616.53	653.34	1.06	0.85
β1-S960B	774.53	920.66	1.19	0.95

Secondary bending stress

The interaction between the average load and the secondary bending stress for the different weld type is shown in **Figure 4-29(a)**. For each steel grade and for average stresses up to $0.2f_y$ small difference in the secondary bending stress is observed. For average stress above $0.2f_y$, the secondary bending stresses for the fillet-welded joints are larger than for the butt-welded joints. This is due to the uneven stiffness distribution of the weld and the one-sided fillet welds.

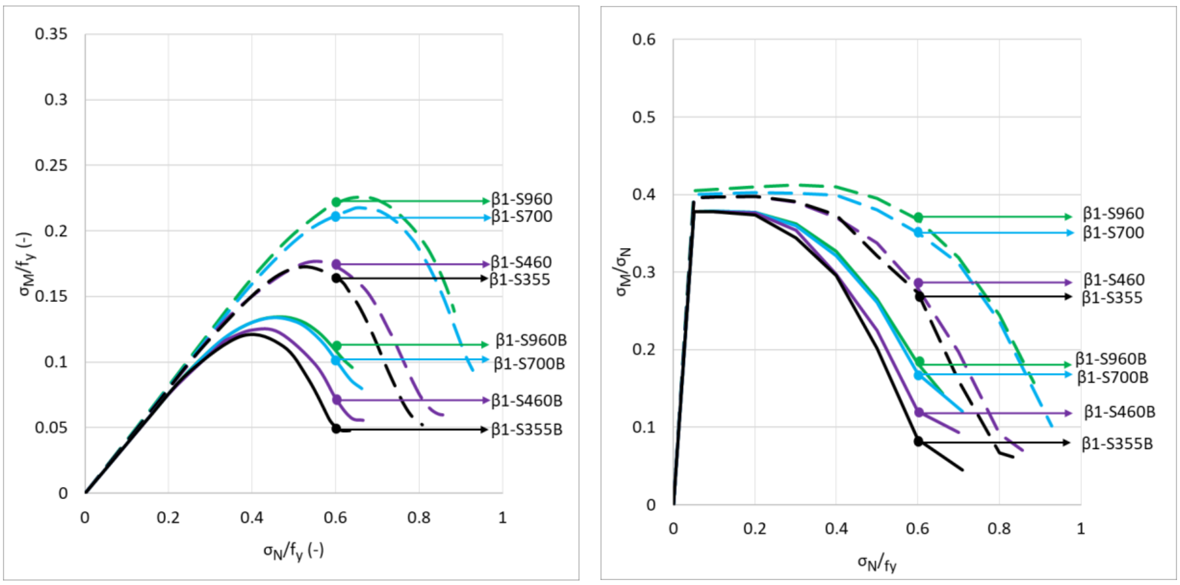

Figure 4-29: (a) Secondary bending stress and (b) level of secondary bending stress

The maximum secondary bending stresses for the butt-welded joints and the fillet-welded joints are in the range of $0.12f_y$ – $0.13f_y$ and $0.16f_y$ – $0.22f_y$, respectively. The largest is obtained for joints with S960 and the lowest for S355. The maximum secondary bending stresses for β_1-S355 is 37% larger than that for β_1-S355B. For β_1-S460, β_1-S700 and β_1-S960

the maximum secondary bending stresses are 44%, 58% and 69%, respectively larger when compared to the butt-welded joints. For higher yield strength, the fillet welded joints result in larger secondary bending stresses.
At ultimate load resistance the average stresses (N_{FEA}/A) are around $0.66f_y$ – $0.71f_y$ and $0.84f_y$ – $0.93f_y$ for the butt-welded joints and the fillet-welded joints. At this load the secondary bending stresses are maximum $0.07f_y$ for joints with mild-strength steel. For the butt-welded joints with HSS the secondary bending stresses are $0.09f_y$, whereas the secondary bending stresses are $0.09f_y$ and $0.14f_y$ for the fillet welded joints with S700 and S960, respectively.

Figure 4-29(b) shows the level of secondary bending stresses ($\sigma_m/\sigma_{average}$) obtained for each model. The $\sigma_m/\sigma_{average}$ ratios for fillet welded joints are larger than for the butt-welded joints. **Table 4-26** and **Table 4-27** summarize the level of secondary bending stresses in the joints. The maximum $\sigma_m/\sigma_{average}$ ratio is in the range 40% – 41% for the fillet-welded joints. This level is around 38% for all the butt-welded joints. The maximum $\sigma_m/\sigma_{average}$ ratio for the fillet welded joint β_1-S960 is 8% larger when compared to the butt-welded joint β_1-S960B. This percentage is around 5% for the other models. Large $\sigma_m/\sigma_{average}$ ratios are obtained for average stresses up to $0.5f_y$.
At ultimate load resistance the $\sigma_m/\sigma_{average}$ ratio is in the range of 5% – 9% for FE models with mild-strength steels, 10% – 12% for joints with S700 and 14% – 16% for joints with S960. Compared to butt-welded joints, the secondary bending stresses and the $\sigma_m/\sigma_{average}$ ratios are larger for the fillet welded joints. The large secondary bending stresses at ultimate load resistance for the high-strength hollow sections joints should be considered in the design.

Table 4-26: Level of secondary bending stress for the fillet-welded joints with β_1

β1-S355			β1-S460			β1-S700			β1-S960		
σ_N/f_y	σ_M/f_y	σ_M/σ_N	σ_N/f_y	σ_M/f_y	σ_M/σ_N	σ_N/f_y	σ_M/f_y	σ_M/σ_N	σ_N/f_y	σ_M/f_y	σ_M/σ_N
0	0	0	0	0	0	0	0	0	0	0	0
0.05	0.02	0.40	0.05	0.02	0.40	0.05	0.02	0.40	0.05	0.02	0.40
0.10	0.04	0.40	0.10	0.04	0.40	0.10	0.04	0.40	0.10	0.04	0.41
0.20	0.08	0.40	0.20	0.08	0.40	0.20	0.08	0.40	0.20	0.08	0.41
0.30	0.12	0.39	0.30	0.12	0.39	0.30	0.12	0.40	0.30	0.12	0.41
0.40	0.15	0.37	0.40	0.15	0.37	0.40	0.16	0.40	0.40	0.16	0.41
0.50	0.16	0.32	0.50	0.17	0.34	0.50	0.19	0.38	0.50	0.20	0.39
0.60	0.16	0.27	0.60	0.17	0.28	0.60	0.21	0.35	0.60	0.22	0.37
0.70	0.11	0.16	0.70	0.14	0.20	0.70	0.22	0.31	0.70	0.22	0.32
0.80	0.05	0.07	0.80	0.07	0.09	0.80	0.19	0.24	0.80	0.20	0.24
0.84	0.05	0.06	0.86	0.06	0.07	0.93	0.09	0.10	0.88	0.14	0.16

Table 4-27: Level of secondary bending stress for the butt-welded joints with β_1

β1-S355B			β1-S460B			β1-S700B			β1-S960B		
σ_N/f_y	σ_M/f_y	σ_M/σ_N	σ_N/f_y	σ_M/f_y	σ_M/σ_N	σ_N/f_y	σ_M/f_y	σ_M/σ_N	σ_N/f_y	σ_M/f_y	σ_M/σ_N
0	0	0	0	0	0	0	0	0	0	0	0
0.05	0.02	0.38	0.05	0.02	0.38	0.05	0.02	0.38	0.05	0.02	0.38
0.10	0.04	0.38	0.10	0.04	0.38	0.10	0.04	0.38	0.10	0.04	0.38
0.20	0.07	0.37	0.20	0.08	0.38	0.20	0.08	0.38	0.20	0.08	0.38
0.30	0.10	0.34	0.30	0.11	0.35	0.30	0.11	0.36	0.30	0.11	0.36
0.40	0.12	0.30	0.40	0.12	0.30	0.40	0.13	0.32	0.40	0.13	0.33
0.50	0.10	0.20	0.50	0.11	0.23	0.50	0.13	0.26	0.50	0.13	0.27
0.60	0.05	0.08	0.60	0.07	0.12	0.60	0.10	0.17	0.60	0.11	0.18
0.71	0.07	0.05	0.70	0.07	0.09	0.71	0.09	0.12	0.66	0.09	0.14

4.3.5.2 Effect of the weld for the parameter β2

Ultimate load resistance

Figure 4-30 shows the load displacement curves for joints with different weld type and parameter β_2. The FE models with fillet welds result in approximately 33% for S960, 26% for S700, 17% for S460 and S355 larger ultimate load resistance when compared with butt-welded joints. Largest differences are obtained for the high-strength steel S700 and S960.

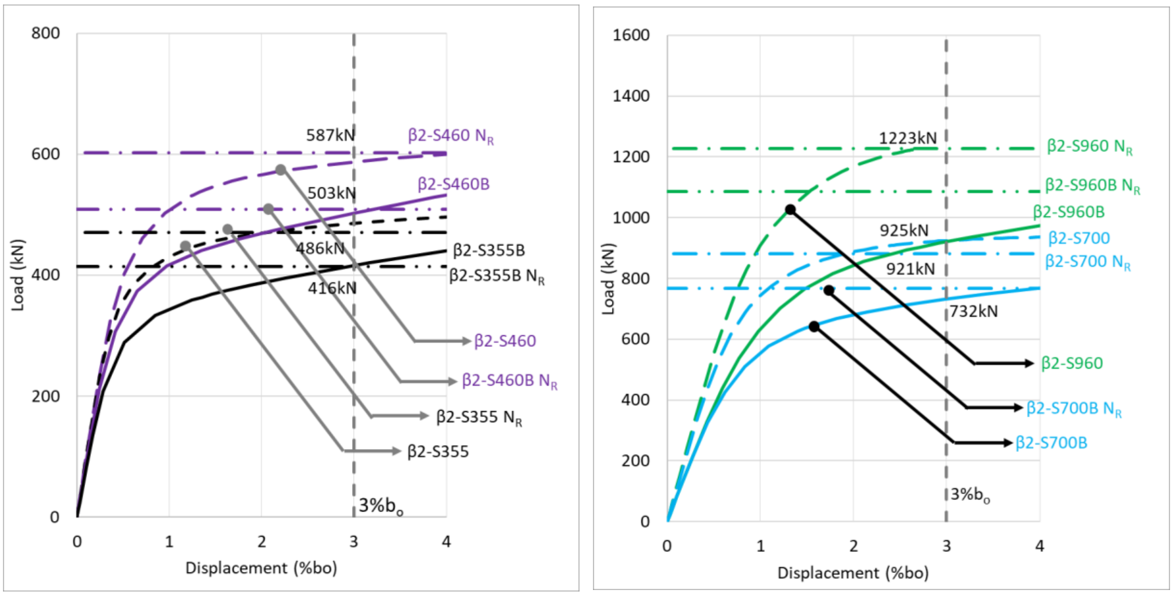

Figure 4-30: Load displacement curve for FE models with different weld type and β_2

Figure 4-28 summarizes the design resistance which should be considered for hollow section joints within the validity range. The material factor and the partial safety factor are not considered. For the butt-welded and fillet-welded joints, the governing failure mode is the chord face failure. The joint design resistance and the ultimate load resistance is summarized in **Table 4-29**. Compared to the resistance, the FE β2-S960B, β2-S700B, β2-S460B and β2-S460 obtained lower ultimate load resistance. Differences up to 18% are obtained. Compared to the fillet-welded joints, higher ratios are observed for the butt-welded joints. Reduction 0.8 for steel grade S960 and S700, 0.9 for steel grade S460 and 1.0 for steel grade S355 are considered for the FEM. These reductions are consistent with the material reduction factors summarized in **Table 2-4**. The ratio design resistance $N_{R;Cf}$ over the ultimate load resistance were lower than 1.0.

Table 4-28: Design resistance for joints with β_2

Model	CFF (kN)	CSF (kN)	BF (kN)	PSF (kN)	Failure mode
β2-S355	470.87	848.07	517.45	1236.98	CFF
β2-S460	602.69	1000.28	610.33	1459.00	CFF
β2-S700	881.43	1452.59	886.30	2118.72	CFF
β2-S960	1226.50	2044.06	1247.19	2981.43	CFF
β2-S355B	414.73	848.07	517.45	1236.98	CFF
β2-S460B	509.25	1000.28	610.33	1459.00	CFF
β2-S700B	766.73	1452.59	886.30	2118.72	CFF
β2-S960B	1085.33	2044.06	1247.19	2981.43	CFF

Table 4-29: Ratio resistance over failure load for joints with β_2

Model	N_{FEA} (kN)	N_R (kN)	N_R/N_{FEA} (-)	$N_{R.Cf}/N_{FEA}$ (-)
β2-S355	486.35	470.87	0.97	0.97
β2-S460	587.24	602.69	1.03	0.92
β2-S700	925.00	881.43	0.95	0.76
β2-S960	1223.20	1226.50	1.00	0.80
β2-S355B	415.72	414.73	1.00	1.00
β2-S460B	503.63	509.25	1.01	0.91
β2-S700B	731.74	766.73	1.05	0.84
β2-S960B	921.12	1085.33	1.18	0.94

Secondary bending stresses

The secondary bending stress values is shown in **Figure 4-31**. The maximum secondary bending stress for the butt-welded joints and the fillet-welded joints are around $0.13f_y$ – $0.17f_y$ and $0.19f_y$ – $0.26f_y$. The largest is obtained for joints with S960 and the lowest for S355. The maximum secondary bending stress for β_1-S355 was 42% larger than that for β_1-S355B. For β_1-S460, β_1-S700 and β_1-S960 the maximum secondary bending stress are 38%, 60% and 60%, respectively larger when compared to the butt-welded joints. For higher yield strength, the fillet welded joints result in larger secondary bending stresses.

At ultimate load resistance the average stresses are around $0.67f_y$ – $0.74f_y$ and $0.84f_y$ – $0.88f_y$ for the butt-welded joints and the fillet-welded joints. For this load, the secondary bending stresses are maximum $0.06f_y$ for joints with mild-strength steel. For the butt-welded joints with HSS the secondary bending stresses are maximum $0.08\ f_y$, whereas the secondary bending stresses are $0.09\ f_y$ and $0.16\ f_y$ for the fillet welded joints with S700 and S960, respectively.

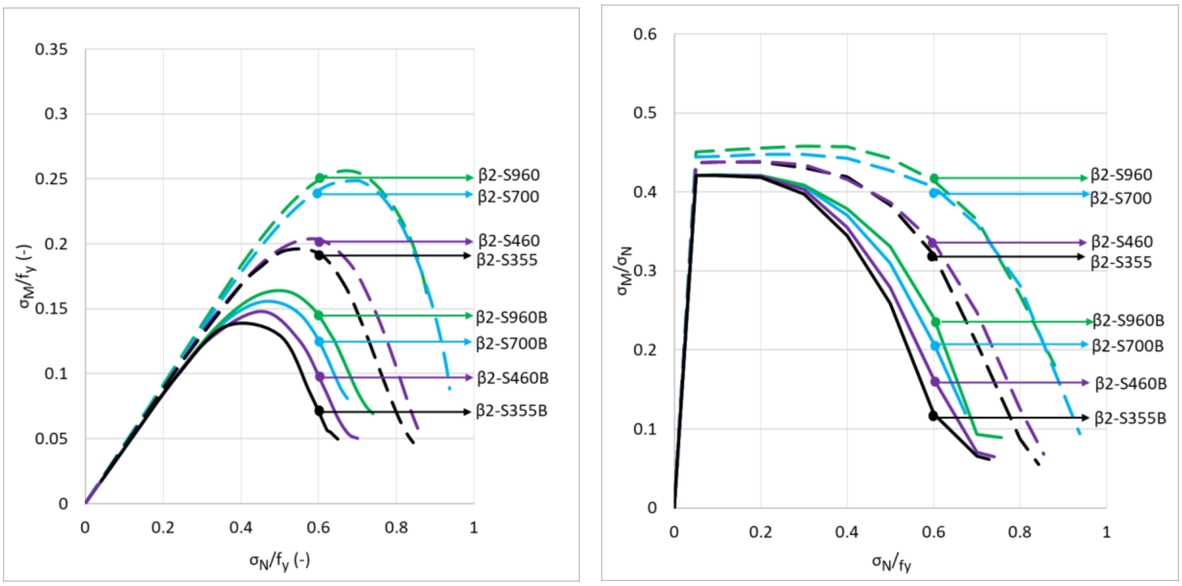

Figure 4-31: (a) Secondary bending stress and (b)level of secondary bending stress

Figure 4-31(b) shows the level of secondary bending stresses ($\sigma_m/\sigma_{average}$) obtained for each model and **Table 4-30** and **Table 4-31** summarize the $\sigma_m/\sigma_{average}$ ratios for the joints. The maximum $\sigma_m/\sigma_{average}$ ratio is 42% for all the butt-welded joints and varies from 44% to 46% for the fillet-welded joints. The maximum $\sigma_m/\sigma_{average}$ ratio for the fillet welded joint β_1-S700 and β_1-S960 is 7% and 10%, respectively larger when compared to the butt-welded joints. Lower differences are obtained for the joints with mild-strength steels. Large $\sigma_m/\sigma_{average}$ ratio is obtained for average stress up to $0.7f_y$. At ultimate load resistance, the $\sigma_m/\sigma_{average}$ ratio is maximum 7% and 9% for FE models with mild-strength steel and steel grade S700, respectively. The largest $\sigma_m/\sigma_{average}$ ratio at failure is obtained for the models β_1-S960B and β_1-S960 with 12% 18%, respectively.

Table 4-30: Level of secondary bending stress for the fillet-welded joints with β_2

β2-S355			β2-S460			β2-S700			β2-S960		
σ_N/f_y	σ_M/f_y	σ_M/σ_N	σ_N/f_y	σ_M/f_y	σ_M/σ_N	σ_N/f_y	σ_M/f_y	σ_M/σ_N	σ_N/f_y	σ_M/f_y	σ_M/σ_N
0	0	0	0	0	0	0	0	0	0	0	0
0.05	0.02	0.44	0.05	0.02	0.44	0.05	0.02	0.44	0.05	0.02	0.45
0.10	0.04	0.44	0.10	0.04	0.44	0.10	0.04	0.45	0.10	0.05	0.45
0.20	0.09	0.44	0.20	0.09	0.44	0.20	0.09	0.45	0.20	0.09	0.46
0.30	0.13	0.43	0.30	0.13	0.43	0.30	0.13	0.45	0.30	0.14	0.46
0.40	0.17	0.42	0.40	0.17	0.42	0.40	0.18	0.44	0.40	0.18	0.46
0.50	0.19	0.38	0.50	0.19	0.39	0.50	0.21	0.43	0.50	0.22	0.44
0.60	0.19	0.32	0.60	0.20	0.34	0.60	0.24	0.41	0.60	0.25	0.41
0.70	0.15	0.21	0.70	0.17	0.25	0.70	0.25	0.36	0.70	0.26	0.36
0.80	0.07	0.09	0.80	0.10	0.13	0.80	0.23	0.28	0.80	0.22	0.27
0.84	0.05	0.06	0.85	0.06	0.07	0.94	0.09	0.09	0.88	0.16	0.18

Table 4-31: Level of secondary bending stress for the butt-welded joints with β_2

β2-S355B			β2-S460B			β2-S700B			β2-S960B		
σ_N/f_y	σ_M/f_y	σ_M/σ_N	σ_N/f_y	σ_M/f_y	σ_M/σ_N	σ_N/f_y	σ_M/f_y	σ_M/σ_N	σ_N/f_y	σ_M/f_y	σ_M/σ_N
0	0	0	0	0	0	0	0	0	0	0	0
0.05	0.02	0.42	0.05	0.02	0.42	0.05	0.02	0.42	0.05	0.02	0.42
0.10	0.04	0.42	0.10	0.04	0.42	0.10	0.04	0.42	0.10	0.04	0.42
0.20	0.08	0.42	0.20	0.08	0.42	0.20	0.08	0.42	0.20	0.08	0.42
0.30	0.12	0.40	0.30	0.12	0.40	0.30	0.12	0.41	0.30	0.12	0.41
0.40	0.13	0.34	0.40	0.14	0.35	0.40	0.15	0.38	0.40	0.15	0.37
0.50	0.13	0.26	0.50	0.14	0.28	0.50	0.17	0.33	0.50	0.15	0.31
0.60	0.07	0.12	0.60	0.10	0.16	0.60	0.14	0.24	0.60	0.12	0.21
0.70	0.05	0.07	0.70	0.05	0.07	0.70	0.07	0.09	0.67	0.08	0.12
0.73	0.04	0.06	0.74	0.05	0.06	0.76	0.07	0.09			

4.3.5.3 Effect of the weld for the parameter β_3

Ultimate load resistance

Figure 4-32 shows the load displacement curves for joints with different weld type and β_3. The FE models with fillet welds result in approximately 30% for S960, 26% for S700, 18% for S460 and 16% for S355 larger joint resistance when compared to models with butt welds. Larger differences are obtained for the high strength steel S900 and S700.

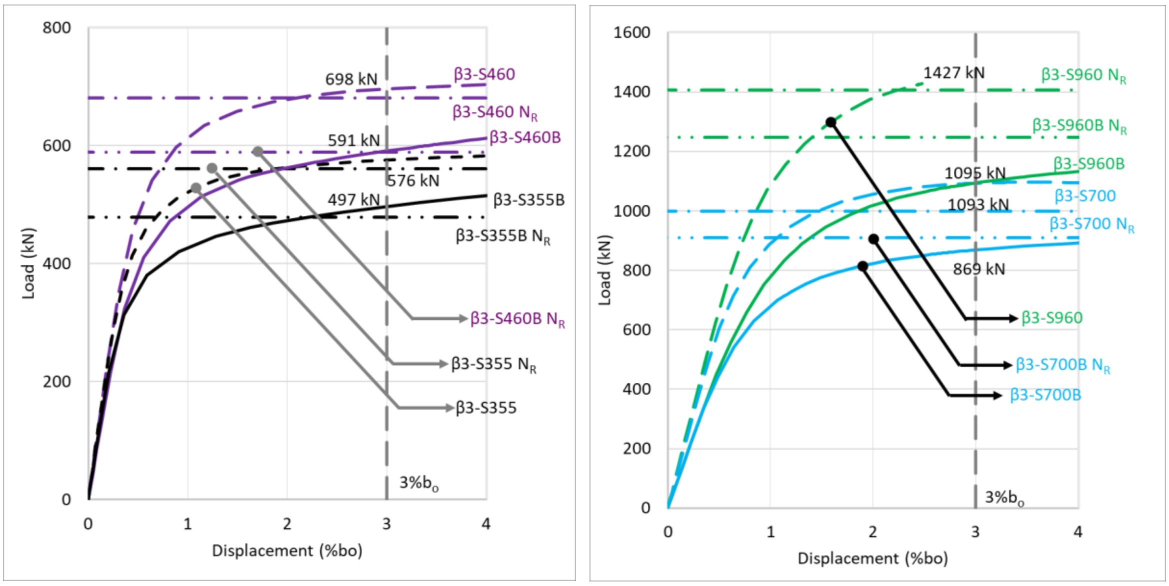

Figure 4-32: Load displacement curve for FE models with β_3

Table 4-32 summarizes the joint resistance without the reductions. For each steel grade, fillet welded joint result in larger resistance. The governing failure mode is the chord face failure. The joint resistance, ultimate load resistance and the ratio between the joint resistance and the failure load is summarized in **Table 4-33**. Compared to the resistance, the FE β_3-S960B results in higher ultimate load resistance which is around 14% larger than the resistance. The resistance for the FE β_3-S700B and β_3-S960B are 2% and 14% larger than the ultimate load resistance. Reduction of 0.8 for steel grade S960 and S700, 0.9 for steel grade S460 and 1.0 for steel grade S355 are considered for the FEM. These reductions are consistent with the material reduction factors summarized in **Table 2-4**. The ratio design resistance $N_{R;Cf}$ over ultimate load resistance were lower than 1.0.

Table 4-32: Joint resistance N_R for joints β3

Model	CFF (kN)	CSF (kN)	BF (kN)	PSF (kN)	Failure mode
β3-S355	561.48	848.07	587.01	1391.60	CFF
β3-S460	681.49	1000.28	692.37	1641.37	CFF
β3-S700	999.57	1452.59	1005.44	2383.56	CFF
β3-S960	1407.28	2044.06	1414.84	3354.11	CFF
β3-S355B	363.52	678.45	469.61	1113.28	CFF
β3-S460B	588.96	1000.28	692.37	1641.37	CFF
β3-S700B	885.74	1452.59	1005.44	2383.56	CFF
β3-S960B	1247.65	2044.06	1414.84	3354.11	CFF

Table 4-33: Ratio resistance over failure load for joints with β_3

Model	N_{FEA} (kN)	N_R (kN)	N_R/N_{FEA} (-)	$N_{R.Cf}/N_{FEA}$ (-)
β3-S355	576.15	561.48	0.97	0.97
β3-S460	697.57	681.49	0.98	0.88
β3-S700	1092.94	999.57	0.91	0.73
β3-S960	1427.38	1407.28	0.99	0.79
β3-S355B	496.90	363.52	0.73	0.73
β3-S460B	591.03	588.96	1.00	0.90
β3-S700B	869.02	885.74	1.02	0.82
β3-S960B	1095.96	1247.65	1.14	0.91

Secondary bending stresses

The secondary bending stress values are shown in **Figure 4-33**(a). The maximum secondary bending stresses for the butt-welded joints and fillet-welded joints are around 0.166_{fy} – $0.19f_y$ and $0{,}23f_y – 0.3f_y$. The largest is obtained for joints with S960 and the lowest for S355. The maximum secondary bending stress for β_1-S355 is 42% larger than that for β_1-S355B. For β_1-S460, β_1-S700 and β_1-S960 the maximum secondary bending stress is 40%, 46%, and 63%, respectively larger when compared to the butt-welded joints. The fillet welded joints with HSS result in larger secondary bending stresses.

At ultimate load resistance the average stresses are around $0.70f_y$ – $0.78f_y$ and $0.88f_y$ – $0.98f_y$ for the butt-welded joints and the fillet-welded joints. The secondary bending stresses are maximum $0.05f_y$ for joints with mild-strength steel. For the butt-welded joints with HSS the secondary bending stresses are maximum $0.06f_y$, whereas the secondary bending stresses are $0.09f_y$ and $0.19f_y$ for the fillet welded joints with S700 and S960, respectively.

Figure 4-33(b) shows the level of secondary bending stress ($\sigma_m/\sigma_{average}$) obtained for each model. **Table 4-34** and **Table 4-35** summarize the level of secondary bending stresses in the joints. The maximum $\sigma_m/\sigma_{average}$ ratio is 45% for all the butt-welded joints and around 48% –

50% for the fillet-welded joints. The maximum $\sigma_m/\sigma_{average}$ ratio for the fillet welded joint β_1-S960 and β_1-S700 is 11% and 9%, respectively larger when compared to the butt-welded joints. This percentage is much lower for the mild strength joints. Large $\sigma_m/\sigma_{average}$ ratio is obtained for average stress up to $0.5f_y - 0.7f_y$.
At ultimate load resistance the average stresses are around $0.70f_y$ – $0.78f_y$ and $0.88\ f_y$ – $0.91f_y$ for the butt-welded joints and the fillet-welded joints, respectively. At this ultimate load resistance, the $\sigma_m/\sigma_{average}$ ratio is lower than 6% for most of the joints. The largest $\sigma_m/\sigma_{average}$ ratio of around 21% is obtained for the models β_1-S960B. At ultimate load, high secondary bending stresses and level of secondary bending are obtained for the fillet welded joints with HSS. This increases the stresses in the joints zone significantly and contributes to failure.

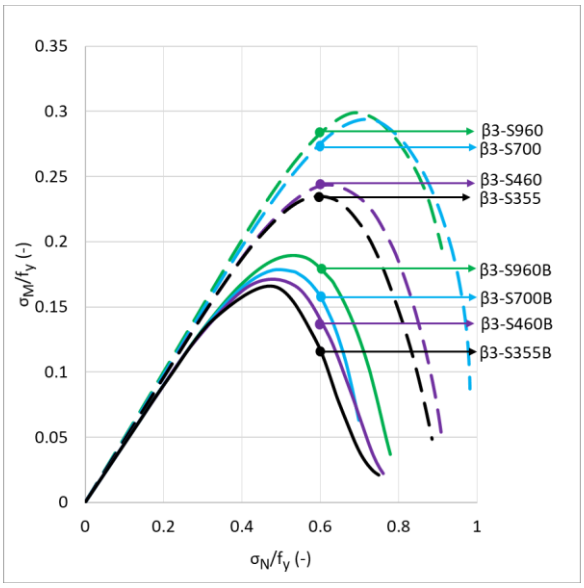

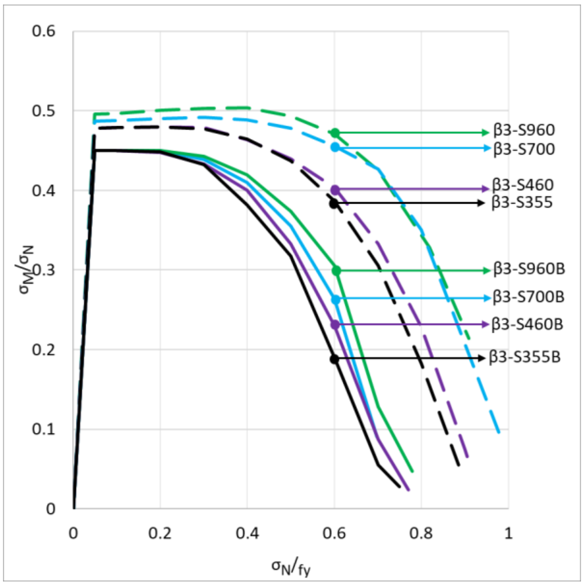

Figure 4-33: (a) Secondary bending stress and (b) level of secondary bending stress

Table 4-34: Level of secondary bending stress for the fillet-welded joints with β_3

β3-S355			β3-S460			β3-S700			β3-S960		
σ_N/f_y	σ_M/f_y	σ_M/σ_N	σ_N/f_y	σ_M/f_y	σ_M/σ_N	σ_N/f_y	σ_M/f_y	σ_M/σ_N	σ_N/f_y	σ_M/f_y	σ_M/σ_N
0	0	0	0	0	0	0	0	0	0	0	0
0.05	0.02	0.48	0.05	0.02	0.48	0.05	0.02	0.49	0.05	0.02	0.50
0.10	0.05	0.48	0.10	0.05	0.48	0.10	0.05	0.49	0.10	0.05	0.50
0.20	0.10	0.48	0.20	0.10	0.48	0.20	0.10	0.49	0.20	0.10	0.50
0.30	0.14	0.48	0.30	0.14	0.48	0.30	0.15	0.49	0.30	0.15	0.50
0.40	0.19	0.46	0.40	0.19	0.46	0.40	0.20	0.49	0.40	0.20	0.50
0.50	0.22	0.44	0.50	0.22	0.44	0.50	0.24	0.48	0.50	0.25	0.49
0.60	0.23	0.39	0.60	0.24	0.40	0.60	0.27	0.46	0.60	0.28	0.47
0.70	0.21	0.31	0.70	0.23	0.33	0.70	0.30	0.43	0.70	0.30	0.42
0.80	0.15	0.18	0.80	0.18	0.23	0.80	0.28	0.35	0.82	0.27	0.33
0.88	0.05	0.05	0.90	0.07	0.07	0.98	0.09	0.09	0.91	0.19	0.21
			0.91	0.05	0.06						

Table 4-35: Level of secondary bending stress for the butt-welded joints with β3

β3-S355B			β3-S460B			β3-S700B			β3-S960B		
σ_N/f_y	σ_M/f_y	σ_M/σ_N	σ_N/f_y	σ_M/f_y	σ_M/σ_N	σ_N/f_y	σ_M/f_y	σ_M/σ_N	σ_N/f_y	σ_M/f_y	σ_M/σ_N
0	0	0	0	0	0	0	0	0	0	0	0
0.05	0.02	0.45	0.05	0.02	0.45	0.05	0.02	0.45	0.05	0.02	0.45
0.10	0.04	0.45	0.10	0.04	0.45	0.10	0.05	0.45	0.10	0.05	0.45
0.20	0.09	0.45	0.20	0.09	0.45	0.20	0.09	0.45	0.20	0.09	0.45
0.30	0.13	0.43	0.30	0.13	0.43	0.30	0.13	0.44	0.30	0.13	0.44
0.40	0.15	0.38	0.40	0.16	0.40	0.40	0.17	0.42	0.40	0.16	0.41
0.50	0.16	0.32	0.50	0.17	0.33	0.50	0.19	0.37	0.50	0.18	0.36
0.60	0.11	0.19	0.60	0.14	0.23	0.60	0.18	0.31	0.60	0.16	0.26
0.70	0.04	0.06	0.70	0.06	0.09	0.70	0.09	0.13	0.70	0.06	0.09
0.75	0.02	0.03	0.77	0.02	0.02	0.78	0.04	0.05			

4.4 Weld strength

The welds have to have sufficient deformation and rotation capacity for redistribution of stresses. Therefore, the welds should be designed either “full strength” or to resist the ultimate load resistance (see section 2.2.1.1). The throat thickness required for a full-strength fillet weld are summarized in **Table 4-36**. The minimum throat thickness required for a full-strength fillet welds are larger than the throat thickness used in the FEM. The single-sided fillet welds in the FEM are not designed for “full strength”.

Table 4-36: Required throat thickness fillet weld

Steel grade	β_w	$\gamma_{m,2}$	$\gamma_{m,0}$	f_y	f_u	Full-strength [4] a/t	FEM a/t
	(-)	(-)		(N/mm²)	(N/mm²)	(mm)	(mm)
S355	0.9	1.25	1	390	521	1.19	1.00
S460	0.85	1.25	1	460	575.5	1.20	1.00
S700	1.1	1.25	1	700	835	1.63	1.20
S960	1.24	1.25	1	960	1175	1.79	1.40

The welds should be able to resist the ultimate load resistance of the joints. To determine the throat thickness of the weld, the effective length of the RHS brace perimeters should be considered. The throat thickness required to transmit the ultimate load resistance is summarized in **Table 4-37**. For the complete table a reference is made to Appendix C.4. The throat thickness in the FEM are equal to or larger than the required throat thickness. Based on the considered effective length and the ultimate load resistance, the weld designed in the FEM is sufficient to prevent failure of the weld and to ensure sufficient ductility of the joints.

Table 4-37: Required throat thickness to resist the ultimate load resistance

model	$b_{e;p}$	l_{eff}	f_u	β_w	γ_{m2}	N_{FEA}	Required [4] a	FEM a
	(mm)	(mm)	(N/mm^2)	(-)	(-)	(kN)	(mm)	(mm)
G1-S355	33.33	193.33	521	0.9	1.25	421.69	3.33	5
G1-S460	33.33	193.33	575.5	0.85	1.25	503.99	3.40	5
G1-S700	33.33	193.33	835	1.1	1.25	773.35	4.66	6
G1-S960	33.33	193.33	1175	1.24	1.25	1018.81	4.92	7
G0-S355	33.33	193.33	521	0.9	1.25	445.11	3.52	5
G0-S460	33.33	193.33	575.5	0.85	1.25	534.74	3.61	5
G0-S700	33.33	193.33	835	1.1	1.25	845.17	5.09	6
G0-S960	33.33	193.33	1175	1.24	1.25	1141.92	5.51	7
β1-S355	31.5	171.50	521	0.9	1.25	413.03	3.68	5
β1-S460	31.5	171.50	575.5	0.85	1.25	500.00	3.81	5
β1-S700	31.5	171.50	835	1.1	1.25	787.00	5.34	6
β1-S960	31.5	171.50	1175	1.24	1.25	1061.00	5.77	7
β2-S355	36	196.00	521	0.9	1.25	486.35	3.79	5
β2-S460	36	196.00	575.5	0.85	1.25	587.20	3.91	5
β2-S700	36	196.00	835	1.1	1.25	925.00	5.50	6
β2-S960	36	196.00	1175	1.24	1.25	1223.00	5.82	7
β3-S355	40.5	220.50	521	0.9	1.25	576.20	3.99	5
β3-S460	40.5	220.50	575.5	0.85	1.25	697.60	4.13	5
β3-S700	40.5	220.50	835	1.1	1.25	1093.00	5.77	6
β3-S960	40.5	220.50	1175	1.24	1.25	1427.40	6.04	7

4.5 Yield Line Patterns in the FEA

In this section, an attempt is done to predict the join resistance with the help of yield line mechanism method. This is done by equating the internal work and the external work. For this, the finite element models described in the previous section is used. **Table 4-38** summarizes the RHS joints.

Table 4-38: The joint geometry for β1

Geometry	b_0	t_0	b_i	t_i	θ_i	e	g	β	β_{mod}
	(mm)	(mm)	(mm)	(mm)	(°)	(mm)	(mm)	(-)	(-)
β1-S355	140	6.3	70	5	30	-18.04	40	0.5	0.60
β1-S460	140	6.3	70	5	30	-18.04	40	0.5	0.60
β1-S700	140	6.3	70	5	30	-18.04	40	0.5	0.62
β1-S960	140	6.3	70	5	30	-18.04	40	0.5	0.64
β1-S355B	140	6.3	70	5	30	-18.04	40	0.5	
β1-S460B	140	6.3	70	5	30	-18.04	40	0.5	
β1-S700B	140	6.3	70	5	30	-18.04	40	0.5	
β1-S960B	140	6.3	70	5	30	-18.04	40	0.5	
β2-S355	140	6.3	80	5	30	-12.26	40	0.57	0.67
β2-S460	140	6.3	80	5	30	-12.26	40	0.57	0.67
β2-S700	140	6.3	80	5	30	-12.26	40	0.57	0.69
β2-S960	140	6.3	80	5	30	-12.26	40	0.57	0.71
β2-S355B	140	6.3	80	5	30	-12.26	40	0.57	
β2-S460B	140	6.3	80	5	30	-12.26	40	0.57	
β2-S700B	140	6.3	80	5	30	-12.26	40	0.57	
β2-S960B	140	6.3	80	5	30	-12.26	40	0.57	

The deformed joint at ultimate load resistance are used to obtain the yield lines. The governing failure mode for the square hollow section joints is the chord face plastification, therefore the axial stress distribution in the chord are evaluated. It is observed that the stress at the chord face is non-uniformly distributed and along the brace perimeter the largest. Along the yield lines in the chord face, stresses are equal to the yield strength as shown in **Figure 4-34**.

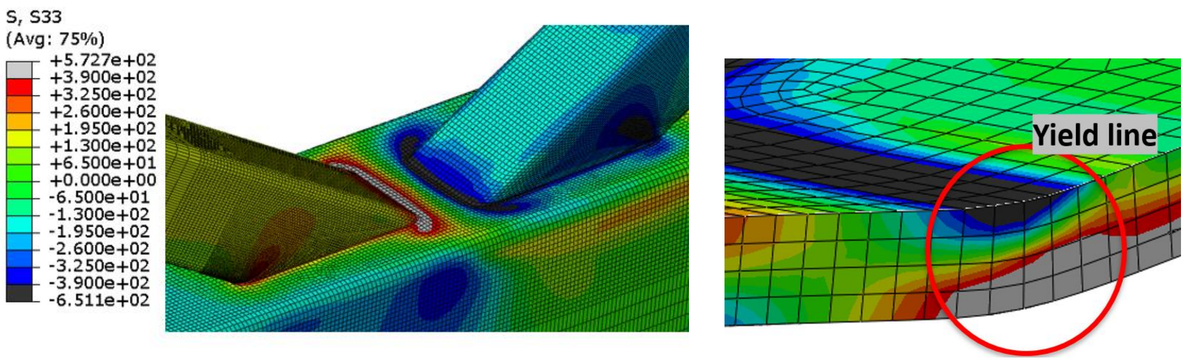

Figure 4-34: Plastic moment at ultimate load resistance for FEM (B1-S355B)

With help of the basic rules, described in section 2.5, the yield lines and the internal work can be determined. The plastic moment and the rotation along the yield line are assumed to be constant. Yield lines are straight and change slope only when intersection another yield line. Furthermore, the elastic deformations are neglected when calculating the internal work. When calculating the internal work, the yield line patterns are fitted in order to obtain a load close to the ultimate load resistance. **Figure 4-35** shows the two type of yield line patterns which are clearly observed in the finite element models. The yield line pattern for most the joints are observed at the brace toe. For the fillet welded joints β2-S355 and β2-S460 additional yield lines are observed at the brace heel side.

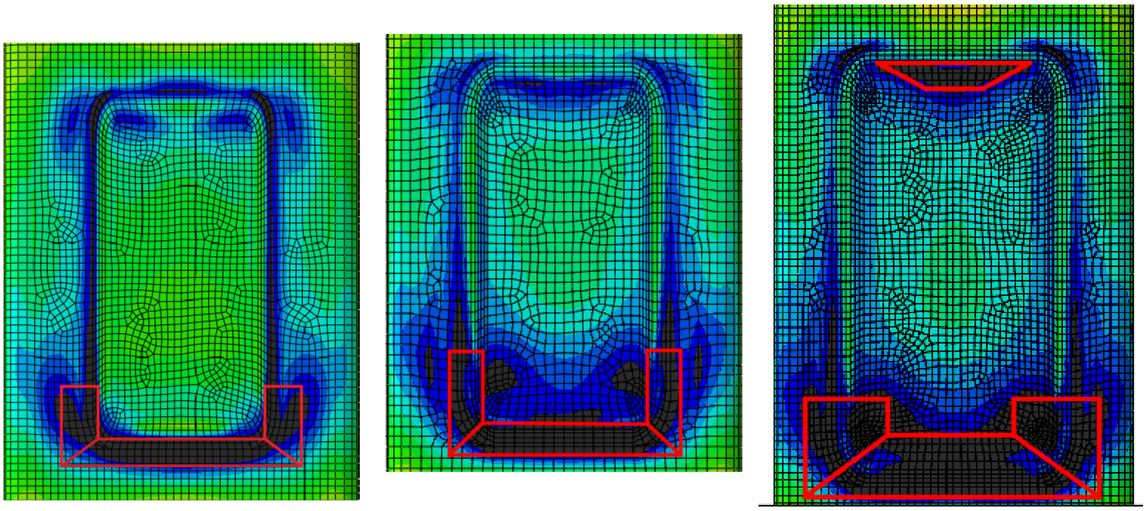

Figure 4-35: Yield line pattern for the FE β1-S355B , β1-S355 and β2-S355

The internal work is determined using the plastic moment ($m_p = \frac{1}{4} f_{yo} t_o^2$) and the displaced, rotated yield lines ($\Sigma l_i \varphi_i$). The length of the yield lines is measured in ABAQUS® using the tool "path". The joint resistance is determined by equating the internal work and the external work. The external work is equal to the joint resistance multiplied by a small deflection of the chord face. The ultimate load resistance obtained by the observed yield line patterns are summarized in **Table 4-39**. The ratio between the ultimate load resistance obtained by the FEA and by the yield line patterns is also show in the before mentioned table. Compared to the ultimate load resistance obtained the FEA, ultimate load resistance obtained by the yield line patterns were 9% and 19% lower predicted.

Table 4-39: Ultimate load resistance obtained from FEA and yield lines (YL)

Model	Ultimate load resistance FEA N_{FEA} (kN)	Ultimate load resistance using yield lines N_{YL} (kN)	N_{YL}/N_{FEA} (-)
β1-S355B	351.16	319.28	0.91
β1-S460B	418.20	381.84	0.91
β1-S700B	629.60	552.46	0.88
β1-S960B	789.08	698.33	0.88
β2-S355B	420.20	432.54	0.91
β2-S460B	503.63	432.54	0.86
β2-S700B	730.79	661.93	0.91
β2-S960B	917.18	903.06	0.98
β1-S355	416.03	352.96	0.85
β1-S460	416.03	383.61	0.92
β1-S700	786.92	697.46	0.89
β1-S960	1059.50	933.45	0.88
β2-S355	486.3498	424.50	0.87
β2-S460	586.8166	516.24	0.88
β2-S700	926.1824	819.71	0.89
β2-S960	1223.199	1030.74	0.84

4.6 Summary

In this section the parametric study is performed in order to obtain the secondary bending stresses in RHS joints made of high strength steels. The geometry, material properties, loading and boundary condition are taken from the literature. In this parametric study, the steel grade, the gap size, the parameter β and the weld type are varied. In total 32 finite element models are built. In case of a fillet-welded joint, a gap of 0.15 mm between the brace and the chord is considered in the FEM to account for the gap in the real joint. Valuable results are obtained with this parametric study. For each parameter the following is observed.

Effect of the material properties

- The ultimate load resistance is for each joint the load corresponding to the *3%bo* deformation limit. Joints with steel grade S460, S700 and S960 resulted in 20%, 83% and 142% larger ultimate load resistance compared to the joint with steel grade S355. Larger ratio joint resistance to ultimate load resistance is obtained for the high-strength RHS joints. The joint resistance is around 14%, 2% and 4% larger than the ultimate load resistance for joints with steel grade S960, S700 and S460, respectively. For joints with steel grade S355 the resistance is smaller or equal to the ultimate load resistance. The governing failure mode is the chord face failure. Reduction factor 0.8, 0.8, 0.9 and 1.00 are considered for G1-S960, G1-S700, G1-S460 and G1-355. These reductions are consistent with the material reduction factors shown in **Table 2-4**. Also, the yield strength of the steel grade is smaller or equal to $0.8f_u$.

- At ultimate load resistance, the ratio maximum von mises stress to yield stress (σ_{mises}/f_y) are 27% for S960 and S700 and 44% for S460 and 55% for S355. Furthermore, at this load level the ratio of axial stresses in the compressive brace over the average stress ($\sigma/\sigma_{average}$) is for high-strength joints lower when compared to the mild-strength joints. The obtained ratios are 203%, 199%. 220% and 231% for joints with steel grade S960, S700, S460 and S355, respectively. The σ_{mises}/f_y ratio and $\sigma/\sigma_{average}$ ratio at ultimate load resistance in the high-strength hollow sections joints are lower when compared to mild-strength joints. This can be explained by the low f_u/f_y ratio. Due to this the difference between the yield strength and the ultimate strength decreases for the increasing yield strength. Therefore, the maximum stresses in high-strength joints are lower when compared to the joints with mild-strength steel.

- The secondary bending moment are obtained from the uneven stress distribution in the compression brace at the cross-section as shown in Figure 4-11. This section is around 95 mm away from chord rectangular to the compressive brace. The secondary bending moment is integrated via a free body cut with element set and node set shown in before mentioned figure. The secondary bending stress is calculated based on FE secondary bending moment and moment inertia.

- The secondary bending moment in the RHS gap K joints is larger for joints with high yield strength. As the axial load increases the secondary bending stresses increases and decreases after the peak secondary bending stress has reached. For mild strength steel the maximum secondary bending stresses are around $0.22f_y$. For joints with steel grade S700 and S960, the maximum secondary bending stresses are around 23% and 30%, respectively larger. At ultimate load resistance the average stresses are in the range of $0.73f_y$ – $0.75f_y$ and the secondary bending stresses are around $0.04f_y$ – $0.06f_y$ for joints with HSS.

- The peak secondary bending stresses for joints with steel grade S355, S460, S700 and S960 occur at a deformation of around *0.31%*b_o, *0.36%*b_o, *0.80%*b_o, *1.10%*b_o and the average stresses are around $0.48f_y$, $0.47f_y$, $0.58f_y$, and $0.58f_y$. At this load level the the peak axial stresses in the compressive brace for joints with mild strength steel are equal to the yield strength and for joints with HSS, the peak axial stresses are 125%f_y. The reason for the high stresses in high-strength joints is the shorter or missing yielding plateau in the stress strain curve. Due to this, the strain hardening in which the stresses and the strain increases significantly, start immediately. Therefore, large stresses occur in joints at the before mentioned deformation.

- Joints with HSS exhibit higher $\sigma_m/\sigma_{average}$ ratios. The maximum $\sigma_m/\sigma_{average}$ ratio for joints with mild-strength steel is around 53%. For joints with steel grade S700 and S960 this level is 54% and 56%, respectively. At ultimate load resistance the $\sigma_m/\sigma_{average}$ ratio is 5% and 8% for joints with steel grade S700 and S960. For joints with mild strength steels, the secondary bending stresses disappeared.

Effect of the gap size

- The impact of the lower gap size on the ultimate load resistance increases with increasing yield strength. Comparisons are made with two gap sizes. For steel grade S355 and S460, the joint with lower gap size exhibit 6% larger resistance. This percentage is around 9% and 12% for joints with steel grade S700 and S960, respectively.

- Compared to the ultimate load resistance, larger resistance is predicted for the high-strength RHS joints with larger gap. The resistance for joints with larger gap and steel grade S960, S700 and S460 is 14%, 2% and 4% larger than the ultimate load resistance. The resistance for joints with lower gap size is approximately equal to the ultimate load resistance.

- Joints with lower gap size, exhibit larger secondary bending stresses. Comparing both the gap sizes, the FE models with the lower gap size result in maximum 15% larger secondary bending moment. The largest percentage is obtained for joints with HSS. For steel grade S355 this percentage is the lowest of around 7%. At ultimate load resistance the average stresses are $0.77f_y$ – $0.86f_y$ and $0.72f_y$ – $0.75f_y$ for joints with G0 and G1, respectively. The secondary bending stresses are maximum $0.06f_y$ for joints with mild strength steel. For joints with S700 and gap size G1 and G0, the secondary bending stresses are around $0.04\ f_y$ and $0.12f_y$, respectively. These stresses are around $0.06\ f_y$ and $0.14f_y$ for joints with S960 and gap size G1 and G0, respectively.

- Joints with lower gap size exhibit for low axial load lower $\sigma_m/\sigma_{average}$ ratios than joint with larger gap size. The difference is maximum 5%. The largest percentage is obtained for joints with HSS. After the peak secondary bending stress, in the decreasing stage, the joints with lower gap size result in larger $\sigma_m/\sigma_{average}$ ratio. At ultimate load resistance, the $\sigma_m/\sigma_{average}$ ratio is larger for joints with lower gap size and for joints with higher yield strength. The $\sigma_m/\sigma_{average}$ ratio at ultimate load resistance are 14%, 22%,5% and 8% for G0-S700, G0-S960, G1-S700 and G1-S960, respectively. This level is maximum 5 % for the joints with mild strength steels.

Effect of the parameter β

- Comparisons are made using three β-values. As already known joints with larger β-values and higher yield strength exhibit larger ultimate load resistance. The difference in ultimate load resistance for different β-values is lower for HSS. For joints with mild strength steel and β3 40% larger resistance is obtained when compared to β1. Similar comparisons are made for the other steel grade. The percentage is around 39% for S700 and 34% for S960.

- The resistance predicted for steel grade S460, S700 and S960 is maximum 3% larger than the ultimate load resistance. Reductions factor which are consistent with the material reduction factors shown in **Table 2-4** were considered. Moreover, the yield strength of the steel grade was smaller or equal to $0.8f_u$. Due to these reductions, the resistance was smaller or equal to the ultimate load resistance

- For each steel grade, larger β-values result in larger secondary bending stresses. The obtained secondary bending stresses in joint with β3 and β2 are compared with joints with β1. The lowest percentage is obtained for S960 and the largest is obtained for S355. The impact of the larger β-values for high-strength hollow section joints are lower when compared to mild-strength hollow section joints. At ultimate load resistance the average stresses are in the range of $0.84f_y$ – $0.98f_y$. At this load, the joints with mild-strength steel have obtained maximum $0.06f_y$ secondary bending stresses. The secondary bending stresses are between $0.09f_y$ – $0.19f_y$ for joints with HSS. The largest is obtained for joints with S960 and β3.

- Furthermore, larger $\sigma_m/\sigma_{average}$ ratio is obtained in joints with large β-value. The impact of large β-value on high-strength joints are larger when compared to mild-strength joints. For mild-strength joints the maximum $\sigma_m/\sigma_{average}$ ratio in joints with β2 and mild-strength steel and HSS are 10% and 13% larger than that in joints with β1. Compared to β1, the maximum $\sigma_m/\sigma_{average}$ ratio in joints with β3 and mild strength steel and HSS is 20% and 23% larger. At ultimate load resistance, the $\sigma_m/\sigma_{average}$ ratio is maximum 7% for FE models with S355 and S460. This level is maximum 10% for models with steel grade S700. The largest $\sigma_m/\sigma_{average}$ ratio in the range of 16%-21% are obtained for the models with S960. The lowest and the largest is obtained for β1 and β3, respectively.

Effect of the weld

- Two weld types: butt-welded joints and fillet-welded joints are varied in order to obtain the joint behavior. Fillet-welded joints exhibit larger ultimate load resistance when compared to the butt-welded joints. For fillet-welded joints with steel grade S960 and S700 the ultimate load resistance is at least 30% and 26% larger when compared to the butt-welded joints. For S355 and S460, the increase is at least 16% and 17%.

- The resistance for the butt-welded joints with S700 and S960 is maximum 9% and 18% larger than the ultimate load resistance. The material reduction factors (see **Table 2-4**) are considered in the design resistance in order to obtain a joint resistance smaller or equal to the ultimate load resistance.

- For each steel grade, the secondary bending stresses in the fillet-welded joints are larger than that in the butt-welded joints. The increase of the maximum secondary bending stress is at least 37% for S355, 38% for S460, 46% for S700 and 60% for S960. At ultimate load resistance the average stresses are around $0.66f_y$ – $0.74f_y$ and $0.84f_y$ – $0.98f_y$ for the butt-welded joints and the fillet-welded joints. The secondary bending stresses are large for the joints with HSS and fillet welds. In case of the joints with mild-strength steel maximum $0.07f_y$ secondary bending stresses are present. This is around $0.04f_y$ – $0.09f_y$ for the butt-welded joints with HSS. For the fillet welded joints made of steel grade S700 and S960, the secondary bending stress is maximum $0.09f_y$ and $0.19f_y$ respectively.

- Fillet-welded joints obtained $\sigma_m/\sigma_{average}$ ratios when compared to the butt-welded joints. The maximum $\sigma_m/\sigma_{average}$ ratio in the fillet-welded joints is at least 5% for S355, S460 and S700 and 8% for S960 larger when compared to the butt-welded joints. At ultimate load resistance the $\sigma_m/\sigma_{average}$ ratio is large for the joints with HSS and fillet welds. In case of the joints with mild-strength steel maximum 9% level of secondary bending stresses are present. This level is maximum 12% and 14% for the butt-welded joints with steel grade S700 and S960. Maximum 10% and 21% are obtained for fillet welded joints made of steel grade S700 and S960, respectively.

Level of secondary bending stress

- **Table 4-40** summarize the maximum secondary bending stresses and level of secondary bending stresses obtained at every load step for various steel grades. The highest values are obtained for average stress up to $0.6f_y$ – $0.7f_y$. At ultimate load resistance the level of secondary bending stress is 6%,7% 14% and 22% for joints with steel grade S355 S460, S700 and S960, respectively.

Table 4-40: Maximum level of secondary bending stress for various steel grades

S355			S460			S700			S960		
σ_N/f_y	σ_M/f_y (max)	σ_M/σ_N (max)	σ_N/f_y	σ_M/f_y (max)	σ_M/σ_N (max)	σ_N/f_y	σ_M/f_y (max)	σ_M/σ_N (max)	σ_N/f_y	σ_M/f_y (max)	σ_M/σ_N (max)
0	0	0	0	0	0	0	0	0	0	0	0
0.05	0.03	0.53	0.05	0.03	0.53	0.05	0.03	0.54	0.05	0.03	0.55
0.1	0.05	0.53	0.1	0.05	0.53	0.1	0.05	0.54	0.1	0.06	0.56
0.2	0.11	0.53	0.2	0.11	0.53	0.2	0.11	0.55	0.2	0.11	0.56
0.3	0.16	0.52	0.3	0.16	0.53	0.3	0.16	0.55	0.3	0.17	0.56
0.4	0.20	0.49	0.4	0.19	0.49	0.5	0.25	0.52	0.4	0.22	0.56
0.5	0.22	0.45	0.5	0.23	0.46	0.5	0.25	0.50	0.5	0.26	0.53
0.6	0.23	0.39	0.6	0.24	0.40	0.6	0.28	0.47	0.6	0.30	0.50
0.7	0.21	0.31	0.7	0.23	0.33	0.7	0.30	0.43	0.7	0.31	0.44
0.8	0.15	0.18	0.8	0.18	0.23	0.8	0.28	0.35	0.8	0.27	0.33
0.85	0.05	0.06	0.9	0.07	0.07	0.9	0.12	0.14	0.9	0.19	0.22

Yield line patterns

- Additionally, an attempt is done to determine the joint resistance using the yield line mechanism method. Using the basic rules for the yield line mechanism, yield lines are observed at the brace toe and brace heel. The displaced, rotated yield lines and the plastic moment are used to determine the internal work. The joint resistance is determined by dividing the internal work by the displacement of the chord face. The joint resistance obtained by the yield line mechanism is 9%-19% lower compared to the ultimate load resistance obtained by the FEA.

CHAPTER 5 CONCLUSION AND RECOMMENDATIONS

The main goal of this research is to study the secondary bending stresses in hollow section joints made of HSS. In mild-strength joints, these stresses are neglected, since these joints have sufficient stiffness and ultimate capacity to resist and to redistribute stresses [6]. Compared to the normal strength steel, high strength steel may not have sufficient ductility to redistribute stresses. This can be explained by the stress-strain curve of HSS, which lack the yielding plateau, have smaller ultimate strain and low f_u/f_y ratio. The impact of HSS on the secondary bending stresses of hollow section joint may be different and is therefore investigated. Another goal is to investigate the magnitude of the material reduction factors recommended by the proposed 2020 version of the Eurocode 3 part 1-8. In this chapter the conclusions of the numerical analyses are presented and the recommendations for future work are suggested.

5.1 Conclusions

The scope of the parametric study is limited to individual gap K-joints made with square hollow sections. In the parametric study, four parameters are varied: steel grade ranging from S355 to S960, three β-values: 0.5, 0.57 and 0.64, two gap sizes: 25 mm and 40 mm and two weld types: fillet and butt welds. Based on the obtained finite element results, the following conclusions can be drawn:

- The ultimate load resistance for the hollow section joints is the load corresponding to the *3%bo* deformation limit. At this ultimate load resistance, the stresses in the hollow section joints are investigated and compared with the average and yield stress. The stresses in the hollow section joint near the joint zone are large and non-uniformly distributed due to discontinuity and uneven stiffness distribution. Also, stress concentrations occur in the corner of the brace in the joint zone. For comparison, the ratio maximum von mises stresses in the joint to yield strength (σ_{mises}/f_y), the ratio maximum axial stresses in the compressive brace to yield strength (σ_{axial}/f_y) and the ratio maximum axial stresses in the compressive brace to average stress ($\sigma_{axial}/\sigma_{average}$) are investigated. The ratios obtained for joints with HSS are lower compared to mild strength joints (see **Table 5-1**). The low ratios for joints with HSS can be explained by the low f_u/f_y ratio for HSS. The f_u/f_y ratios are 1.34, 1.25, 1.19 and 1.22 for the steel grade S355, S460, S700 and S960, respectively. With the increase in steel grade, the stress ratios at failure decrease which indicated the limitation of use of HSS. Therefore, it can be concluded that the capacity of HSS is not completely utilized at ultimate load resistance.

Table 5-1: Ratio stress to average stress or yield strength

Model	σ_{mises}/f_y (-)	σ_{axial}/f_y (-)	$\sigma_{axial}/\sigma_{average}$ (-)
G1-S355	1.55	1.70	2.31
G1-S460	1.43	1.64	2.20
G1-S700	1.27	1.55	1.99
G1-S960	1.27	1.49	2.03

- The ultimate load resistance, which is the load corresponding to the *3%bo* deformation limit is compared with the resistance without considering the material factor (C_f). The resistance is determined using EN 1993-1-8:2005 [20]. The ratio resistance to ultimate load resistance (N_R/N_{FEA}) were maximum 1.00, 1.04, 1.06 and 1.19 for joints with steel grade S355, S460, S700 and S960. The material reduction factors recommended by the proposed 2020 version of the Eurocode 3 part 1-8 [4] seems to be necessary since higher resistance are predicted.

- The maximum secondary bending stresses (σ_m) and the maximum $\sigma_m/\sigma_{average}$ ratios obtained for the joints is summarized in **Table 5-2**. In **Table 5-3,** the average stresses and the secondary bending stresses at ultimate load resistance is given. It is found that the secondary bending stresses are dependent on the steel grade. The secondary bending stresses (σ_m) and the ratio $\sigma_m/\sigma_{average}$ in hollow section joints increase with the increasing steel grade. Also, at ultimate load resistance, large secondary bending stresses exists in joints made from HSS. This increases the local stresses significantly. For joints with steel grade above S460, the high material reduction parameters recommended by the proposed 2020 version of the Eurocode 3 part 1-8 [4] seems to be necessary to include the effects of the secondary bending stresses in the static design strength.

Table 5-2: Maximum secondary bending stresses and $\sigma_m/\sigma_{average}$

Joints with steel grade	maximum Secondary bending stresses	maximum $\sigma_m/\sigma_{average}$
S355	$0.12f_y - 0.23f_y$	$0.38f_y - 0.53f_y$
S460	$0.12f_y - 0.24f_y$	$0.38f_y - 0.53f_y$
S700	$0.13f_y - 0.30f_y$	$0.38f_y - 0.55f_y$
S960	$0.13f_y - 0.31f_y$	$0.38f_y - 0.56f_y$

Table 5-3: Average stresses and secondary bending stresses at ultimate load resistance

joints with steel grade	Average stress	Secondary bending stress
S355	$0.71f_y - 0.88f_y$	$0 - 0.07f_y$
S460	$0.70f_y - 0.91f_y$	$0 - 0.07f_y$
S700	$0.71f_y - 0.98f_y$	$0.04f_y - 0.12f_y$
S960	$0.66f_y - 0.91f_y$	$0.06f_y - 0.19f_y$

- The maximum secondary bending stresses for joints with steel grade S355, S460, S700 and S960 occur at a deformation of *0.31%b₀*, *0.36%b₀*, *0.80%b₀*, *1.10%b₀* and the average stresses are $0.48f_y$, $0.47f_y$, 0.58 f_y, and 0.58 f_y. At this load level the secondary bending stresses starts to decrease due to the redistribution of stresses. In the compressive brace the peak axial stresses which occur in the welded area are evaluated. It can be concluded that the peak axial stresses are equal to the yield stress in joints with mild-strength steel and for joints with HSS, the peak axial stresses are 125%f_y. The high peak stresses in the high-strength joints can be explained by the lack of the yielding plateau in the stress strain curve for HSS. Due to this, the strain hardening stage starts immediately after the yield stress and therefore, large stresses may occur in joints at the before mentioned deformation.

- Four parameters are varied in this parametric study. For each parameter, the conclusions regarding the ultimate load resistance are:
    - Joints with steel grade S460, S700 and S960 resulted in 20%, 83% and 142% larger ultimate load resistance compared to the joint with steel grade S355. The ultimate load resistance is for each joint, the load corresponding to the *3%bo* deformation limit.
    - Joints with smaller gap size (25 mm) and steel grade S355, S460, S700 and S960 have obtained 6%, 6%, 9% and 12%, respectively larger ultimate load resistance compare to joints with larger gap size (40 mm).
    - Joints with β_2 and β_3 have obtained 15% – 18% and 34% – 40% larger ultimate load resistance when compared to joints with β_1. Largest difference is obtained for joints with steel grade S355 and the lowest for joints with S960.
    - The ultimate load resistance for the fillet-welded joints with steel grade S355, S460, S700 and S7960 is at least 16%, 17%, 26% and 30% larger when compared to the butt-welded joints

  For each parameter, the conclusions regarding the secondary bending stresses are:
    - A comparison is made using the maximum secondary bending stresses for each joint. The maximum secondary bending stress for joints with mild strength steel is 0.22f_y. For joints with steel grade S700 and S960, the maximum secondary bending stresses are 23% and 30%, respectively larger.
    - The maximum secondary bending stresses in joints with the smaller gap and steel grade S355, S460, S700 and S960 are 5%, 8%, 14% and 12%, respectively larger compared to the joints with larger gap size.
    - The obtained maximum secondary bending stresses in joint with β3 and β2 are compared with joints with β1. The obtained maximum secondary bending stresses in joint with β3 and steel grade S355, S460, S700 and S960 are 44%, 44%, 37% and 33% larger compared to joints with β1.
    - The maximum secondary bending stresses in the fillet welded joints with steel grade S355, S460, S700 and S960 are at least 37%, 38%, 46% and 60% larger compared to the butt-welded joints.

  It can be concluded that for joints with fillet welds, smaller gap sizes, larger β-values and high yield strength larger ultimate load resistance and secondary bending stresses are obtained. For joints with HSS the impact of smaller gap sizes and fillet welds are larger when compared to mild strength joints. The impact of larger β-values on high-strength joints are lower when compared to joints with mild-strength steels.

5.2 Recommendations

From the finite element results the following recommendations for future work are proposed:

- In this study, the truss girder and the T-joint are roughly validated against experimental data. It is recommended to calibrate the FEM more comprehensively in order to investigate the secondary bending stresses in hollow section joints. Next, it is recommended to validate the individual gap K-joint against test data.

- Furthermore, it is recommended to experimentally investigate the influence of other joint geometries (such as: brace thickness to chord thickness ratio τ, chord width to chord thickness ratio 2γ, overlap, weld strength and weld size) on the joint behavior and secondary bending stresses in hollow section joints.

- In this research the design rules described in the proposed 2020 version of the Eurocode 3 part 1-8 [4] are extrapolated to steel grade S960. Results regarding the ultimate load resistance and the secondary bending stresses are evaluated. The ultimate load resistance is defined as the load corresponding to the *3%bo* deformation limit. The resistance determined by [4] is maximum 19% larger than the ultimate load resistance. At the ultimate load resistance, the average stresses are in between $0.66f_y$ and $0.91f_y$ and the secondary bending stresses vary from $0.06f_y$ to $0.19f_y$. The obtained results indicate that joints with S960 have lower ultimate capacity and high secondary bending stresses are present at ultimate load resistance. Further study is recommended to investigate the behavior of joints made from steel grade S960.

BIBLIOGRAPHY

1. Ban, H. and G. Shi, *A review of research on high-strength steel structures.* Proceedings of the Institution of Civil Engineers - Structures and Buildings, 2018. **171**(8): p. 625-641.
2. Gogou, E., *Use of High Strength Steel Grades for Economical Bridge Design. Master's thesis, TU Delft.* 2012.
3. Sjors H.J. van Es, H.M., *Application of HSS and VHSS in civil engineering structures – requirements regarding material properties.* First Workshop of High Performance Steel Structures Research Council., 2018.
4. Standardization, E.C.f., *NEN-EN1993-1-8-V4.2. Eurocode 3: Design of steel structures - Part 1-8: Design of joints. Revised version v4.2.* 2018.
5. T. Björk, N.T.T.L., *Effect of the secondary bending moment on K-joint capacity.* Tubular Structures XV : proceedings of the 15th International Symposium on Tubular Structures, Rio de Janeiro, Brazil, 27-29 May 2015, 2015: p. 557-565.
6. Wardenier, J.A.P., J & Zhao, Xiao-Ling & J Van Der Vegte, G. , *Hollow sections in structural applications.* 2010.
7. Linwei He; Matthew Gilbert, M.A.a.M.S., *Automatic Yield-Line Analysis of Practical Slab Configurations via Discontinuity Layout Optimization.* Journal of Structural Engineering Volume 143 Issue 7, 2017.
8. Wardenier, J., *Hollow Section Joints . Delft University Press.* 1982: p. 236,406.
9. Gang Shi, F.B., Milan Veljkovic, Xuhong Qiang, *First Workshop Proceedings of High Performance Steel Structures Research Council (HPSSRC). Delft University of Technology.* 2018.
10. Standardization, E.C.f., *NEN-EN 1993-1-12. Eurocode 3: Design of steel structures - Part 1-12: Additional rules for the extension of EN 1993 up to steel grades S 700.* 2011.
11. F. Schroter, M.M., *Current world-wide trends in the usage of modern steel plates for bridge constructions.* Steelbridge 2004, 2004.
12. Ma, J.-L., T.-M. Chan, and B. Young, *Tests on high-strength steel hollow sections: a review.* Proceedings of the Institution of Civil Engineers - Structures and Buildings, 2017. **170**(9): p. 621-630.
13. Michel Bruneau, P.D., P.Eng., P.D. Chia-Ming Uang, and S.E. Rafael Sabelli, *Ductile Design of Steel Structures*. Second Edition ed. 2011: The McGraw-Hili Companies, Inc.
14. Pavlovic, M. and M. Veljkovic, *Compact cross-sections of mild and high-strength steel hollow-section beams.* Proceedings of the Institution of Civil Engineers - Structures and Buildings, 2017. **170**(11): p. 825-840.
15. Es, S.H.J.v., *Effect of TIG-dressing on fatigue strength and weld toe geometry of butt welded connections in high strength steel. Master Thesis.TU Delft.* 2012.
16. Standardization, E.C.f., *NEN-EN 1993-1-1. Eurocode 3: Design of steel structures - Part 1-1: General rules and rules for buildings.* 2006.
17. NORDENSTAM, J. and G. SVANTESSON, *High strength steel in conventional building structures. Master's thesis, CHALMERS UNIVERSITY OF TECHNOLOGY.* 2016.

18. Weynand, K., Jaspart, Jean-Pierre, *Design of joints in steel and composite structures: Eurocode 3 : design of steel structures : part 1-8 : design of joints, Eurocode 4 : design of composite steel and concrete structures : part 1-1 : general rules and rules for buildings.* 2016.
19. Javidan, F., et al., *Effect of weld on the mechanical properties of high strength and ultra-high strength steel tubes in fabricated hybrid sections.* Engineering Structures, 2016. **118**(C): p. 16-27.
20. Standardization, E.C.f., *NEN-EN1993-1-8. Eurocode 3: Design of steel structures - Part 1-8: Design of joints.* 2005.
21. Smith, M.C., *An Analysis of Secondary Stresses in Steel Parallel Chord Pratt Trusses. Master's thesis, Kansas State University, Manhattan, Kansas.* 2009.
22. A.J. Börger, A.R., J. Wardenier, *Secondary Stresses in Lattice Girders. Influence on the fatigue strength of tubular trusses with uniplanar K-joints.* Proceedings of The Fourteenth International Offshore and Polar Engineering Conference Toulon, France 2004.
23. Prof. ir. A.C.W.M. Vrouwenvelder, P.i.J.W., *Plasticity: The plastic behaviour and the calculation of plates subjected to bending . Lecture notes CT4150.* 2003.
24. Koning, C.H.M.d., & Wardenier, J., *Test on welded joints in complete girders made of square hollow sections. Cidect Report 5Q/79/*. 1979, Delft University of Technology: Delft, The Netherlands.
25. Petr Jehlička, F.W., *Experimental investigation of weld type and size effect on resistance of hollow section joints, CTU in Prague, Faculty of Civil Engineering Department of Steel and Timber Structures, DRAFT.* 2018.
26. O. Fleischer, J.W., *Effect of chord tensile stress on the capcity of RHS K joints with gap in real girder.* Tubular Structures XVI: Proceedings of the 16th International Symposium for Tubular Structures, 2018: p. 185-192.
27. Hibbitt, K.a.S., *ABAQUS Version 6.2.* 2001.
28. Yun, X. and L. Gardner, *Stress-strain curves for hot-rolled steels*. Vol. 133. 2017. 36-46.
29. Maheninggalih, G., *A demountable structural system of multi-storey building Case study of car park building. Master's thesis, TU Delft*. 2017, Technical University of Delft: The Netherlands.
30. Pereira, D.J.R., et al., *Effect of fillet welds on T-joints with thin-walled chords.* Proceedings of the Institution of Civil Engineers - Structures and Buildings. **0**(0): p. 1-12.
31. Fleischer, O.H., Stefan & Koenig, D., *Comparison of Different Configurations of Thick-walled K-joints with Gap made of RHS and CHS.* 2014.
32. Oliver Fleischer, R.P., *Evaluation of experimental results on slender RHS K-gap joints.* Conference: 11th International Symposium and IIW International Conference on Tubular Structures At: Québec City, Canada, 2006.

APPENDIX

APPENDIX A LITERATURE REVIEW

Appendix A.1 Yield line model for gap K-joints

Bjork [5] has described the yield line model for a gap K-joint. The yield line model for this joint is shown in Figure 36.

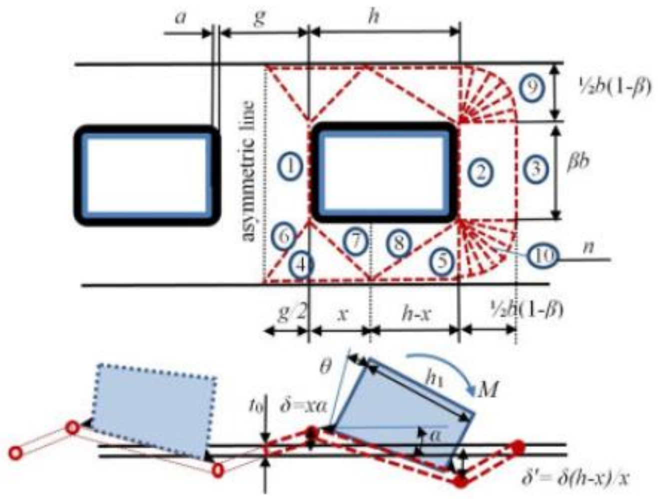

Figure A-1: Yield line model [5]

The derivation of the moment capacity is adopted from the work done by Björk T. et al [5]. This method is based on the yield lines is based on K-joints with equal brace angle and brace outer dimensions. The following simplifications are made:

$$b = b_0 - t_0$$
$$\beta = (b_1 + 2k_a a)/b_0$$
$$h = h_1 / \sin\theta + (k_2 + k_3)a$$
$$g = g_0 - 2k_3 a$$

where

b is the width of the chord member

t is the wall thickness of the flange in a chord

a is the throat thickness of the weld

k_1,k_2,k_3 are shape factor between 0 and 1. These factors include the weld effect on the location of the plastic hinge

g_0 is the distance between tensions and compression brace member

g is the distance between the plastic hinges in the gap

The virtual work (W) of each hinge is given by the following expression

$$W_i = m_p l_i a_i$$

where

m_p *is the plastic moment of a hinge i*

l_i *is length of a hinge i*

a_i *is the rotation angle of a hing i*

Table A-1: Work of plastic hinge[5]

ID	n_i	$m_{p0.i}$	l_i	α_i	W_i
1	1	$\frac{f_y t_0^2}{4}$	βb	$\left[\frac{1}{x}+\frac{2}{g}\right]\delta$	$\frac{f_y t_0^2}{4}\left[\frac{\beta b}{x}+\frac{2\beta b}{g}\right]\delta$
2	1	$\frac{f_y t_0^2}{4}$	βb	$\left[\frac{1}{x}+\frac{2(h-x)}{xb(1-\beta)}\right]\delta$	$\frac{f_y t_0^2}{4}\left[\frac{\beta b}{x}+\frac{2\beta(h-x)}{x(1-\beta)}\right]\delta$
3	1	$\frac{f_y t_0^2}{4}$	βb	$\left[\frac{2(h-x)}{xb(1-\beta)}\right]\delta$	$\frac{f_y t_0^2}{4}\left[\frac{2\beta(h-x)}{x(1-\beta)}\right]\delta$
4	2	$\frac{f_y t_0^2}{4}$	$\frac{g}{2}+x$	$\left[\frac{2}{b(1-\beta)}\right]\delta$	$\frac{f_y t_0^2}{4}\left[\frac{2g+4x}{b(1-\beta)}\right]\delta$
5	2	$\frac{f_y t_0^2}{4}$	$h-x$	$\left[\frac{2(h-x)}{xb(1-\beta)}\right]\delta$	$\frac{f_y t_0^2}{4}\left[\frac{4(h-x)^2}{xb(1-\beta)}\right]\delta$
6	2	$\frac{f_y t_0^2}{4}$	$\frac{1}{2}\sqrt{g^2+b^2(1-\beta)^2}$	$\left[\frac{g}{b(1-\beta)}+\frac{b(1-\beta)}{g}\right]\frac{\delta}{l_6}$	$\frac{f_y t_0^2}{4}\left[\frac{2g}{b(1-\beta)}+\frac{2b(1-\beta)}{g}\right]\delta$
7	2	$\frac{f_y t_0^2}{4}$	$\frac{1}{2}\sqrt{4x^2+b^2(1-\beta)^2}$	$\left[\frac{2x}{b(1-\beta)}+\frac{b(1-\beta)}{2x}\right]\frac{\delta}{l_7}$	$\frac{f_y t_0^2}{4}\left[\frac{4x}{b(1-\beta)}+\frac{b(1-\beta)}{x}\right]\delta$
8	2	$\frac{f_y t_0^2}{4}$	$\frac{1}{2}\sqrt{4(h-x)^2+b^2(1-\beta)^2}$	$\left[\frac{2(h-x)^2}{bx(1-\beta)}+\frac{b(1-\beta)}{2x}\right]\frac{\delta}{l_8}$	$\frac{f_y t_0^2}{4}\left[\frac{4(h-x)^2}{xb(1-\beta)}+\frac{b(1-\beta)}{x}\right]\delta$
9	2	$\frac{f_y t_0^2}{4}$	$\frac{\pi b(1-\beta)}{4}$	$\left[\frac{2(h-x)}{xb(1-\beta)}\right]\delta$	$\frac{f_y t_0^2}{4}\left[\frac{\pi(h-x)}{x}\right]\delta$
10	2	$\frac{f_y t_0^2}{4}$	$\frac{nb(1-\beta)}{2}$	$\left[\frac{\pi(h-x)}{nxb(1-\beta)}\right]\delta$	$\frac{f_y t_0^2}{4}\left[\frac{\pi(h-x)}{x}\right]\delta$

In **Table A-1**, the work of all the possible 10 yield lines is tabulated. The total internal work can be expressed by:

$$W_{in}=\sum_{i=1}^{10}W_i=\frac{f_y t_o^{\,2}}{2}\alpha\left[b+\pi h+\frac{2h(\beta b+2h)}{b(1-\beta)}+\left(\frac{b}{g}-\frac{2\beta b+8h-2g}{b(1-\beta)}-\pi\right)x+\left(\frac{8}{b(1-\beta)}\right)x^2\right]$$

The ‘x’ is determined by the outer work of the system

$$W_0=M\alpha$$

$$\frac{dW}{dx}=\frac{d(W_{in}-W_o)}{dx}=\frac{16}{b(1-\beta)}x+\frac{b}{g}-\frac{2\beta b+8h-2g}{b(1-\beta)}-\pi=0$$

$$x=\frac{1}{16}\left[8h+2\beta b-2g-b\left(\frac{b}{g}-\pi\right)(1-\beta)\right]$$

Finally, the moment capacity of the K joint can be determined using the following expressions:

$$M=\frac{f_y t_o^{\,2}}{2}\left[b+\pi h+\frac{2h(\beta b+2h)}{b(1-\beta)}+\left(\frac{b}{g}-\frac{2\beta b+8h-2g}{b(1-\beta)}-\pi\right)x+\left(\frac{8}{b(1-\beta)}\right)x^2\right]$$

in which

$$x=\frac{1}{16}\left[8h+2\beta b-2g-b\left(\frac{b}{g}-\pi\right)(1-\beta)\right]$$

APPENDIX B JOINT RESISTANCE TRUSS GIRDER 1 AND T-JOINT

Appendix B.1 Experimental results

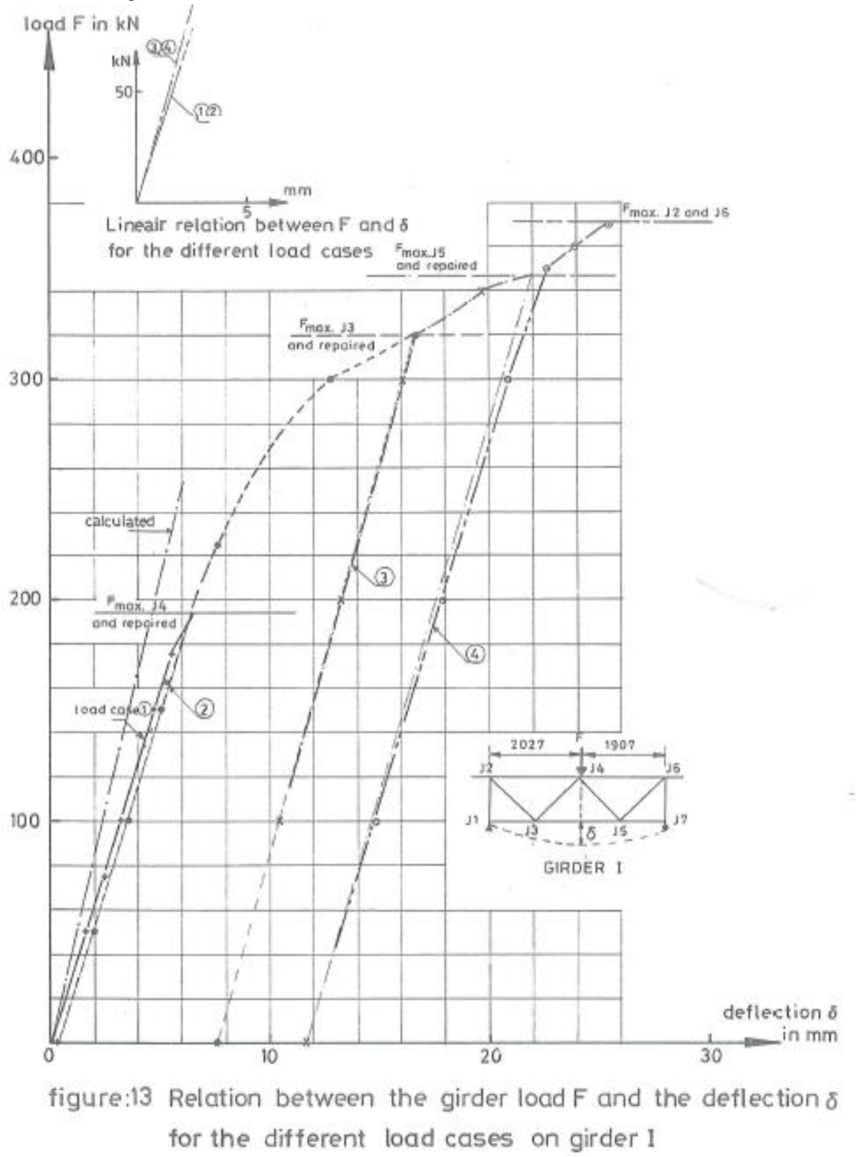

Figure B-1: Load – deflection of the girder 1 [24]

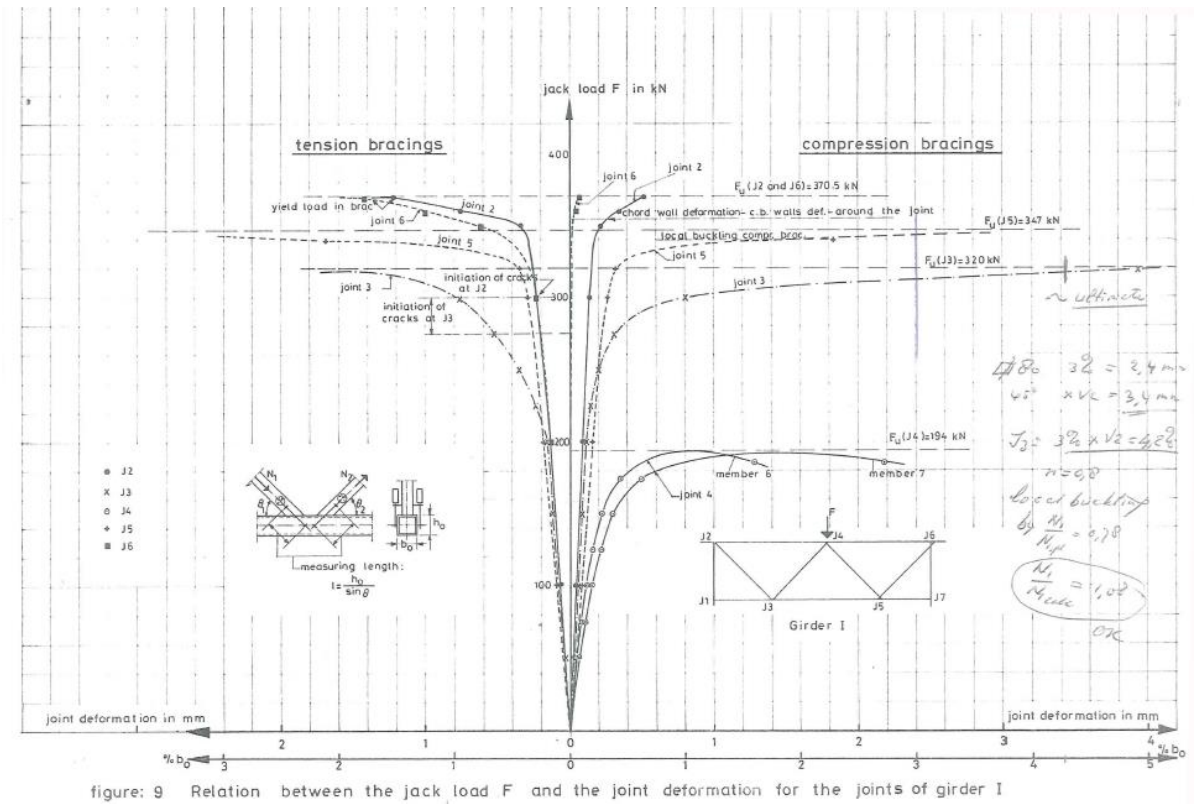

Figure B-2: Load-joint deformation girder 1 [24]

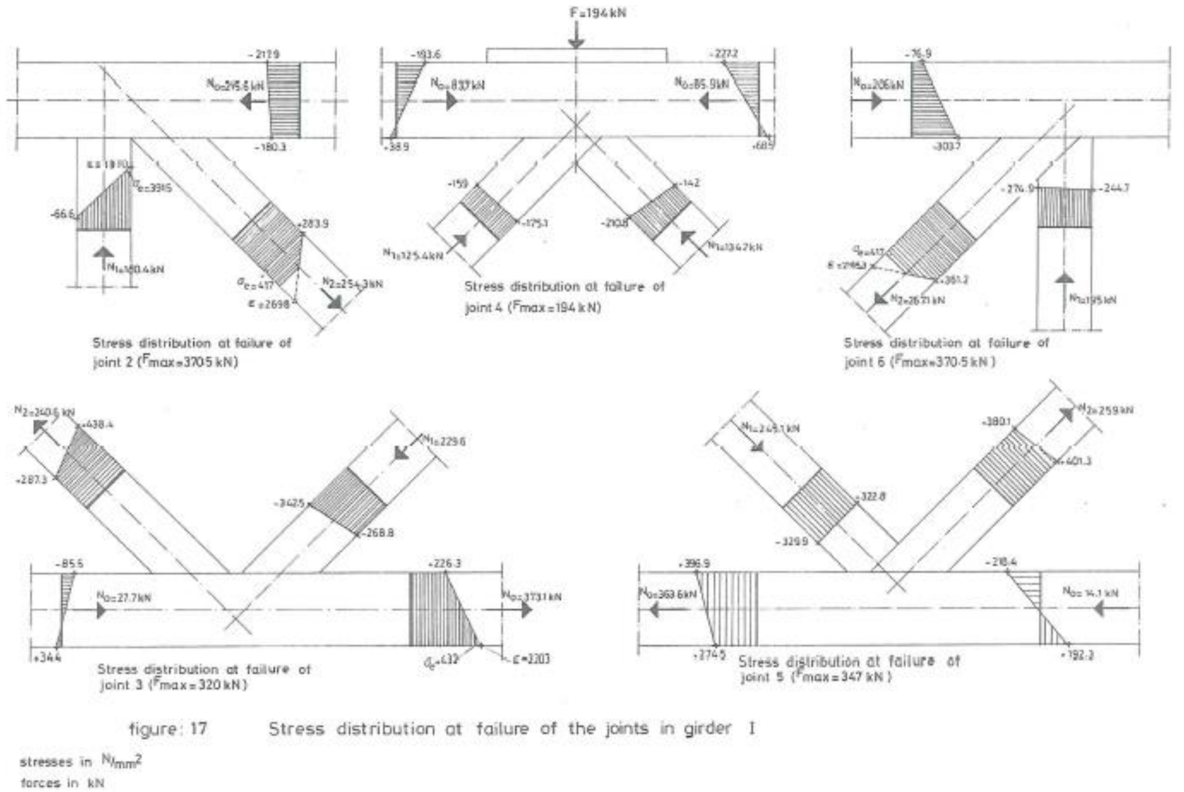

Figure B-3: Stress distribution at failure in joint 1 [24]

Appendix B.2 Joint resistance of J6

Table B-1: Range of Validity girder 1, part 1

												eccentricity		
Joint	class.	b_0	t_o	f_{yo}	b_i	t_i	f_{yi}	θ_i	e	gap	lap	min: –0.55*h_o	max: 0.25*h_o	check
		(mm)	(mm)	(MPa)	(mm)	(mm)	(Mpa)	(º)	(mm)	(mm)	(%)	(mm)	(mm)	
j6	N lap	79.8	3.56	432	60	2.96	417	45	-15.3		79.61	-43.89	19.95	within limit
					60.2	3.28	391.5	90						

Table B-2: Range of Validity girder 1, part 2

	RHS brace					RHS chord				Aspect ratio			
Joint	b_i/b_o>0.25	b_i/t_i<35	c/t	class 1: c/t<33e		bo/to<35	C/t	Class c/t<33e		0.5<h_o/b_o<2	0.5<h_i/b_i<2	t_i/t_o <1	f_{yi}/f_{yo}≤1
	(-)	(-)	(-)				(-)			(-)	(-)	(-)	(-)
j6	0.25	20.27			class 1	22.42	18.73	24.34	class 1	1	1	0.75	0.97
	0.25	18.35	14.52	25.57	class 1						1	0.75	0.91

Table B-3: Range of Validity girder 1, part 3

	Gap: 0.5(1-β) <g/bo <1.5(1-β)							
Joint	min: $g=t_1+t_2$	0.5(1-β)*b_o	1.5(1-β)*b_o	check	t_i/t_j<1	b_i/b_j>0.75	λ_{ov}>25%	Satisfied
	(mm)	(-)	(-)		(-)		(%)	
j6					1.00	1.00	79.61	Good

Table B-4: Joint resistance Girder 1

			BF	PSF	chord member failure			Brace shear resistance				Resistance
Joint	γ_{m5}	C_f	N_{iRd}	$N_{i,Rd}$	σ_o	f_{yo}	σ_o/f_y≤1	$N_{s,Rd}$	Ni_{ED}	Ni_{ED}*cosθ+ N_{jED}cosθ	check	$N_{i,Rd}$
	(-)	(-)	(kN)	(kN)	(Mpa)	(Mpa)	(-)	(kN)	(kN)	(kN)		(kN)
j6	1	1	202.85		432	-303.7	0.70	228.42	267.10	188.87	0.83	202.85

Table B-5: Member design strength

Joint	b=h (mm)	t (mm)	A (mm^2)	f_y (Mpa)	f_u (Mpa)	Loading	$N_{pl,Rd}$ (kN)	Buckl. length (-)	$i=\sqrt{(I/A)}$ (mm)	λ_E	λ	$\lambda^*=\lambda/\lambda_E$	α	X	$X*N_{pl,Rd}$
j6	79.8	3.56	1083	432	490	Compression	467.86	1.8	31.22	69.27	57.65	0.83	0.21	0.78	363.40
	60	2.96	663	417	490	Tension	276.47								
	60.2	3.28	751	391.5	500	compression	294.02	1.06	22.55	72.76	47.02	0.65	0.21	0.87	256.26

Appendix B.3 Joint resistance of T-joint

Table B-6: Parameters of the T-joint

Model	b0 [mm]	to [mm]	fu [Mpa]	fy [Mpa]	bi [mm]	fu [Mpa]	fy [Mpa]	θi [o]	β [-]	γ	ti/to (-)	η=bi/bo [-]
Tjoint	200	8	512	429	150	530	420	90	0.75	12.5	0.625	0.75

Table B-7: Joint Resistance T-joint

Model	bi/bo>0.1+0.01bo/to but>0.25 [-]	bi/ti<35 [-]	class brace	bo/to<35	class chord	ti/to <1 [-]	fyi/ fyo<=1 [-]	bo/to>=15 [-]	σo [Mpa]	Qf≥ 0.4 [-]	Chord face failure Ni,Rd [kN]
Tjoint	0.26	30	class 2	25	class 1	0.75	0.98	25	-180	0.88	340.10

APPENDIX C PARAMETRIC STUDY

Appendix C.1 True stress-strain relationship

Table C-1: Engineering stress-strain and true stress – strain

Material	Engineering stress	Engineering strain	True stress	True strain
	(N/mm^2)	(-)	(N/mm^2)	(-)
S355	390	0.001857143	390.7242857	0.00185542
	390	0.023	398.97	0.022739487
	475	0.049	498.275	0.047837329
	504	0.075	541.8	0.072320662
	515	0.1	566.5	0.09531018
	521	0.15	599.15	0.139761942
	516	0.2	619.2	0.182321557
	500	0.25	625	0.223143551
	470	0.3	611	0.262364264
S460	460	0.002190476	461.007619	0.002188081
	492.4	0.005	494.862	0.004987542
	492.4	0.016	500.2784	0.015873349
	505.8	0.02	515.916	0.019802627
	551.4	0.05	578.97	0.048790164
	575.5	0.1	633.05	0.09531018
	575.5	0.15	661.825	0.139761942
	555	0.2	666	0.182321557
	505	0.22	616.1	0.198850859
	455	0.23	559.65	0.207014169
S650	650	0.003095238	652.0119048	0.003090458
	740	0.006	744.44	0.005982072
	750	0.01	757.5	0.009950331
	800	0.05	840	0.048790164
	800	0.075	860	0.072320662
	790	0.1	869	0.09531018
	750	0.128	846	0.120446153
	650	0.151	748.15	0.14063113
	570	0.162	662.34	0.150142658
S700	700	0.003333333	702.3333333	0.00332779
	820	0.005	824.1	0.004987542
	835	0.05	876.75	0.048790164
	820	0.09	893.8	0.086177696
	800	0.1	880	0.09531018
	700	0.13	791	0.122217633

	600	0.146	687.6	0.136277618
S960	960	0.004571429	964.3885714	0.004561011
	1050	0.0065	1056.825	0.006478966
	1120	0.01	1131.2	0.009950331
	1155	0.017	1174.635	0.016857117
	1175	0.035	1216.125	0.034401427
	1150	0.05	1207.5	0.048790164
	1000	0.077	1077	0.074179398
	920	0.086	999.12	0.082501222

Appendix C.2 Validity Range and Joint Resistance

Table C-2:Joint geometry FEM with G0 and G1

Model	b_0	t_o, r_0	r_u	A_o	f_u	$f_y \leq .8f_u$	b_i	t_i, r_i	r_u	A_i	θ_i	e	g	β	β_{mod}	γ	t_i/t_o
	(mm)	(mm)	(mm)	(mm^2)	(MPa)	(MPa)	(mm)	(mm)	(mm)	(mm^2)	(°)	(mm)	(mm)		(-)		(-)
G1-S355	120	5	9	2270	520	390	80	5	7.5	1470	30	-2.26	40	0.67	0.78	12	1
							80	5	7.5	1470	30						
G1-S460	120	5	7.5	2270	575	460	80	5	7.5	1470	30	-2.26	40	0.67	0.78	12	1
							80	5	7.5	1470	30						
G1-S700	120	5	7.5	2270	835	668	80	5	7.5	1470	30	-2.26	40	0.67	0.81	12	1
							80	5	7.5	1470	30						
G1-S960	120	5	7.5	2270	1175	940	80	5	7.5	1470	30	-2.26	40	0.67	0.83	12	1
							80	5	7.5	1470	30						
G0-S355	120	5	7.5	2270	520	390	80	5	7.5	1470	30	-6.60	25	0.67	0.78	12	1
							80	5	7.5	1470	30						
G0-S460	120	5	7.5	2270	575	460	80	5	7.5	1470	30	-6.60	25	0.67	0.78	12	1
							80	5	7.5	1470	30						
G0-S700	120	5	7.5	2270	835	668	80	5	7.5	1470	30	-6.60	25	0.67	0.81	12	1
							80	5	7.5	1470	30						
G0-S960	120	5	7.5	2270	1175	940	80	5	7.5	1470	30	-6.60	25	0.67	0.83	12	1
							80	5	7.5	1470	30						

Table C-3: Validity range FEM with G0 and G1

	eccentricity			brace to chord width ratio		Cross-section classification							
Model	Min. $-0.55*h_o$	Max. $0.25*h_o$	e	$b_i/b_o>0.1+0.01b_o/t_o$ but>0.25		$b_i/t_i<35$	$\varepsilon=\sqrt{235/fy}$	c/t	Class 1 ($c/t<33\varepsilon$)	class brace	$b_o/t_o<35$	C/t	Class chord
	(mm)	(mm)	(mm)	(-)		(-)	(-)	(-)				(-)	
G1-S355	-66	30	-2.26	0.25	good	16	0.78	12	25.62	class 1	24	20.00	Class 1
G1-S460	-66	30	-2.26	0.25	good	16	0.71	12	23.59	class 1	24	20.00	class 1
G1-S700	-66	30	-2.26	0.25	good	16	0.59	12	19.57	class 1	24	20.00	Class 2
G1-S960	-66	30	-2.26	0.25	good	16	0.50	12	16.50	class 1	24	19.00	
G0-S355	-66	30	-6.60	0.25	good	16	0.78	12	25.6	class 1	24	20	Class 1
G0-S460	-66	30	-6.60	0.25	good	16	0.71	12	23.58	class 1	24	20	class 1
G0-S700	-66	30	-6.60	0.25	good	16	0.59	12	19.57	class 1	24	20	Class 2
G0-S960	-66	30	-6.60	0.25	good	16	0.5	12	16.5	class 1	24	19	

Table C-4: Validity range and additional validity range FEM with G0 and G1

	Gap						Additional validity range		
Model	Min. $g=t_1+t_2$	$0.5(1-\beta)*b_o$	$1.5(1-\beta)*b_o$	check	ti/to <1	f_{yi}/f_{yo}<=1	$0.6<b_1+b_2/2b_1<1.3$	$b_o/t_o\geq15$	check
	(mm)	(-)	(-)	(-)	(-)	(-)		(-)	
G1-S355	10	12.93	38.79	good	0.67	1	1	24	
G1-S460	10	20	60	Good	0.67	1	1	24	
G1-S700	10	11.55	34.65	good	0.67	1	1	24	
G1-S960	10	10.1	30.3	good	1.00	1	1	24	
G0-S355	10	13	39	Good	0.67	1	1	24	
G0-S460	10	12.93	38.79	Good	0.67	1	1	24	
G0-S700	10	11.5	34.5	Good	0.67	1	1	24	
G0-S960	10	10.1	30.3	Good	0.67	1	1	24	

Table C-5: Joint resistance FEM with G0 and G1

	Chord face failure							Chord Shear Failure					Brace failure		Punching shear	
Model	γ_{m5}	Cf	σo	n= σo/fyo	C_1	Q_f	Ni,Rd	$V_{pl,RD}$	α	$A_{v,o,gap}$	$N_{i,Rd}$	$N_{0,Rd}$	beff	NiRd	$b_{e,p}$	Ni,Rd
	(-)	(-)	(MPa)	(-)		(-)	(kN)	(kN)	(-)	(mm^2)	(kN)	(kN)	(mm)	(kN)	(mm)	(kN)
G1-S355	1	1	-250	-0.64	0.11	0.90	422.34	284.74	0.11	1264.57	569.48	723.76	33.33	494.00	33.33	975.72
	1						422.34				569.48		33.33	494.00	33.33	975.72
G1-S460	1	1	-200	-0.43	0.11	0.94	522.17	335.85	0.11	1264.57	671.69	982.96	33.33	582.67	33.33	1150.85
	1						522.17				671.69		33.33	582.67	33.33	1150.85
G1-S700	1	1	-240	-0.36	0.10	0.96	796.64	487.71	0.11	1264.57	975.42	1186.43	33.33	846.13	33.33	1671.24
	1						796.64				975.42		33.33	846.13	33.33	1671.24
G1-S960	1	1	-328	-0.35	0.08	0.96	1162.36	686.30	0.11	1264.57	1372.59	1741.67	33.33	1190.67	33.33	2351.74
	1						1162.36				1372.59		33.33	1190.67	33.33	2351.74
G0-S355	1	1	-200	-0.51	0.11	0.93	435.64	293.26	0.17	1302.40	586.51	708.13	33.33	494.00	33.33	975.72
	1						435.64				586.51		33.33	494.00	33.33	975.72
G0-S460	1	1	-200	-0.43	0.11	0.94	523.12	345.89	0.17	1302.40	691.78	825.18	33.33	582.67	33.33	1150.85
	1						523.12				691.78		33.33	582.67	33.33	1150.85
G0-S700	1	1	-280	-0.42	0.10	0.95	790.14	502.30	0.17	1302.40	1004.59	1476.66	33.33	846.13	33.33	1671.24
	1						790.14				1004.59		33.33	846.13	33.33	1671.24
G0-S960	1	1	-300	-0.32	0.08	0.97	1166.75	706.82	0.17	1302.40	1413.65	1631.22	33.33	1190.67	33.33	2351.74
	1						1166.75				1413.65		33.33	1190.67	33.33	2351.74

Table C-6: Joint geometry FEM with β1,β2,β3

Model	b_0	t_o, r_0	r_u	A_o	f_u	$f_y \leq 0.8f_u$	b_i	t_i, r_i	r_u	A_i	θ_i	e	g	β	β_{mod}	γ	t_i/t_o
	(mm)	(mm)	(mm)	(mm^2)	(MPa)	(MPa)	(mm)	(mm)	(mm)	(mm^2)	(°)	(mm)	(mm)		(-)		(-)
β1-S355	140	6.3	9.45	3330	520	390	70	5	7.5	1270	30	-18.04	40	0.50	0.60	11.11	0.79
							70	5	7.5	1270	30						
β1-S460	140	6.3	9.45	3330	575	460	70	5	7.5	1270	30	-18.04	40	0.50	0.60	11.11	0.79
							70	5	7.5	1270	30						
β1-S700	140	6.3	9.45	3330	835	668	70	5	7.5	1270	30	-18.04	40	0.50	0.62	11.11	0.79
							70	5	7.5	1270	30						
β1-S960	140	6.3	9.45	3330	1175	940	70	5	7.5	1270	30	-18.04	40	0.50	0.64	11.11	0.79
							70	5	7.5	1270	30						
β2-S355	140	6.3	9.45	3330	520	390	80	5	7.5	1479	30	-12.26	40	0.57	0.67	11.11	0.79
							80	5	7.5	1479	30						
β2-S460	140	6.3	9.45	3330	575	460	80	5	7.5	1470	30	-12.26	40	0.57	0.67	11.11	0.79
							80	5	7.5	1470	30						
β2-S700	140	6.3	9.45	3330	835	668	80	5	7.5	1470	30	-12.26	40	0.57	0.69	11.11	0.79
							80	5	7.5	1470	30						
β2-S960	140	6.3	9.45	3330	1175	940	80	5	7.5	1470	30	-12.26	40	0.57	0.71	11.11	0.79
							80	5	7.5	1470	30						
β3-S355	140	6.3	9.45	3330	520	390	90	5	7.5	1670	30	-6.49	40	0.64	0.74	11.11	0.79
							90	5	7.5	1670	30						
β3-S460	140	6.3	9.45	3330	575	460	90	5	7.5	1670	30	-6.49	40	0.64	0.74	11.11	0.79
							90	5	7.5	1670	30						
β3-S700	140	6.3	9.45	3330	835	668	90	5	7.5	1670	30	-6.49	40	0.64	0.76	11.11	0.79
							90	5	7.5	1670	30						
β3-S960	140	6.3	9.45	3330	1175	940	90	5	7.5	1670	30	-6.49	40	0.64	0.78	11.11	0.79
							90	5	7.5	1670	30						

Table C-7: Validity range FEM with β1,β2,β3

	eccentricity			brace to chord width ratio		Cross-section classification							
Model	Min. $-0.55*h_o$	Max. $0.25*h_o$	e	$b_i/b_o>0.1+0.01b_o/t_o$ but>0.25		$b_i/t_i<35$	$\varepsilon=\sqrt{235/fy}$	c/t	Class 1 (c/t<33ε)	class brace	$b_o/t_o<35$	C/t	Class chord
	(mm)	(mm)	(mm)	(-)		(-)	(-)	(-)				(-)	
β1-S355	-77	35	-18.04	0.25	good	14	0.78	10	25.62	class 1	22.22	18.22	class 1
β1-S460	-77	35	-18.04	0.25	good	14	0.71	10	23.59	class 1	22.22	18.22	class 1
β1-S700	-77	35	-18.04	0.25	good	14	0.59	10	19.57	class 1	22.22	18.22	class 1
β1-S960	-77	35	-18.04	0.25	good	14	0.5	10	16.5	class 1	22.22	17.22	Class 2
β2-S355	-77	35	-12.26	0.25	good	16	0.78	12	25.62	class 1	22.22	18.22	class 1
β2-S460	-77	35	-12.26	0.25	good	16	0.71	12	23.59	class 1	22.22	18.22	class 1
β2-S700	-77	35	-12.26	0.25	good	16	0.59	12	19.57	class 1	22.22	18.22	class 1
β2-S960	-77	35	-12.26	0.25	good	16	0.50	12	16.50	class 1	22.22	17.22	Class 2
β3-S355	-77	35	-6.49	0.25	good	18	0.78	14	25.62	class 1	22.22	18.22	class 1
β3-S460	-77	35	-6.49	0.25	good	18	0.71	14	23.59	class 1	22.22	18.22	class 1
β3-S700	-77	35	-6.49	0.25	good	18	0.59	14	19.57	class 1	22.22	18.22	class 1
β3-S960	-77	35	-6.49	0.25	good	18	0.50	14	16.50	class 1	22.22	17.22	Class 2

Table C-8: Validity range and additional validity range FEM with β1, β2,β3

	Gap						Additional validity range		
Model	Min. $g=t_1+t_2$	$0.5(1-\beta)*b_o$	$1.5(1-\beta)*b_o$	check	ti/to <1	$f_{yi}/ f_{yo}<=1$	$0.6<b_1+b_2/2b_1<1.3$	$b_o/t_o\geq15$	check
	(mm)	(-)	(-)	(-)	(-)	(-)		(-)	
β1-S355	10	27.93	83.79	Good	0.50	1	1	22.22	
β1-S460	10	27.93	83.79	Good	0.50	1	1	22.22	
β1-S700	10	26.5	79.5	Good	0.50	1	1	22.22	
β1-S960	10	25.1	75.3	Good	0.50	1	1	22.22	
β2-S355	10	22.93	68.79	Good	0.57	1	1	22.22	
β2-S460	10	22.93	68.79	Good	0.57	1	1	22.22	
β2-S700	10	21.5	64.5	Good	0.57	1	1	22.22	
β2-S960	10	20.1	60.3	Good	0.57	1	1	22.22	
β3-S355	10	17.93	53.79	Good	0.64	1	1	22.22	
β3-S460	10	17.93	53.79	Good	0.64	1	1	22.22	
β3-S700	10	16.52	49.56	Good	0.64	1	1	22.22	
β3-S960	10	15.1	45.3	Good	0.64	1	1	22.22	

Table C-9: Joint resistance FEM with β1, β2,β3

	Chord face failure							Chord Shear Failure					Brace failure		Punching shear	
Model	γ_{m5}	Cf	σo	n= σo/fyo	C_1	Q_f	Ni,Rd	$V_{pl,RD}$	α	$A_{v,o,gap}$	$N_{i,Rd}$	$N_{0,Rd}$	beff	NiRd	$b_{e,p}$	Ni,Rd
	(-)	(-)	(MPa)	(-)		(-)	(kN)	(kN)	(-)	(mm^2)	(kN)	(kN)	(mm)	(kN)	(mm)	(kN)
β1-S355	1	1	-280	-0.72	0.25	0.73	402.25	424.03	0.14	1883.20	848.07	1205.71	39.69	447.90	31.5	1082.35
	1						402.25				848.07		39.69	447.90	31.50	1082.35
β1-S460	1	1	-280	-0.61	0.25	0.79	514.92	500.14	0.14	1883.20	1000.28	1415.82	39.69	528.29	31.50	1276.62
	1						514.92				1000.28		39.69	528.29	31.50	1276.62
β1-S700	1	1	-425	-0.64	0.25	0.78	759.20	726.29	0.14	1883.20	1452.59	2023.85	39.69	767.16	31.50	1853.88
	1						759.20				1452.59		39.69	767.16	31.50	1853.88
β1-S960	1	1	-630	-0.67	0.25	0.76	1076.01	1022.03	0.14	1883.20	2044.06	2873.04	39.69	1079.54	31.50	2608.75
	1						1076.01				2044.06		39.69	1079.54	31.50	2608.75
β2-S355	1	1	-280	-0.72	0.21	0.76	470.87	424.03	0.14	1883.20	848.07	1251.21	45.36	517.45	36.00	1236.98
	1						470.87				848.07		45.36	517.45	36.00	1236.98
β2-S460	1	1	-270	-0.59	0.21	0.83	602.69	500.14	0.14	1883.20	1000.28	1531.80	45.36	610.33	36.00	1459.00
	1						602.69				1000.28		45.36	610.33	36.00	1459.00
β2-S700	1	1	-420	-0.63	0.21	0.81	881.43	726.29	0.14	1883.20	1452.59	2197.32	45.36	886.30	36.00	2118.72
	1						881.43				1452.59		45.36	886.30	36.00	2118.72
β2-S960	1	1	-650	-0.69	0.21	0.78	1226.50	1022.03	0.14	1883.20	2044.06	3130.20	45.36	1247.19	36.00	2981.43
	1						1226.50				2044.06		45.36	1247.19	36.00	2981.43
β3-S355	1	1	-260	-0.67	0.18	0.82	561.48	424.03	0.14	1883.20	848.07	1251.21	51.03	587.01	40.50	1391.60
	1						561.48				848.07		51.03	587.01	40.50	1391.60
β3-S460	1	1	-280	-0.61	0.18	0.85	681.49	500.14	0.14	1883.20	1000.28	1286.40	51.03	692.37	40.50	1641.37
	1						681.49				1000.28		51.03	692.37	40.50	1641.37
β3-S700	1	1	-430	-0.64	0.18	0.83	999.57	726.29	0.14	1883.20	1452.59	1795.09	51.03	1005.44	40.50	2383.56
	1						999.57				1452.59		51.03	1005.44	40.50	2383.56
β3-S960	1	1	-650	-0.69	0.18	0.81	1407.28	1022.03	0.14	1883.20	2044.06	2627.11	51.03	1414.84	40.50	3354.11
	1						1407.28				2044.06		51.03	1414.84	40.50	3354.11

Table C-10: Joint geometry butt-welded joints

Model	b_0	t_o	r_i	r_u	A_o	f_u	$f_y \le 0.8f_u$	bi	ti	ri	ru	Ai	θi	e	gap	β , η	γ	ti/to
	(mm)	(mm)	(mm)	(mm)	(mm^2)	(Mpa)	(Mpa)	(mm)	(mm)	(mm)	(mm)	(mm^2)	(o)	(mm)	(mm)	(-)	(-)	(-)
β1-S355B	140	6.3	6.3	9.45	3330	520	390	70	5	5	7.5	1270	30	-18.04	40	0.50	11.11	0.79
								70	5	5	7.5	1270	30					
β1-S460B	140	6.3	6.3	9.45	3330	575	460	70	5	5	7.5	1270	30	-18.04	40	0.50	11.11	0.79
								70	5	5	7.5	1270	30					
β1-S700B	140	6.3	6.3	9.45	3330	835	668	70	5	5	7.5	1270	30	-18.04	40	0.50	11.11	0.79
								70	5	5	7.5	1270	30					
β1-S960B	140	6.3	6.3	9.45	3330	1175	940	70	5	5	7.5	1270	30	-18.04	40	0.50	11.11	0.79
								70	5	5	7.5	1270	30					
β2-S355B	140	6.3	6.3	9.45	3330	520	390	80	5	5	7.5	1479	30	-12.26	40	0.57	11.11	0.79
								80	5	5	7.5	1479	30					
β2-S460B	140	6.3	6.3	9.45	3330	575	460	80	5	5	7.5	1470	30	-12.26	40	0.57	11.11	0.79
								80	5	5	7.5	1470	30					
β2-S700B	140	6.3	6.3	9.45	3330	835	668	80	5	5	7.5	1470	30	-12.26	40	0.57	11.11	0.79
								80	5	5	7.5	1470	30					
β2-S960B	140	6.3	6.3	9.45	3330	1175	940	80	5	5	7.5	1470	30	-12.26	40	0.57	11.11	0.79
								80	5	5	7.5	1470	30					
β3-S355B	140	6.3	6.3	9.45	3330	520	390	90	5	5	7.5	1670	30	-6.49	40	0.64	11.11	0.79
								90	5	5	7.5	1670	30					
β3-S460B	140	6.3	6.3	9.45	3330	575	460	90	5	5	7.5	1670	30	-6.49	40	0.64	11.11	0.79
								90	5	5	7.5	1670	30					
β3-S700B	140	6.3	6.3	9.45	3330	835	668	90	5	5	7.5	1670	30	-6.49	40	0.64	11.11	0.79
								90	5	5	7.5	1670	30					
β3-S960B	140	6.3	6.3	9.45	3330	1175	940	90	5	5	7.5	1670	30	-6.49	40	0.64	11.11	0.79
								90	5	5	7.5	1670	30					

Table C-11: Validity range butt-welded joints

	eccentricity			Brace to chord width ratio		Cross-section classification							
Model	Min. $-0.55*h_o$	Max $0.25*h_o$	e	$b_i/b_o>0.1+0.01b_o/t_o$ but>0.25		$b_i/t_i<35$	c/t	Class 1 c/t<33ε	Class brace	$b_o/t_o<35$	C/t	Class chord	check
	(mm)	(mm)	(mm)	(-)		(-)	(-)				(-)		
β1-S355B	-77	35	-18.04	0.25	good	14	10	25.62	class 1	22.22	18.22	class 1	good
β1-S460B	-77	35	-18.04	0.25	good	14	10	23.59	class 1	22.22	18.22	class 1	good
β1-S700B	-77	35	-18.04	0.25	good	14	10	19.57	class 1	22.22	18.22	class 1	good
β1-S960B	-77	35	-18.04	0.25	good	14	10	16.50	class 1	22.22	18.22	Class 2	good
β2-S355B	-77	35	-12.26	0.25	good	16	12	25.62	class 1	22.22	18.22	class 1	good
β2-S460B	-77	35	-12.26	0.25	good	16	12	23.59	class 1	22.22	18.22	class 1	good
β2-S700B	-77	35	-12.26	0.25	good	16	12	19.57	class 1	22.22	18.22	class 1	good
β2-S960B	-77	35	-12.26	0.25	good	16	12	16.50	class 1	22.22	17.22	Class 2	good
β3-S355B	-77	35	-6.49	0.25	good	18	14	25.62	class 1	22.22	18.22	class 1	good
β3-S460B	-77	35	-6.49	0.25	good	18	14	23.59	class 1	22.22	18.22	class 1	good
β3-S700B	-77	35	-6.49	0.25	good	18	14	19.57	class 1	22.22	18.22	class 1	good
β3-S960B	-77	35	-6.49	0.25	good	18	14	16.50	class 1	22.22	17.22	Class 2	good

Table C-12: Validity range and additional validity range butt-welded joints

Model	Gap							Additional validity range		
	Min g=t1+t2	0.5(1-β)*bo	1.5(1-β)*bo	Check:	t_i/t_o <1	f_{yi}/f_{yo}≤1	Θ≥ 30°	0.6≤b1+b2/2b1≤1.3	bo/to≥15	check
β1-S355B	(mm)	(-)	(-)	(-)	(-)	(-)	(-)		(-)	
	10	35	105	Gap within limit	0.5	1	good	1	22.22	good
β1-S460B										
	10	35	105	Gap within limit	0.5	1	good	1	22.22	good
β1-S700B										
	10	35	105	Gap within limit	0.5	1	good	1	22.22	good
β1-S960B										
	10	35	105	Gap within limit	0.5	1	good	1	22.22	good
β2-S355B										
	10	30	90	Gap within limit	0.57	1	good	1	22.22	good
β2-S460B										
	10	30	90	Gap within limit	0.57	1	good	1	22.22	good
β2-S700B										
	10	30	90	Gap within limit	0.57	1	good	1	22.22	good
β2-S960B										
	10	30	90	Gap within limit	0.57	1	good	1	22.22	good
β3-S355B										
	10	25	75	Gap within limit	0.64	1	good	1	22.22	good
β3-S460B										
	10	25	75	Gap within limit	0.64	1	good	1	22.22	good
β3-S700B										
	10	25	75	Gap within limit	0.64	1	good	1	22.22	good
β3-S960B										
	10	25	75	Gap within limit	0.64	1	good	1	22.22	good

Table C-13: Joint resistance butt-welded joints

	Chord face failure							Chord Shear Failure					Brace failure		Punching shear	
Model	γ_{m5}	C_f	σ_o	$n=\sigma_o/f_{yo}$	C_1	Q_f	Ni,Rd	$V_{pl,RD}$	α	$A_{v,o,gap}$	$N_{i,Rd}$	$N_{0,Rd}$	b_{eff}	$N_{i;Rd}$	$b_{e,p}$	$N_{i,Rd}$
	(-)	(-)	(Mpa)	(-)		(-)	(kN)	(kN)	(-)	(mm^2)	(kN)	(kN)	(mm)	(kN)	(mm)	(kN)
β1-S355B	1	1	-260	-0.67	0.25	0.76	348.93	424.03	0.14	1883.20	848.07	1232.78	39.69	447.90	31.5	1082.35
	1						348.93				848.07		39.69	447.90	31.5	1082.35
β1-S460B	1	1	-275	-0.60	0.25	0.80	431.33	500.14	0.14	1883.20	1000.28	1452.46	39.69	528.29	31.5	1276.62
	1						431.33				1000.28		39.69	528.29	31.5	1276.62
β1-S700B	1	1	-350	-0.52	0.25	0.83	653.34	726.29	0.14	1883.20	1452.59	2197.32	39.69	767.16	31.5	1853.88
	1						653.34				1452.59		39.69	767.16	31.5	1853.88
β1-S960B	1	1	-490	-0.52	0.25	0.83	920.66	1022.03	0.14	1883.20	2044.06	2998.20	39.69	1079.54	31.5	2608.75
	1						920.66				2044.06		39.69	1079.54	31.5	2608.75
β2-S355B	1	1	-260	-0.67	0.21	0.79	414.73	424.03	0.14	1883.20	848.07	1251.21	45.36	517.45	36	1236.98
	1						414.73				848.07		45.36	517.45	36	1236.98
β2-S460B	1	1	-275	-0.60	0.21	0.82	509.25	500.14	0.14	1883.20	1000.28	1413.99	45.36	610.33	36	1459.00
	1						509.25				1000.28		45.36	610.33	36	1459.00
β2-S700B	1	1	-350	-0.52	0.21	0.85	766.73	726.29	0.14	1883.20	1452.59	2197.32	45.36	886.30	36	2118.72
	1						766.73				1452.59		45.36	886.30	36	2118.72
β2-S960B	1	1	-480	-0.51	0.21	0.86	1085.33	1022.03	0.14	1883.20	2044.06	2940.27	45.36	1247.19	36	2981.43
	1						1085.33				2044.06		45.36	1247.19	36	2981.43
β3-S355B	1	1	-270	-0.69	0.18	0.81	478.36	424.03	0.14	1883.20	848.07	1159.42	51.03	587.01	40.5	1391.60
	1						478.36				848.07		51.03	587.01	40.5	1391.60
β3-S460B	1	1	-280	-0.61	0.18	0.85	588.96	500.14	0.14	1883.20	1000.28	1364.41	51.03	692.37	40.5	1641.37
	1						588.96				1000.28		51.03	692.37	40.5	1641.37
β3-S700B	1	1	-300	-0.45	0.18	0.90	909.15	726.29	0.14	1883.20	1452.59	1974.49	51.03	1005.44	40.5	2383.56
	1						909.15				1452.59		51.03	1005.44	40.5	2383.56
β3-S960B	1	1	-490	-0.52	0.18	0.88	1247.65	1022.03	0.14	1883.20	2044.06	2854.24	51.03	1414.84	40.5	3354.11
	1						1247.65				2044.06		51.03	1414.84	40.5	3354.11

Appendix C.3 Stress and strain distribution

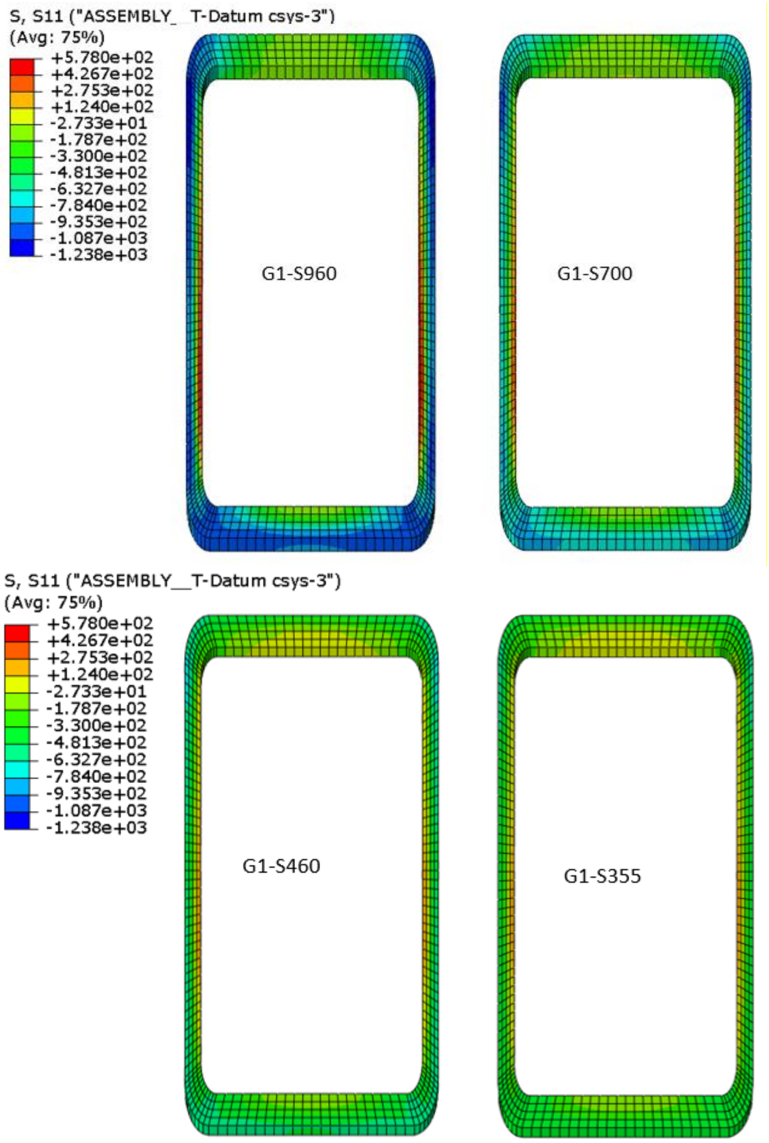

Figure C-1: Stress distribution in cross-section 2

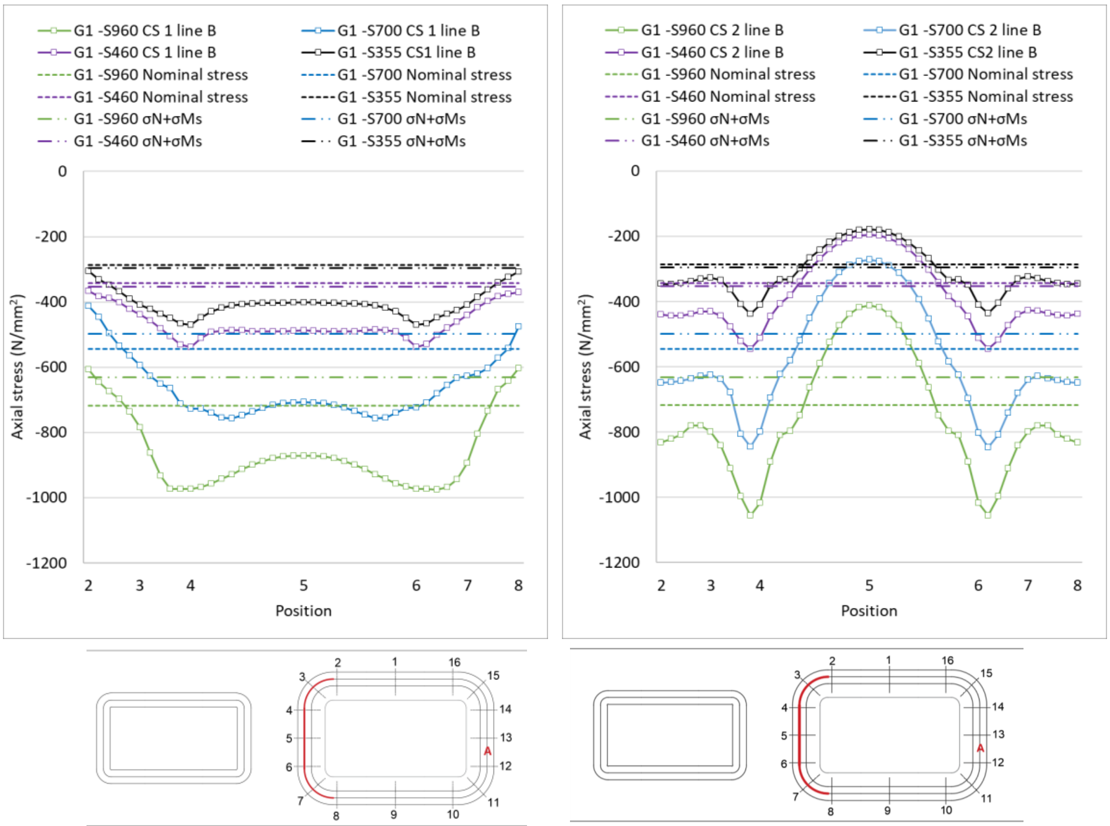

Figure C-2: Axial stress in cross-section 1 and 2 in the positions 2-8

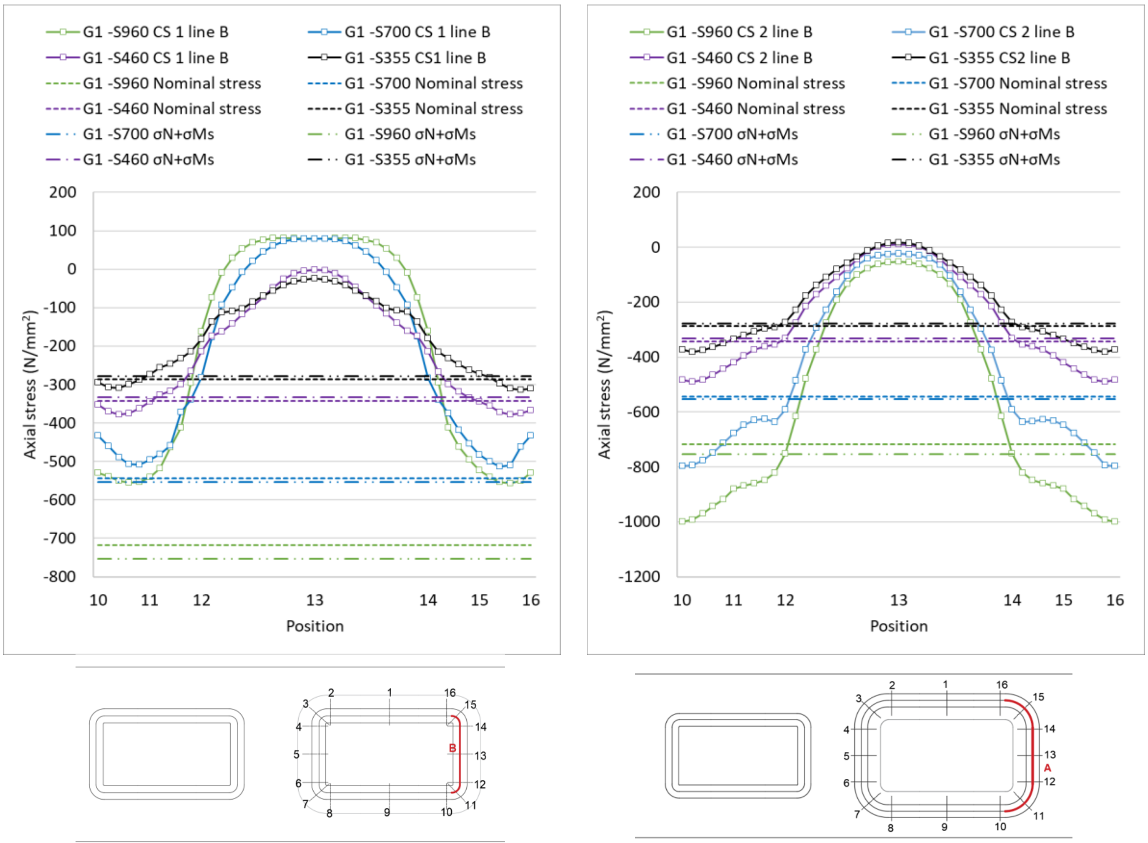

Figure C-3: Axial stress in cross-section 1 and 2 in the positions 10-16

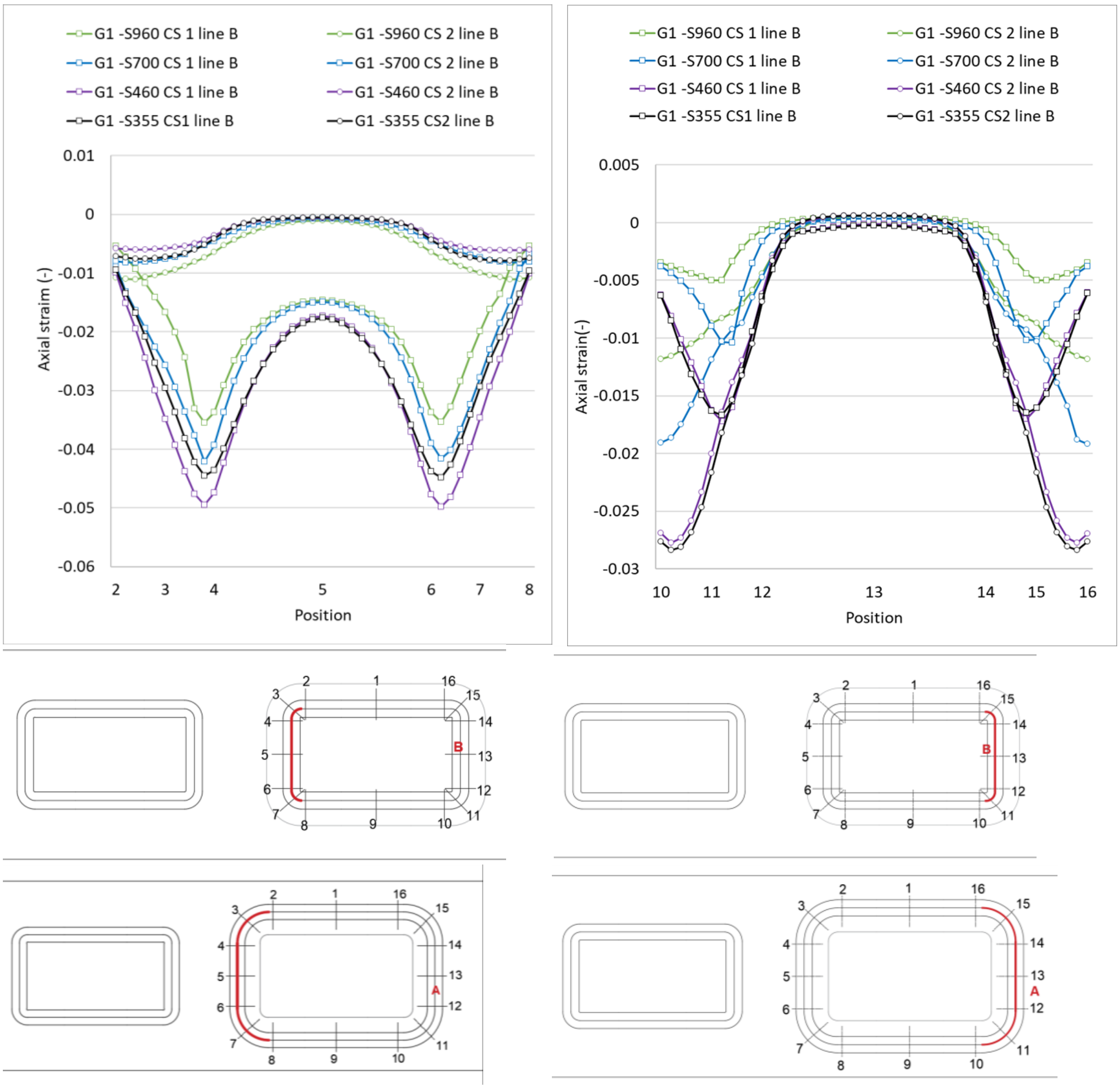

Figure C-4: Axial strain in cross section 1 and 2 in position 2-8 and 10-16

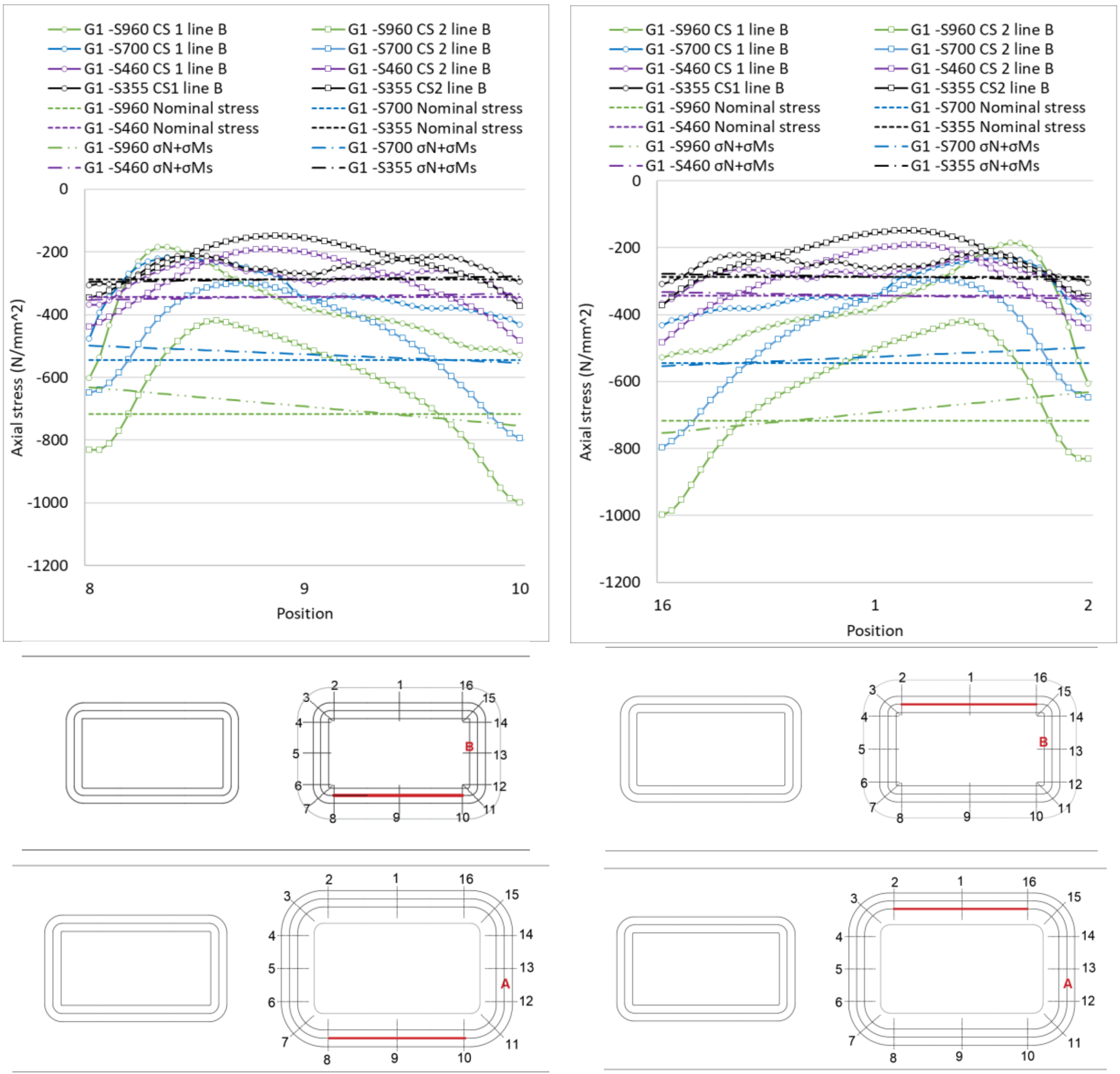

Figure C-5: Axial stress in position 8-10 and 16-2

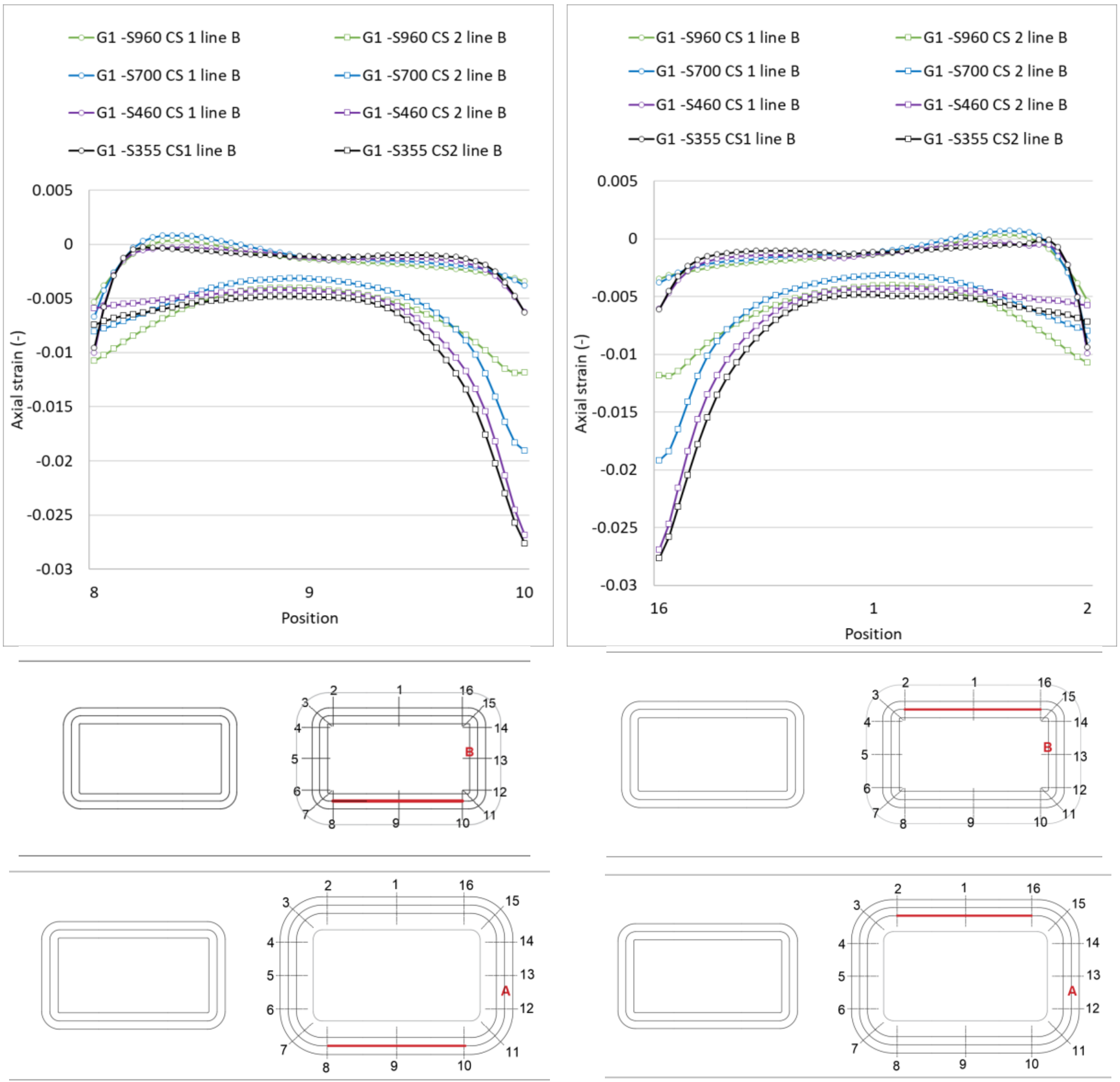

Figure C-6: Axial strain in position 8-10 and 16-2

Table C-14: Stresses in cross section 1

	CS1 line B											
	G1-S355			G1-S460			G1-S700			G1-S960		
	Stress	Nominal stress	Ratio	Stress	Nominal stress	Ratio	Stress	Nominal stress	Ratio	Stress	Nominal stress	Ratio
	(N/mm²)	(N/mm²)	(-)	(N/mm²)	(N/mm²)	(-)	(N/mm²)	(N/mm²)	(-)	(N/mm²)	(N/mm²)	(-)
1	-263.01	-286.73	0.92	-285.08	-342.85	0.83	-344.97	-544.61	0.63	-381.98	-717.47	0.53
2	-306.04	-286.73	1.07	-367.38	-342.85	1.07	-412.35	-544.61	0.76	-606.86	-717.47	0.85
3	-408.73	-286.73	1.43	-438.61	-342.85	1.28	-594.68	-544.61	1.09	-785.40	-717.47	1.09
4	-470.57	-286.73	1.64	-537.81	-342.85	1.57	-727.00	-544.61	1.33	-974.11	-717.47	1.36
5	-400.74	-286.73	1.40	-485.91	-342.85	1.42	-707.61	-544.61	1.30	-871.04	-717.47	1.21
6	-470.87	-286.73	1.64	-537.81	-342.85	1.57	-724.07	-544.61	1.33	-973.92	-717.47	1.36
7	-408.67	-286.73	1.43	-440.01	-342.85	1.28	-627.17	-544.61	1.15	-894.26	-717.47	1.25
8	-307.61	-286.73	1.07	-369.76	-342.85	1.08	-476.39	-544.61	0.87	-603.13	-717.47	0.84
9	-267.86	-286.73	0.93	-291.86	-342.85	0.85	-347.18	-544.61	0.64	-380.38	-717.47	0.53
10	-294.72	-286.73	1.03	-352.63	-342.85	1.03	-432.21	-544.61	0.79	-528.66	-717.47	0.74
11	-273.48	-286.73	0.95	-344.63	-342.85	1.01	-494.91	-544.61	0.91	-540.66	-717.47	0.75
12	-181.57	-286.73	0.63	-214.67	-342.85	0.63	-282.15	-544.61	0.52	-161.86	-717.47	0.23
13	-24.16	-286.73	0.08	-1.01	-342.85	0.00	79.88	-544.61	-0.15	79.50	-717.47	-0.11
14	-180.32	-286.73	0.63	-213.81	-342.85	0.62	-282.86	-544.61	0.52	-161.00	-717.47	0.22
15	-271.09	-286.73	0.95	-343.51	-342.85	1.00	-482.64	-544.61	0.89	-522.27	-717.47	0.73
16	-309.81	-286.73	1.08	-367.49	-342.85	1.07	-433.30	-544.61	0.80	-529.34	-717.47	0.74

Table C-15: Stresses in cross section 2

	CS2 line B											
	G1-S355			G1-S460			G1-S700			G1-S960		
Position	Stress	Nominal stress	Ratio	Stress	Nominal stress	Ratio	Stress	Nominal stress	Ratio	Stress	Nominal stress	Ratio
	(N/mm^2)	(N/mm^2)	(-)	(N/mm^2)	(N/mm^2)	(-)	(N/mm^2)	(N/mm^2)	(-)	(N/mm^2)	(N/mm^2)	(-)
1	-155.53	-286.73	0.54	-202.90	-342.85	0.59	-345.55	-544.61	0.63	-502.74	-717.47	0.70
2	-346.18	-286.73	1.21	-439.16	-342.85	1.28	-648.22	-544.61	1.19	-831.73	-717.47	1.16
3	-326.35	-286.73	1.14	-430.97	-342.85	1.26	-624.91	-544.61	1.15	-798.00	-717.47	1.11
4	-410.83	-286.73	1.43	-511.53	-342.85	1.49	-799.46	-544.61	1.47	-1016.78	-717.47	1.42
5	-178.70	-286.73	0.62	-195.50	-342.85	0.57	-272.31	-544.61	0.50	-411.80	-717.47	0.57
6	-410.70	-286.73	1.43	-512.27	-342.85	1.49	-801.67	-544.61	1.47	-1016.78	-717.47	1.42
7	-323.38	-286.73	1.13	-427.35	-342.85	1.25	-640.29	-544.61	1.18	-798.00	-717.47	1.11
8	-345.47	-286.73	1.20	-438.74	-342.85	1.28	-648.69	-544.61	1.19	-831.73	-717.47	1.16
9	-155.37	-286.73	0.54	-200.74	-342.85	0.59	-347.26	-544.61	0.64	-502.74	-717.47	0.70
10	-372.24	-286.73	1.30	-483.29	-342.85	1.41	-795.44	-544.61	1.46	-999.07	-717.47	1.39
11	-334.97	-286.73	1.17	-420.07	-342.85	1.23	-676.77	-544.61	1.24	-880.18	-717.47	1.23
12	-274.16	-286.73	0.96	-331.46	-342.85	0.97	-591.69	-544.61	1.09	-751.60	-717.47	1.05
13	16.13	-286.73	-0.06	10.19	-342.85	-0.03	-22.83	-544.61	0.04	-52.22	-717.47	0.07
14	-274.24	-286.73	0.96	-331.53	-342.85	0.97	-592.51	-544.61	1.09	-751.60	-717.47	1.05
15	-335.45	-286.73	1.17	-420.31	-342.85	1.23	-647.72	-544.61	1.19	-880.18	-717.47	1.23
16	-371.91	-286.73	1.30	-483.11	-342.85	1.41	-796.41	-544.61	1.46	-999.07	-717.47	1.39

Appendix C.4 Required throat thickness

Table C-16: Required throat thickness to resist the ultimate load

model	b_i	t_i	b_o	t_o	$b_{e;p}$	l_{eff}	f_y	f_u	β_w	γ_{m2}	N_{FEA}	Required a	FEM a	Ratio a_{FEM}/a_{req}
	(mm)	(mm)			(mm)	(mm)	(N/mm^2)	(N/mm^2)	(-)	(-)	(kN)	(mm)	(mm)	(-)
G1-S355	80	5	120	5	33.33	193.33	390	521	0.9	1.25	421.69	3.33	5	1.50
G1-S460	80	5	120	5	33.33	193.33	460	575.5	0.85	1.25	503.99	3.40	5	1.47
G1-S700	80	5	120	5	33.33	193.33	700	835	1.1	1.25	773.35	4.66	6	1.29
G1-S960	80	5	120	5	33.33	193.33	960	1175	1.24	1.25	1018.81	4.92	7	1.42
G0-S355	80	5	120	5	33.33	193.33	390	521	0.9	1.25	445.11	3.52	5	1.42
G0-S460	80	5	120	5	33.33	193.33	460	575.5	0.85	1.25	534.74	3.61	5	1.38
G0-S700	80	5	120	5	33.33	193.33	700	835	1.1	1.25	845.17	5.09	6	1.18
G0-S960	80	5	120	5	33.33	193.33	960	1175	1.24	1.25	1141.92	5.51	7	1.27
β1-S355	70	5	140	6.3	31.5	171.50	390	521	0.9	1.25	413.03	3.68	5	1.36
β1-S460	70	5	140	6.3	31.5	171.50	460	575.5	0.85	1.25	500.00	3.81	5	1.31
β1-S700	70	5	140	6.3	31.5	171.50	700	835	1.1	1.25	787.00	5.34	6	1.12
β1-S960	70	5	140	6.3	31.5	171.50	960	1175	1.24	1.25	1061.00	5.77	7	1.21
β2-S355	80	5	140	6.3	36	196.00	390	521	0.9	1.25	486.35	3.79	5	1.32
β2-S460	80	5	140	6.3	36	196.00	460	575.5	0.85	1.25	587.20	3.91	5	1.28
β2-S700	80	5	140	6.3	36	196.00	700	835	1.1	1.25	925.00	5.50	6	1.09
β2-S960	80	5	140	6.3	36	196.00	960	1175	1.24	1.25	1223.00	5.82	7	1.20
β3-S355	90	5	140	6.3	40.5	220.50	390	521	0.9	1.25	576.20	3.99	5	1.25
β3-S460	90	5	140	6.3	40.5	220.50	460	575.5	0.85	1.25	697.60	4.13	5	1.21
β3-S700	90	5	140	6.3	40.5	220.50	700	835	1.1	1.25	1093.00	5.77	6	1.04
β3-S960	90	5	140	6.3	40.5	220.50	960	1175	1.24	1.25	1427.40	6.04	7	1.16

The required throat is determined using the following equations:

$$a \geq \frac{F_{end}\beta_w\gamma_{m2}}{f_u l\sqrt{2}}$$ **Equation C-1**

where a is the throat thickness and l is the effective length of the weld, the factor β_w is the correlation factor and it depends on the steel grade (shown in

Table 2-1). The parameter f_u is the nominal ultimate strength of the weaker part. The parameter γ_{m2} is the partial safety factor for welded connections [4, 18]. The force F_{end} is the external axial load. The effective length of the weld is determined using the following equation:

$$l_{eff} = 2(h_i / \sin(\theta_i) + b_{e,p})$$
$$with$$ **Equation C-2**
$$b_{e,p} = \frac{10}{b_o / t_o} b_i \leq b_i$$

In which h_i is the height of the brace, b_i is the width of the brace member, θ_i is the brace angle, b_o is the width of the chord and t_o is the thickness of the chord.

Appendix C.5 Yield line patterns in FEA

Table C-17: Yield line patterns for the butt-welded joints

Internal work									External work				
Model	Line	No	fy	to	mpl	liφi	n*length	ΣliφiMpl	δ	N_{YLT}	N_{FEA}	Ratio	
			(Mpa)	(mm)	(Nmm/mm)	(mm)	(mm)	(Nmm)	(mm)	(KN)	(kN)	(-)	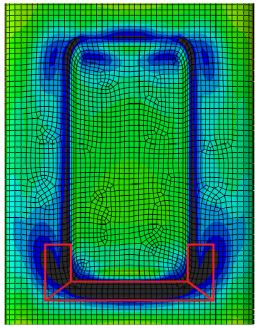
β1-S355B	L1	1	390	6.3	3869.775	91	91	352149.53					
	L2	1	390	6.3	3869.775	60	60	232186.50					
	L3	2	390	6.3	3869.775	16.8	33.6	130024.44					
	L4	2	390	6.3	3869.775	45.75	91.5	354084.41					
	L5	2	390	6.3	3869.775	14.85	29.7	114932.32					
	L6	2	390	6.3	3869.775	24.23	48.46	187529.30					
							354.26	1370906.49	4.29	319.28	351.16	0.91	
β1-S460B	L1	1	460	6.3	4564.35	91.00	91.00	415355.85					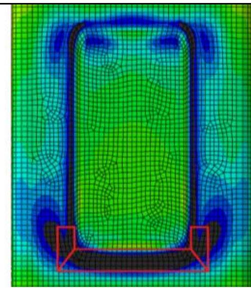
	L2	1	460	6.3	4564.35	60.00	60.00	273861.00					
	L3	2	460	6.3	4564.35	16.80	33.60	153362.16					
	L4	2	460	6.3	4564.35	45.75	91.50	221188.40					
	L5	2	460	6.3	4564.35	14.85	29.70	135561.20					
	L6	2	460	6.3	4564.35	24.23	48.46	417638.03					
						252.63	354.26	1616966.63	4.23	381.84	418.20	0.91	
β1-S700B	L1	1	700	6.3	6945.75	96.02	96.02	666931.61					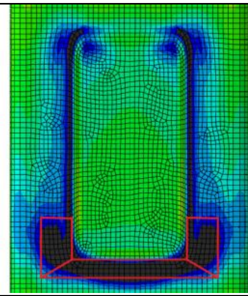
	L2	1	700	6.3	6945.75	64.62	64.62	448862.15					
	L3	2	700	6.3	6945.75	21.79	43.58	302695.79					
	L4	2	700	6.3	6945.75	38.02	76.03	528099.26					
	L5	2	700	6.3	6945.75	16.20	32.40	225028.41					
	L6	2	700	6.3	6945.75	26.22	52.44	364235.13					
						262.87	365.09	2535852.35	4.59	552.46	629.60	0.88	

β1-S960B	L1	1	960	6.3	9525.6	89.78	89.78	855200.75					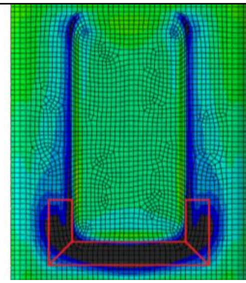
	L2	1	960	6.3	9525.6	64.46	64.46	614007.79					
	L3	2	960	6.3	9525.6	18.58	37.16	353931.29					
	L4	2	960	6.3	9525.6	34.68	69.37	660747.05					
	L5	2	960	6.3	9525.6	13.22	26.44	251887.35					
	L6	2	960	6.3	9525.6	21.91	43.82	417383.22					
						242.63	331.02	3153157.44	4.52	698.33	789.08	0.88	
β2-S355B	L1	1	390	6.3	3869.775	110.14	110.14	426217.02					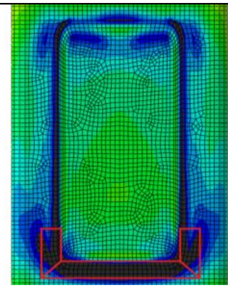
	L2	1	390	6.3	3869.775	73.0509	73.0509	282690.55					
	L3	2	390	6.3	3869.775	21.0486	42.0972	162906.69					
	L4	2	390	6.3	3869.775	35.1595	70.319	272118.71					
	L5	2	390	6.3	3869.775	22.5313	45.0626	174382.12					
	L6	2	390	6.3	3869.775	31.1533	62.3066	241112.52					
							402.9763	1559427.61	4.44	351.32	420.20	0.84	
β2-S460B	L1	1	460	6.3	4564.35	110.14	110.14	502717.51					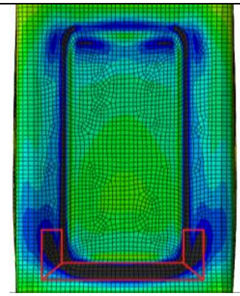
	L2	1	460	6.3	4564.35	73.0509	73.05	333429.88					
	L3	2	460	6.3	4564.35	21.0486	42.10	192146.35					
	L4	2	460	6.3	4564.35	35.1595	70.32	284389.13					
	L5	2	460	6.3	4564.35	22.5313	45.06	205681.48					
	L6	2	460	6.3	4564.35	31.1533	62.31	320960.53					
							402.98	1839324.87	4.25	432.54	503.6304	0.86	
β2-S700B	L1	1	700	6.3	6945.75	109.14	109.14	758059.16					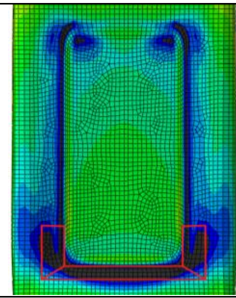
	L2	1	700	6.3	6945.75	72.0509	72.05	500447.54					
	L3	2	700	6.3	6945.75	21.0486	42.10	292396.63					
	L4	2	700	6.3	6945.75	34.1595	68.32	474526.69					
	L5	2	700	6.3	6945.75	22.5313	45.06	312993.55					
	L6	2	700	6.3	6945.75	30.1533	60.31	418874.57					
							396.98	2757298.14	4.17	661.93	730.79	0.91	

β2-S960B	L1	1	960	6.3	9525.6	107.14	107.14	1020572.78					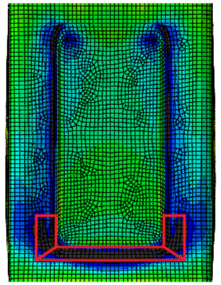
	L2	1	960	6.3	9525.6	72.0509	72.05	686328.05					
	L3	2	960	6.3	9525.6	20.0486	40.10	381949.89					
	L4	2	960	6.3	9525.6	34.1595	68.32	650779.47					
	L5	2	960	6.3	9525.6	20.5313	41.06	391145.90					
	L6	2	960	6.3	9525.6	30.1533	60.31	574456.55					
							388.98	3705232.64	4.10	903.06	917.18	0.98	
β1-S355	L1	1	390	6.3	3869.775	87.5232	87.5232	338695.09					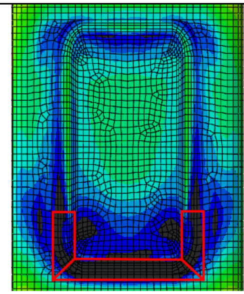
	L2	1	390	6.3	3869.775	57.5969	57.5969	222887.04					
	L3	2	390	6.3	3869.775	20.6044	41.2088	159468.78					
	L4	2	390	6.3	3869.775	57.597	115.194	445774.86					
	L5	2	390	6.3	3869.775	9.6866	19.3732	74969.93					
	L6	2	390	6.3	3869.775	43.2225	86.445	334522.70					
							407.3411	1576318.41	4.47	352.96	416.03	0.85	
β1-S460	L1	1	460	6.3	4564.35	85.5232	85.5232	390357.82					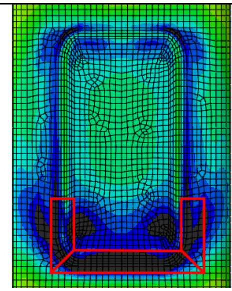
	L2	1	460	6.3	4564.35	52.5969	52.5969	240070.66					
	L3	2	460	6.3	4564.35	19.1044	38.2088	174398.34					
	L4	2	460	6.3	4564.35	50.597	101.194	461884.83					
	L5	2	460	6.3	4564.35	9.6866	19.3732	88426.07					
	L6	2	460	6.3	4564.35	39.2225	78.445	358050.44					
							375.3411	1713188.15	4.47	383.61	416.03	0.92	

β1-S700	L1	1	700	6.3	6945.75	107.802	107.802	748765.74					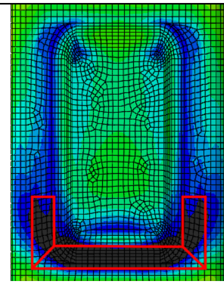
	L2	1	700	6.3	6945.75	75.346	75.346	523334.48					
	L3	2	700	6.3	6945.75	21.966	43.932	305140.69					
	L4	2	700	6.3	6945.75	47.208	94.416	655789.93					
	L5	2	700	6.3	6945.75	17.436	34.872	242212.19					
	L6	2	700	6.3	6945.75	33.681	67.362	467879.61					
							423.73	2943122.65	4.22	697.46	786.92	0.89	
β1-S960	L1	1	960	6.3	9525.6	103.966	103.966	990338.53					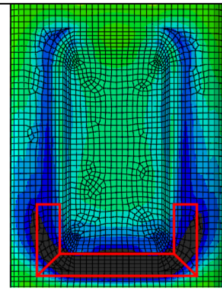
	L2	1	960	6.3	9525.6	75.19	75.19	716229.86					
	L3	2	960	6.3	9525.6	29.654	59.308	564944.28					
	L4	2	960	6.3	9525.6	41.95	83.9	799197.84					
	L5	2	960	6.3	9525.6	12.155	24.31	231567.34					
	L6	2	960	6.3	9525.6	29.654	59.308	564944.28					
							405.982	3867222.14	4.14	933.45	1059.50	0.88	
β2-S355	L1	1	390	6.3	3869.775	92.69	92.69	358689.44					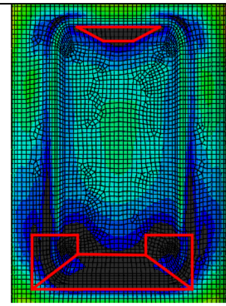
	L2	1	390	6.3	3869.775	41.652	41.652	161183.87					
	L3	2	390	6.3	3869.775	30.434	60.868	235545.46					
	L4	2	390	6.3	3869.775	40	80.398	311122.17					
	L5	2	390	6.3	3869.775	21.63	43.26	167406.47					
	L6	2	390	6.3	3869.775	16.989	33.978	131487.21					
		2	390	6.3	3869.775	19.018	38.036	147190.76					
		1	390	6.3	3869.775	20.7751	20.7751	80394.96					
		1	390	6.3	3869.775	58.8834	58.8834	227865.51					
							352.846	1820885.86	4.289478	424.50	486.3498	0.87	

β2-S460	L1	1	460	6.3	4564.35	92.69	92.69	423069.60					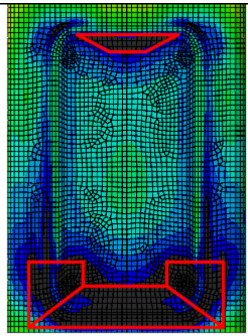
	L2	1	460	6.3	4564.35	41.652	41.652	190114.31					
	L3	2	460	6.3	4564.35	30.434	60.868	277822.86					
	L4	2	460	6.3	4564.35	40	80.398	366964.61					
	L5	2	460	6.3	4564.35	21.63	43.26	197453.78					
	L6	2	460	6.3	4564.35	16.989	33.978	155087.48					
	l7	2	460	6.3	4564.35	19.018	38.036	173609.62					
	l8	1	460	6.3	4564.35	20.7751	20.7751	94824.83					
	l9	1	460	6.3	4564.35	58.8834	58.8834	268764.45					
							352.846	2147711.53	4.160307	516.24	586.8166	0.88	
β2-S700	L1	1	700	6.3	6945.75	120.274	120.274	835393.14					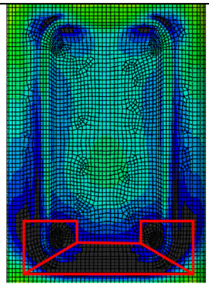
	L2	1	700	6.3	6945.75	57.794	57.794	401422.68					
	L3	2	700	6.3	6945.75	40.609	81.218	564119.92					
	L4	2	700	6.3	6945.75	59.36	118.718	824585.55					
	L5	2	700	6.3	6945.75	39.884	79.768	554048.59					
	L6	2	700	6.3	6945.75	24.829	49.658	344912.05					
							507.43	3524481.92	4.299647	819.71	926.1824	0.89	
β2-S960	L1	1	960	6.3	9525.6	114.528	114.528	1090947.92					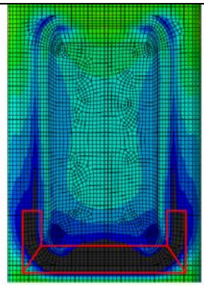
	L2	1	960	6.3	9525.6	86.956	86.956	828308.07					
	L3	2	960	6.3	9525.6	24.61	49.22	468850.03					
	L4	2	960	6.3	9525.6	39.527	79.054	753036.78					
	L5	2	960	6.3	9525.6	13.513	27.026	257438.87					
	L6	2	960	6.3	9525.6	21.004	42.008	400151.40					
							398.792	3798733.08	3.685453	1030.74	1223.199	0.84	